

DEVELOPMENT OF MICROFLUIDIC
PLATFORMS AS A TOOL FOR HIGH-
THROUGHPUT BIOMARKER SCREENING

by
Helena Zec

A dissertation submitted to The Johns Hopkins University in conformity with the
requirements for the degree of Doctor of Philosophy

Baltimore, Maryland
August 2015

© 2015 Helena Zec
All Rights Reserved

Abstract

Droplet microfluidic platforms are in the early stages of revolutionizing high throughput and combinatorial sample screening for bioanalytical applications. However, many droplet platforms are incapable of addressing the needs of numerous applications, which require high degrees of multiplexing, as well as high-throughput analysis of multiple samples. Examples of applications include single nucleotide polymorphism (SNP) analysis for crop improvement and genotyping for the identification of genes associated with common diseases. My PhD thesis focused on developing microfluidic devices to extend their capabilities to meet the needs of a wide array of applications.

Thesis Advisor: Dr. Tza-Huei Wang

Acknowledgments

First and foremost, I must express my sincerest gratitude to my advisor, Dr. Tza-Huei (Jeff) Wang. Throughout my PhD, Dr. Wang has devoted attention to my research and academic training. Dr. Wang has always struck the right balance between providing ample guidance and also allowing me autonomy to explore my research interests. Dr. Wang has opened many opportunities for me and has always believed in me. Dr. Wang is extremely patient and I have seen first-hand how he tailors his mentoring style to suit each of his students. I am truly lucky to be mentored by someone who is a consistent source of support while challenging you to learn and grow.

Dr. Wang's encouraging and positive management style has spilled over in to the lab and created a collaborative, open and friendly working environment. I was lucky to be able to carry out my PhD with an amazing group of motivated and talented researchers. I learned microfluidics from Chris and Tushar, and molecular biology from Vas and Yi during my initial stay in the lab. Dr. Tushar Rane has been a wonderful research partner and mentor in the collaborative research projects we have completed together. I enjoyed collaborating and engaging with other lab members over the course of my PhD including Kelvin, Stephanie, Sarah, Yi, Cyrus, Yunke, Dong Jin, Ye, Liben, Weihua, Natt, and Chrissy. I have enjoyed collaborating with Alejandro and Tom on one of my most recent projects. Wen, who more recently joined our lab, has been a wonderful role model and is skillful at mentoring and inspiring younger students. I have enjoyed working with visiting fellows, like Dr. Chi-Han Chiou and Dr. Wei Liu. I have learned something from each and every one of them.

Throughout my PhD, I am fortunate to have worked with many bright and talented undergraduate students. Polly Ma in particular has contributed to my research and I am grateful for her efforts.

I must also thank my friends Sravanti Kusuma, Liz Jordan, Danya Decoteau, Iwen Wu, and Maggie Kuo for making life fun. I look back fondly on our coffee breaks, weekend outings, and frequent runs by the Baltimore Harbor.

Finally, I would like to thank my family for their unwavering support and encouragement. My parents never stop believing in me. My sisters, Grace and Vivien, who were always just a phone call away. And of course my boyfriend, Elliot, who shared this experience with me from the very beginning. I cherish their support and unconditional love and dedicate this thesis to them.

Table of Contents

Abstract	ii
Acknowledgments	iii
Table of Contents	iv
List of Figures	vii
1 Introduction	1
1.1 Thesis overview.....	2
2 Novel droplet platforms for the detection of disease biomarkers	3
2.1 Biomarkers in diagnostics	3
2.2 Types of droplet platforms	5
2.2.1 Microfluidic droplet platforms.....	5
2.2.2 Surface droplet platforms.....	6
2.2.3 Static droplet arrays	8
2.3 Applications of droplet platforms.....	9
2.3.1 Traditional technologies for digital analysis.....	9
2.4 Microfluidic droplet platforms applications.....	10
2.4.1 Integrated platforms for genetic mutation detection.....	10
2.4.2 Integrated platforms for targeted enrichment for sequence-based studies..	12
2.4.3 Integrated platforms for targeted enrichment for single-cell studies	13
2.5 Surface droplet platform applications	14
2.5.1 Integrated platforms for pathogen detection.....	15
2.6 Static droplet array applications	16
2.6.1 Integrated platforms for genetic mutation detection.....	16
2.6.2 Integrated platforms for protein detection	18
2.7 Expert commentary & five-year view	18
3 Microfluidic platform for on-demand generation of spatially indexed combinatorial droplets	38
3.1 Introduction	38
3.2 Materials and Methods	41
3.2.1 Serial Sampling Loading System.....	42
3.2.2 Fabrication of the Master Molds for the Microfluidic Device.....	42
3.2.3 Microfluidic Device Fabrication.....	43
3.2.4 Capillary-to-Chip Interface.....	43
3.2.5 Device control.....	44
3.2.6 Reagents.....	44

3.2.7	Sample plug and droplet volume estimation.....	44
3.3	Results and Discussion.....	45
3.3.1	Overall Work Flow.....	45
3.3.2	Capillary-to-Chip Interface.....	46
3.3.3	Droplet uniformity using mechanical valve based droplet generation.....	46
3.3.4	Sample Digitization.....	47
3.3.5	Generation of droplets of combinatorial mixtures.....	48
3.4	Conclusion.....	49
3.5	Supplementary section.....	64
3.5.1	Mold Fabrication.....	64
3.5.2	Device Fabrication and Operation.....	64
3.5.3	Fusion Zone design.....	65
3.5.4	Serial Sample Loading System.....	66
3.5.4.1	Background.....	66
3.5.4.2	Materials and Methods.....	69
3.5.4.3	Results.....	71
3.5.4.4	Discussion.....	75
4	Enhancing Throughput of Combinatorial Droplet Devices via Droplet Bifurcation, Parallelized Droplet Fusion, and Parallelized Detection.....	76
4.1	Introduction.....	76
4.2	Experimental Section.....	78
4.2.1	Mask Design and Printing.....	78
4.2.2	Master Mold Microfabrication.....	78
4.2.3	Microfluidic Chip Fabrication.....	79
4.2.4	Experimentation.....	80
4.2.5	Data Acquisition and Analysis.....	81
4.3	3. Results.....	81
4.3.1	Device Design and Workflow.....	81
4.3.2	Uniform Droplet Splitting.....	83
4.3.3	Parallelized Injection of Reagents with Individualized Calibration.....	84
4.3.4	Reliable Droplet Fusion in Parallel.....	85
4.3.5	Parallelized Droplet Imaging.....	86
4.4	Discussion.....	86
4.5	Conclusions.....	88
4.6	Acknowledgments.....	88
5	A Nano Sample Processor for Genotyping of Plant Samples for Marker-Assisted Selection.....	102
5.1	Introduction.....	102
5.2	Materials and Methods.....	105

5.2.1	SNP Genotyping Workflow:.....	105
5.2.2	Multiplexed PCR:	106
5.2.3	Invader® Assay Chemistry:.....	106
5.2.4	Off-chip SNP Genotyping Invader® Assay (Synthetic and Genomic Targets):106	
5.2.5	Hydrophobic Surface Treatment of Microfluidic Device:.....	107
5.2.6	Optimization of Carrier Fluid, Additives, and Surfactants:	108
5.2.7	On-chip SNP Genotyping Invader® Assay (Synthetic and Genomic Targets):108	
5.2.8	Fluorescence Detection Setup and Data Analysis:	109
5.3	Results	110
5.3.1	Droplet-Based Assay Overview:.....	110
5.3.2	Benchmark verification of Invader assays	111
5.3.3	Sample loading into microfluidic device via Nano Sample Processor	113
5.3.4	Robust droplet operation and optical detection in microfluidic device	113
5.3.5	On-Chip SNP Genotyping Invader® with Synthetic Targets	114
5.3.6	On-Chip SNP Genotyping Invader® with Genomic Targets.....	115
5.4	Discussion	115
6	Ultra-thin, evaporation-resistant PDMS devices for absolute quantification of DNA using digital pcr	128
6.1	Introduction	128
6.2	Methods.....	129
6.2.1	Device fabrication.....	129
6.2.2	Device Loading and Thermocycling.....	130
6.2.3	Imaging and Image Processing.....	130
6.2.4	Evaporation.....	130
6.2.5	Digital PCR.....	131
6.3	Discussion	131
7	Conclusions and future work.....	145
	Bibliography	146
	Curriculum Vitae.....	156

List of Figures

Figure 2.1. Schematic of digital PCR.	21
Figure 2.2. A conceptual diagram of droplet microfluidics, surface droplet platforms and static droplet arrays.	23
Figure 2.3. Schematics illustrating various modes of droplet actuation on surface.	25
Figure 2.4. Droplet platform for on-demand generation of combinatorial mixtures of samples and reagents.	27
Figure 2.5. Microdroplet PCR workflow.	29
Figure 2.6. Amplification-free genetic detection of single pathogenic cells on a droplet-based microfluidic device.	31
Figure 2.7. Real-time PCR droplet platforms for integrated sample processing and detection.	33
Figure 2.8. Melting curve analysis for genetic mutation detection using an integrated droplet platform.	35
Figure 2.9. Megapixel digital PCR and SlipChip.	37
Figure 3.1. A schematic of the sample screening platform.	53
Figure 3.2. The Serial Sample Loading (SSL) system.	55
Figure 3.3. Microfluidic Device Design.	57
Figure 3.4. Control of droplet volume and droplet uniformity using mechanical valve based droplet generation.	59
Figure 3.5. Demonstration of reagent injection in sample daughter droplets.	61
Figure 3.6. Photographs of the incubation region indicating the multiplexing capability of the device.	63

Figure 4.1. Improving Throughput of Combinatorial Droplet Devices via Parallelization.....	91
Figure 4.2. Parallelized Combinatorial Droplet Device.	93
Figure 4.3. Uniformity of Droplet Bifurcation.	95
Figure 4.4 Parallelized Quadplex Injection of Reagent Droplets with Capacity for Individualized Calibration.	97
Figure 4.5. Parallel Fusion of Sample Droplets with Reagent Droplets.	99
Figure 4.6. Imaging-Based Parallel Detection of Fused Droplets.....	101
Figure 5.1. SNP Genotyping Workflow.	119
Figure 5.2. Microfluidic Chip Workflow.	121
Figure 5.3 Bench-top SNP Genotyping Invader[®] Assay Results.	123
Figure 5.4. Synthetic Target Results.	125
Figure 5.5. On-chip SNP Genotyping Invader[®] Assay of Genomic Targets.....	127
Figure 6.1. Ensemble versus Digital PCR.....	134
Figure 6.2. Fabrication steps for creation of ultra-thin microfluidic dPCR chip. ..	136
Figure 6.3. Device structure.	138
Figure 6.4. Evaporation during PCR.	140
Figure 6.5. A comparison of expected and measured copies per well.....	142
Figure 6.6. Experimental Results.	144

*Genius is one percent inspiration, ninety-nine percent perspiration.
~Thomas Alva Edison*

For my family

1 ***Introduction***

Microfluidic systems refer to enclosed networks of channels in which fluid is manipulated in a confined geometry where at least one of the dimensions is below 1 mm. In droplet microfluidics, thousands of discrete reaction chambers are generated in the form of droplet emulsions. In these systems, each individual droplet is separated by an immiscible carrier phase (typically oil or gas). At present, there are several different methods for generating droplets in a high-throughput fashion. In these miniaturized systems, droplet volumes typically fall within picoliter to nanoliter range. Reducing reaction volumes by several orders of magnitude significantly lowers the costs of reagents. Furthermore, millions of droplets can be generated and analyzed on a single device, thus improving the accuracy of statistical analysis. In addition, reaction kinetics in droplets are favorable due to improved surface-to-volume ratios (compared with bulk methods). Additional advantages are that carrier fluid shields each droplet, mitigating the problems of absorption onto solid surfaces and contamination. Droplet microfluidics has the potential to satisfy the unmet needs for increased miniaturization, scalability and automation in biosample analysis.

Droplet-based microfluidic systems have a special advantage over other emulsion-generating techniques in that highly monodisperse droplets are generated. Droplets generated with bulk-created emulsions, are limited in applications due to the lack of control over droplet sizes. This size polydispersity limits the ability to perform quantitative measurements. In contrast, generating droplets in microfluidic systems has the advantage of creating monodisperse sample volumes that improves reaction conditions.

On the other hand, two key limitations of most droplet based devices include the difficulty of manipulating droplets after formation and measuring reaction kinetics within individual droplets in real time. Operations required for performing chemical reactions in droplets include droplet fusion, droplet fission, and droplet sorting. Automated manipulation of droplets in microchannels, combined with the ability to perform

biochemical reactions inside microdroplets, has inspired the development of versatile platforms for numerous applications ranging from molecular diagnostics to organic synthesis. In these devices, each individual droplet functions as a miniaturized reaction container. This approach allows the controlled manipulation of small volumes of reaction mixtures and permits the rapid partitioning of single molecules from complex samples that facilitates digital analysis. Interested readers are referred to comprehensive reviews of droplet-based microfluidic systems that review various operations that can be performed with these systems and their applications.

The ability to generate monodisperse droplets at extremely high throughput (kHz frequencies) facilitates experiments previously rendered impossible due to the practical constraint on the number of reactions that can be performed using traditional bench-top technologies. In this thesis, we will overcome some of the limitations of droplet microfluidic technology.

1.1 *Thesis overview*

The overall goal of this thesis was to investigate the use of droplet microfluidic devices to extend their use in bioanalysis applications.

An overview of droplet platforms is presented in *Chapter 2*. *Chapter 3* discusses the development of a microfluidic platform which can perform combinatorial screening operations. In *Chapter 4*, I describe a platform to increase the throughput of this combinatorial screening microfluidic device. *Chapter 5* demonstrates an application of our microfluidic device in the agricultural industry. *Chapter 6* investigates the use of a microfluidic device for digital analysis of DNA molecules in cancer. The thesis will conclude with *Chapter 7* providing a discussion and proposal for future work.

2 *Novel droplet platforms for the detection of disease biomarkers*

Helena Zec, Dong Jin Shin, and Tza-Huei Wang. "Novel droplet platforms for the detection of disease biomarkers." Expert Review of Molecular Diagnostics (2014): 787-801. Reproduced with permission of Informa Healthcare.

Personalized medicine – healthcare based on individual genetic variation – has the potential to transform the way healthcare is delivered to patients. The promise of personalized medicine has been predicated on the predictive and diagnostic power of genomic and proteomic biomarkers. Biomarker screening may help improve health outcomes, for example, by identifying individuals’ susceptibility to diseases and predicting how patients will respond to drugs. Microfluidic droplet technology offers an exciting opportunity to revolutionize the accessibility of personalized medicine. A framework for the role of droplet microfluidics in biomarker detection can be based on two main themes. Emulsion-based microdroplet platforms can provide new ways to measure and detect biomolecules. In addition, microdroplet platforms facilitate high-throughput screening of biomarkers. Meanwhile, surface-based droplet platforms provide an opportunity to develop miniaturized diagnostic systems. These platforms may function as portable benchtop environments that dramatically shorten the transition of a benchtop assay into a point-of-care format.

2.1 *Biomarkers in diagnostics*

Biomarker profiling assays are based on patterns of molecules such as nucleic acids, proteins and metabolites. The clinical applications of biomarker profiling run the gamut:

from examining normal biological processes, to monitoring pathogenic processes or pharmacological responses to a therapeutic intervention [1]. Segmenting patient populations based on biomarkers may facilitate clinical interventions. As clinical sequencing gains traction, there has been increased interest to connect genotype to phenotype. For example, sequencing has been used to correlate rare mutations to previously unidentified disorders [2]. However, several challenges remain. One major challenge is disease heterogeneity [3]. For instance, cancer is a heterogeneous disease characterized by a spectrum of genetic and epigenetic alterations [4]. In heterogeneous diseases like cancer, the use of genetic mutations as biomarkers necessitates sensitive strategies that allow detection of mutations within a milieu of predominantly wild-type DNA molecules [5]. Bulk procedures measure ensemble signals (Fig. 1), which have a very low sensitivity for rare sequences within biological samples. The ability to detect extremely rare populations of nucleic acids from a background of normal targets has the potential to transform clinical medicine. In light of this, technologies enabling digitization of biochemical assays are highly desirable. In addition to resolving genetic heterogeneity in disease, patterns of molecular heterogeneity on the single-cell level may be explored to determine the role in disease pathology and cellular responses to treatment. Molecular biomarker profiling also facilitates new paradigms for patient diagnostics and treatment in a manner that is more rapid and robust, such that efficacious therapeutic intervention can be achieved with minimal delay after diagnosis. In the case of infectious diseases, early diagnostics and treatment may help interrupt transmission of infectious agents and carry an additional importance from a public health standpoint [6]. While infectious agents have traditionally relied on culture-based assessment to identify the pathogen and determine the appropriate antibiotic treatment, the requirement of facilities and trained personnel as well as the time and cost of microbial culture limits the accessibility and efficacy of these assays. The emergence of PCR-based techniques for pathogen detection enables highly sensitive assays that can be performed with a significant reduction in cost and turnaround time [7]. In addition, genetic polymorphisms that have shown clear associations with patient response to therapeutic agents may help improve the efficacy of clinical interventions. One important example is patient sensitivity to the anticoagulant warfarin, which is known to be substantially less effective

in patients with mutations in the VKORC1 gene [8] and may be tested using PCR-based techniques for polymorphism identification. As these diagnostic assays can provide immediately useful information to the practicing clinician, there is a strong motivation to develop technologies in order to deliver these tests outside centralized laboratories. This review will demonstrate how miniaturized droplet technologies will facilitate biomarker analysis by allowing the sensitive detection and quantification of biomolecules. Instead of assays targeting single biomarkers to confer a diagnosis, highthroughput screening technologies allow screening of panels of biomarkers to elucidate patterns in diseases. The importance of testing a panel of biomarkers is particularly relevant to heterogeneous diseases like cancer and complex diseases like chronic inflammation. In addition to reviewing the role of droplet-based microfluidic devices in high-throughput screening applications, we will explore how surface-based miniaturized droplet platforms can be utilized to miniaturize an entire bench-top assay in a portable format. Finally, we will review miniaturized array-based technologies and their applications in biomarker discovery and detection. For the interested reader, there are several reviews that have recently explored the role of continuous flow microfluidic platforms on biomarker analysis [9, 10].

2.2 *Types of droplet platforms*

2.2.1 **Microfluidic droplet platforms**

Microfluidic systems refer to enclosed networks of channels (Fig. 2) in which fluid is manipulated in a confined geometry where at least one of the dimensions is below 1 mm. In droplet microfluidics, thousands of discrete reaction chambers are generated in the form of droplet emulsions. In these systems, each individual droplet is separated by an immiscible carrier phase (typically oil or gas). Droplet-based microfluidic systems have a special advantage over other emulsion-generating techniques in that highly monodisperse droplets are generated. Furthermore, droplets can be generated and manipulated at kHz frequencies in microfluidic systems. At present, there are several different methods for generating droplets in a high-throughput fashion. In these miniaturized systems, droplet volumes typically fall within picoliter to nanoliter range. Reducing reaction volumes by

several orders of magnitude significantly lowers the costs of reagents. Furthermore, millions of droplets can be generated and analyzed on a single device, thus improving the accuracy of statistical analysis. In addition, reaction kinetics in droplets are favorable due to improved surface-to-volume ratios (compared with bulk methods). On the other hand, two key limitations of most droplet based devices include the difficulty of manipulating droplets after formation and measuring reaction kinetics within individual droplets in real time. Automated manipulation of droplets in microchannels, combined with the ability to perform biochemical reactions inside microdroplets, has inspired the development of versatile platforms for numerous applications ranging from molecular diagnostics to organic synthesis. In these devices, each individual droplet functions as a miniaturized reaction container. This approach allows the controlled manipulation of small volumes of reaction mixtures and permits the rapid partitioning of single molecules from complex samples that facilitates digital analysis. Interested readers are referred to comprehensive reviews of droplet-based microfluidic systems that review various operations that can be performed with these systems and their applications [11-19]. The ability to generate monodisperse droplets at extremely high throughput (kHz frequencies) facilitates experiments previously rendered impossible due to the practical constraint on the number of reactions that can be performed using traditional bench-top technologies.

2.2.2 Surface droplet platforms

Surface droplet manipulation is a branch of techniques that has evolved outside the channel-based microemulsion paradigm. In this approach, aqueous reservoirs in the nanoliter-to-microliter range are manipulated individually on an open planar substrate rather than inside microchannels (Fig. 2). Surface droplet platforms focus on scalable fluidic processing mechanisms that do not require to be pressure-driven. Departure from pumps and complex fluidic architecture also lends these platforms to applications in point-of-care diagnostics and mobile medicine. Various modes of actuation (Fig. 3) have been explored for surface droplet manipulation, including electric [20-29], magnetofluidic [26, 30-41], acoustic [42-45], optical [46] and pneumatic actuation [47].

Among these, electric and magnetic actuation have received the most attention due to their advantages in speed, robust operating principles as well as compatibility with biochemical assays. Electrical actuation of droplets is an attractive concept, in part because the transition to electrical rather than mechanical actuators opens up the potential to leverage recent advancements in consumer electronics. While mechanisms such as droplet dielectrophoresis [20-22] and electrophoresis [28] have been explored to varying degrees, electrowetting-on-dielectric (EWOD) has gained the most attention due to the flexibility in device layout and wide range of fluidic operations that can be realized. The main principle of EWOD operation relies on the phenomenon of electrowetting, where the interfacial tension between the liquid droplet and solid substrate is altered when electric field is applied directly across the droplet. In the typical two-layer arrangement as shown in Fig. 3, an electrolyte solution is sandwiched between a reference electrode and a control electrode covered by a dielectric surface. When a voltage is applied across an electrolyte, this induces accumulation of charge along the electrolyte–dielectric interface and subsequent spreading of the liquid along the dielectric surface within the confines of the control electrode. In a typical EWOD device, an array of square electrode tiles is patterned on one substrate in order to facilitate actuation of a droplet on a surface at a resolution of one electrode tile. This mechanism forms the basis of all operations, including transport, mixing and fission of droplets, and has [31] been demonstrated in processes involving multiple fluid handling operations including nucleic acid extraction [25] and pyrosequencing [26]. Magnetofluidic actuation is another approach that has demonstrated its capacity for handling a diverse range of biochemical assays. A typical arrangement of magnetofluidic actuation involves aqueous droplets containing a suspension of magnetic particles and relies on the use of magnetic force and energy barriers to achieve the desired manipulation process. As shown in Fig. 3, magnetic droplet manipulation involves the actuation of magnetic particles by a moving external magnetic field generated by a permanent magnet or an electromagnet. As the magnetic particle is transported, it may either carry the entire volume of the droplet along with itself or become dissociated with the droplet, based on the relative magnitude of force exerted by magnetic particles to drag and capillary forces [27, 30]. Modification of these forces using topographical barriers [31, 32] and hydrophilic patterns [33, 34] has been

utilized in order to enable robust sequential processing of bioanalytes in aqueous reagents. Automation of magnetic particle actuation has been explored using mechanical actuators such as linear [35, 36] and rotary [37, 38, 41][37,38,41] stages, and also using electromagnetic actuators such as a planar coil array [39, 40, 48]. One significant utility of droplet platforms utilizing magnetic particles stems from their scalability to any biochemical assays utilizing solid phase capture of analytes. Commercial efforts to develop integrated nucleic acid testing platforms utilizing magnetic particle-based bioassays have already been demonstrated by Hologic's Tigris DTS system [24] and BD ViperXTR system [49]. Integration of sample preparation and enzymatic amplification chemistries such as PCR has been demonstrated by a number of magnetofluidic droplet platforms [31-34, 40], suggesting that droplet platforms may present a possible future direction toward further miniaturization. In addition to the two main actuation mechanisms, several other modes have been explored for droplet and particle manipulation and are relevant for discussion. Of particular note is surface acoustic waves, which are mechanical waves propagated along the surface of elastic substrate. When a viscous object such as a liquid droplet is placed on the substrate as shown in Fig. 3, surface acoustic waves are strongly absorbed by the liquid and induce an internal streaming inside the droplet. This phenomenon can be utilized at low-wave amplitudes for droplet agitation, while larger amplitudes can deform the droplet to varying extent and facilitate droplet transport and fission as demonstrated by Yeo et al. [43]. Other novel approaches include optical and pneumatic droplet actuation. Park et al. utilized optical tweezers to generate dielectrophoresis-induced droplet transport for cell transport [46]. Meanwhile, Huang et al. recently demonstrated a superhydrophobic polydimethylsiloxane membrane that was pneumatically actuated to facilitate efficient droplet agitation and transport [47].

2.2.3 Static droplet arrays

Many of the aforementioned droplet-based devices – particularly microfluidic droplets –are limited in their ability to manipulate and monitor droplets after formation. Measuring reaction kinetics within individual microemulsion droplets is difficult because droplets are continuously transported throughout the device: real-time measurements

would require sophisticated tracking techniques for millions of individual droplets. Surface-droplet platforms to some extent overcome these challenges, but their throughput is limited. To overcome these difficulties, miniaturized droplets can also be indexed into static arrays (Fig. 2). Spatial indexing is convenient when large numbers of discrete reactions must be executed and monitored. Such array-based technologies have wide-ranging applications in diagnostics, drug discovery and cell biology. Arrayed reactors allow for parallel processing and real-time monitoring of biological assays. Several techniques have been developed to enable facile generation of static droplet arrays. The ability to create high-density arrays of small volume chambers in microfluidic devices provides a useful platform for digital analysis of biomarkers. Emulsion-based methods can achieve high numbers of reactions, but many have complicated workflows and often require offline incubation. In contrast, array-based devices offer advantages of simplified workflow and analysis speed. Fluidigm has commercialized a number of valve-based digital PCR devices with single nucleotide resolution. In addition, Life Technologies has developed platforms for digital PCR after acquiring collaborator BioTrove. In addition, there have been a number of technologies developed in academic settings. Recently, Men et al. demonstrated digital PCR in an array of femtoliter chambers allowing for a reaction density of 20000 mm² [50]. Heyries et al. developed a valvfree microfluidic digital PCR device that performs a million single-molecule PCRs in uniform arrays of picoliter-volume chambers with densities up to 440,000 reactions cm⁻² [51]. The different platforms for microfluidic arrays and their applications will be reviewed in more detail in the following sections.

2.3 *Applications of droplet platforms*

2.3.1 **Traditional technologies for digital analysis**

In 1992, Sykes et al. introduced digital PCR as a method to quantify initial template numbers from unknown samples [52]. An additional benefit of this technique was the ability to detect rare targets in a milieu of competing sequences. In 1999, Vogelstein and Kinzler invented the term ‘digital PCR’ [53]. This work paved the way toward digital analysis of nucleic acids as well as single cells. An excellent review on digital PCR

strategies and their role in personalized medicine was recently published [54]. To make dPCR feasible as a clinical tool required miniaturization. True digital PCR requires performing hundreds of thousands of reactions per sample. Liquid handling robotic systems have reached their limits as the smallest reaction volumes now approach approximately 1 ml. As a step toward realizing dPCR as a clinical tool, Vogelstein and Kinzler developed a technology called Beads, Emulsion, Amplification, Magnetics (BEAMing) [55, 56]. Beaming refers to the process of emulsification in bulk. In one study, circulating mutant cDNA was quantified using BEAMing, representing a personalized approach for assessing disease in subjects with cancer [57]. However, bulk-created emulsions are limited due to the lack of control over droplet sizes. The size polydispersity in BEAMing limits the reliability of encapsulating a single DNA molecule per droplet and the ability to perform quantitative measurements. In contrast, generating droplets in microfluidic systems has the advantage of creating monodisperse sample volumes that improves reaction conditions (Fig. 1). Commercially available platforms for emulsion digital PCR are marketed by Bio-Rad Laboratories and RainDance Technologies. Monodisperse droplets are generated and then collected in an Eppendorf tube to order to perform PCR thermocycling step off-chip. Detection of the PCR products requires reinjection of droplets into a microfluidic channel to analyze the fluorescent signal. Commercial emulsion-based PCR systems are becoming more prevalent in the research community for digital analysis of biomarkers, and microfluidic droplet technology is expected to play a pivotal role as an enabling technology.

2.4 *Microfluidic droplet platforms applications*

2.4.1 **Integrated platforms for genetic mutation detection**

Droplet microfluidics affords the opportunity to perform sensitive and quantitative methods for detecting genetic markers. RainDance technologies has developed a droplet-based method, based on digital PCR, which allows the highly sensitive and quantitative detection of mutations within a large excess of wild-type sequences [58]. In a recent study, single-target DNA molecules were encapsulated in microdroplets with fluorogenic TaqMan probes specific for mutated and wild-type KRAS. After droplet generation,

droplets were collected in an Eppendorf tube and incubated. Then the fluorescence of each individual droplet was measured. Because amplified mutant DNA and wild-type DNA gave fluorescent signals in different channels, the ratio of wild-type to mutant DNA was able to be calculated. This strategy enabled the precise determination of mutant allelic specific imbalance in several cancer cell lines and the precise quantification of a single mutated KRAS gene in a background of 200,000 unmutated KRAS genes. Furthermore, a 6-plex assay for six common mutations in KRAS codon 12 was demonstrated with just two fluorophores in a single experiment. This multiplexing was achieved by varying the concentration of the different fluorogenic probes, leading to an identification of the targeted gene alteration on the basis of fluorescent color and intensity [59]. This platform was recently used to perform multiplex emulsion-based PCR applied to detecting mutations in circulating DNA (ctDNA) prepared from clinical plasma samples [60]. In conventional techniques, the moderate sensitivity of mutation detection has limited the detection of ctDNA. In contrast, with this droplet-based platform, the sensitivity was high enough to detect mutations in ctDNA obtained by noninvasive blood collection. Another recent study demonstrated high-throughput droplet digital PCR for absolute quantification of DNA copy number [61]. This high-throughput system enabled processing of 20,000 PCR reactions per sample using conventional TaqMan assays with a 96-well plate workflow. Massive partitioning by the droplet digital PCR system resulted in higher precision and sensitivity than conventional real-time PCR. Accurate measurement of germline copy number variation was demonstrated. In addition, for rare alleles, sensitive detection of mutant DNA in a 100,000-fold excess of wild-type background was demonstrated. Finally, absolute quantitation of circulating fetal and maternal DNA from cell-free plasma was performed. The analysis was performed by endpoint fluorescence analysis of the content of the droplets. This platform is now being commercialized by Bio-Rad and has been demonstrated in other studies [61]. Both of these platforms have demonstrated the capability of high-resolution detection of biological molecules. However, they are limited to the analysis of a homogeneous sample and are incapable of high-throughput analysis of multiple samples against a large library of probes. Examples of applications that require high degrees of multiplexing include single-nucleotide polymorphism analysis and genotyping required for identification of

genes associated with common diseases. To address this need, we recently developed a droplet platform (Fig. 4) capable of on-demand generation of microfluidic droplets of combinatorial mixtures of samples and reagents [62]. This platform employs a linear array of sample plugs as an input to the device. A preformed linear array of sample plugs separated by a carrier fluid is injected from the cartridge into the microfluidic device, where each plug is chopped by a pneumatic valve into daughter droplets. The daughter droplets are then directly injected with reagents. The microfluidic design features a robust fusion module, which exploits local channel geometry, for synchronization-free injection of reagents into each sample daughter droplet. After reagent injection into a sample droplet, our microfluidic device introduces additional carrier fluid containing surfactant to the channel containing the sample-reagent hybrid droplet array to prevent unwanted merging of these droplets on the device. We believe this approach has the potential to broaden the applications of microfluidic droplets by allowing the generation of combinatorial mixtures of droplets, which many screening reactions require.

2.4.2 Integrated platforms for targeted enrichment for sequence-based studies

Attempts have been made to expand the capacity of droplet platforms for multiplexed analysis. One well-known platform has been developed by RainDance Technologies for massively parallel PCR enrichment for DNA sequencing. Microdropletbased PCR enrichment for large-scale targeted sequencing is valuable in enabling sequencing-based studies of genetic variation in large populations. Recently, this enrichment approach based on microdroplet PCR, which enables 1.5 million amplifications in parallel, was described [63]. This platform involves generation of a large library of PCR reagent droplets by a microchip. These droplets are then collected off-chip and merged with sample droplets generated from a DNA sample on a second droplet generation device. These sample–reagent hybrid droplets are then collected in standard PCR tubes for thermocycling, followed by fluorescence detection and sequencing. Fig. 5 shows a schematic of this microdroplet PCR workflow. Since then, this same method has been used for detecting somatic tumor mutations in heterogeneous samples [64]. More recently, this PCR enrichment method in microdroplets was used to identify 43 forms of monogenic diabetes or obesity [65]. Although promising, this platform cannot be used for

applications that require real-time detection. Namely, in this scheme the content of each individual droplet is unknown and is decoded offline by nucleic acid sequencing. One solution to this problem is to associate an optical code (based on fluorescence intensity) with each reagent prior to mixing with the sample. This approach is limited to a small number of codes due to the small allowable number of fluorophores without spectral crosstalk and the dynamic range of the optical detection setup being used. One way to circumvent the need for barcoding would be to perform spatial indexing of droplets [62].

2.4.3 **Integrated platforms for targeted enrichment for single-cell studies**

Droplets can be used for confinement and manipulation of single cells into microfluidic droplets, making them ideal for conducting high-throughput single-cell studies. The potential of droplet microfluidics to be a powerful tool for single-cell studies has been shown with demonstrations of single-cell screening assays. Because of the small operating volumes of droplets (picoliter-to-nanoliter range), concentrations of cellular genetic or proteomic materials are higher and can increase measurement sensitivity. Huebner et al. described the preparation of droplets containing individual cells and subsequent detection of fluorescent proteins in the cells with simultaneous measurement of droplet size, fluorescence and cell occupancy [66]. Joensson et al. demonstrated detection of the cell-surface biomarkers CCR5 and CD19 on single human monocytic cells using enzymatic amplification in droplets [67]. Boedicker et al. demonstrated the rapid detection and drug susceptibility of single bacterial cells in droplets using a fluorescent cell viability indicator assay [68]. Brouzes et al. performed high-throughput screening of a drug library for its cytotoxic effect against human monocytic U937 cells [69]. However, this method required an optical barcoding scheme that limits the applications of this method – only eight library members (different concentrations of the drug) were screened. Zeng et al. demonstrated the detection of pathogenic *Escherichia coli* cells in a background of normal *E. coli* K12 cells using a microfluidic droplet generator array [70]. However, this platform requires PCR reactions to be performed off-chip. Rane et al. recently demonstrated amplification-free genetic detection of single pathogenic cells [71]. This device (Fig. 6) offers a simple and fully integrated approach to include all assay steps, including cell isolation, lysis, probe-target binding and

fluorescence detection. Each of these steps is performed within microfluidic droplets. Single-cell sensitivity was achieved through the platform by a two-pronged approach. Stochastic confinement of single cells within picoliter droplets was used to maintain a low-abundance intracellular target of interest from single cells at high concentrations. In addition, the microfluidic platform was coupled with highly sensitive confocal fluorescence spectroscopy for sensitive detection of target biomolecules from individual droplets. The capability of the device to perform ‘sample to answer’ pathogen detection of single cells was demonstrated using *E. coli* as a model pathogen. This indicated the promise in utilization of the platform with clinical samples with appropriate testing and optimization of assay conditions. Although the functioning of the device was demonstrated for pathogen detection, the platform is versatile enough to be applied toward other single-cell studies.

2.5 Surface droplet platform applications

Testing of nucleic acid biomarkers is another major arena where microfluidic droplet technology is being studied. While immunoassays may be useful in assessing the presence of abundant macromolecular targets, the high level of sensitivity and specificity provided by enzymatic amplification of nucleic acid targets provides a strong motivation for developing these technologies. The wide range of fluidic operations enabled by open-surface droplet platforms, together with their capacity for miniaturization, places these technologies in a unique vantage point in delivering enzymatic nucleic acid amplification tests in point-of-care settings. A ubiquitous feature of droplet-based nucleic acid platforms is surface-modified magnetic particles, which are essential for extraction and retention of nucleic acids through various washing and incubation steps. Initially demonstrated by Vogenstein and Gilliespie [72] using glass beads, solid-phase extraction involving the adsorption of duplex DNA to silica is a convenient technique for purifying DNA from biological samples and transporting them through various reagents. In this section, examples of surface droplet platforms that explore the various aspects of nucleic acid testing, including sample preparation and enzymatic amplification, will be discussed. To date, various droplet platforms have made significant progress in combining sample preparation and detection into a single workflow, as described in the following examples.

2.5.1 Integrated platforms for pathogen detection

Nucleic acid detection via amplification is an effective technique in identifying pathogens and provides some key advantages over culture-based techniques including shorter turnaround time, assay sensitivity and the ability to assess fastidious samples [73]. Magnetofluidic droplet platforms demonstrated by Pipper et al. [34] and Zhang et al. [31] combined solid-phase DNA extraction and PCR amplification to create sample-to-answer analytical platforms (Fig. 7). Isolation of pathogenic nucleic acid targets and subsequent detection via real-time PCR demonstrates the potential of such platforms in mobile biosurveillance, including pathogen identification and viral load quantification. In addition, these platforms could be extended to perform multiplexed reactions in a single mixture with molecular beacon probes in order to detect a panel of pathogens simultaneously [74]. An alternative method of detecting multiple gene targets is by performing amplification reactions from the same DNA isolate in separate reaction wells. To this end, Zhang and Wang developed a SET-based integrated platform capable of extracting and aliquoting genomic DNA before performing multiple PCR reactions simultaneously using unique primer sets [41]. Integrated platforms for genetic mutation detection

Alongside pathogen identification, genetic mutation detection is also an important aspect of genetic diagnostics. Droplet based platforms designed to retrieve sequence-specific information have been proposed in several instances. Miniaturized pyrosequencing platforms have been pioneered on EWOD devices by Boles et al. [26], suggesting a potential direction for a small-scale DNA sequencer if sample preparation could be integrated. While sequencing techniques provide the most comprehensive information regarding an unknown nucleic acid target, the high level of fidelity and time required to process sequencing samples preclude their use in point-of-care settings. A recent work by Huang et al. [47] utilized gold nanoparticles functionalized with oligonucleotide probes on a pneumatically actuated droplet device, inducing visible color changes based on hybridization mismatches. While the simplicity of readout and the ability to detect sequence mismatches is encouraging, this approach has only been demonstrated for abundant copies of single-stranded synthetic targets and may be

difficult to apply in biological samples where amplified DNA targets are double-stranded and sequence variation is more often heterogeneous. In light of this, melting curve analysis has recently emerged as a potential alternative to sequencing in rapid diagnostic applications [75]. This technique monitors the dissociation of double-stranded DNA during heating by measuring the fluorescence emitted by DNA intercalating dyes [76]. By monitoring the fraction of remaining double-stranded DNA as the temperature is gradually increased, thermodynamic properties associated with the sequence are resolved as a function of temperature. Since the dissociation characteristics of a DNA strand are a function of base composition and length, samples containing mutations generate melting profiles that are different from their wildtype counterparts. Melting curve analysis is directly compatible with conventional real-time PCR workflow since it requires only a single universal primer pair for product amplification, in contrast to other PCR-based genotyping assays such as allele specific PCR [77] and allele-specific oligonucleotide probes [78] that require additional probes for mutation identification. In a recent study, Shin et al. demonstrated identification of a single-nucleotide polymorphism in the KRAS oncogene using a melting curve-based approach [32]. In this work, open-surface magnetic droplet manipulation was used to combine DNA extraction and amplification via PCR into a single streamlined process (FIGURE 8).

2.6 *Static droplet array applications*

Droplets immobilized in high-density indexed arrays enable high throughput time-lapse imaging of biological reactions. For example, in the case of PCR, arrays afford the ability to monitor the ‘response curve’ – or how levels of DNA change over the course of amplification. In turn, this capability can help eliminate false readings caused by nonspecific labeling of DNA sequencing [79]. In the following section, we will review some commercial technologies as well as technologies developed in academic research labs for performing array-based reactions.

2.6.1 **Integrated platforms for genetic mutation detection**

Two companies that have developed various commercialized microfluidic PCR platforms are Fluidigm and Life Technologies. Fluidigm has an array of digital PCR products, including one for real-time digital PCR, Fluidigm qdPCR 37K™ IFC. Life Technologies offers OpenArray, with custom formats to allow tailored analysis according to the level of sensitivity or precision required. Both platforms have isolated microfluidic reaction chambers that allow real-time monitoring of amplification. Results are generated by calculating the number of positive reaction chambers and equating it to the number of target copies present. A different approach to partitioning chambers for digital PCR is achieved with the ‘SlipChip’ (Fig. 9). The SlipChip is a microfluidic platform that manipulates liquid samples from picoliter-to-microliter scales by relative movement of patterned glass plates [80]. The SlipChip has been previously used for PCR [81, 82] and digital isothermal amplification [83]. In one recent paper, HIV and hepatitis C loads were detected on a platform for use in point-of-care and resource limited settings using the SlipChip [84]. In addition to the SlipChip, several other platforms have been proposed. Recently, Heyries et al. [51] developed a megapixel digital PCR device that partitions samples based on surface tension. High-fidelity single DNA molecule amplification was achieved in 1,000,000 parallel reactors. Furthermore, this device boasted a dynamic range of 10^7 and single-nucleotide-variant detection below one copy per 100,000 wildtype (FIGURE 9). In another recent study, an integrated on-chip valve-free and power-free microfluidic digital PCR device was developed by making use of a novel method for self-priming compartmentalization and simple dehydration control for single DNA molecule detection [85]. The device contains 5120 independent 5 nl microchambers, allowing the samples to be compartmentalized completely. Using this platform, three different abundances of lung cancer-related genes were detected to demonstrate the ability of the microchip to amplify single copies of target DNA. In a different approach, a spinning disk platform for microfluidic digital PCR was developed [86]. This design loads the sample into nanoliter-sized compartments by centrifugation, eliminating the need for valves and pumps and reducing microfluidic loading time. The disk passively divides a spun sample into thousands of compartments, reducing chip disposable costs. PCR is performed on the rotating disk by rapid thermocycling in an air chamber, reducing

thermocycling time. After PCR, each compartment is interrogated for a positive/negative signal by fluorescence imaging. PCR was demonstrated in less than 35 min.

2.6.2 Integrated platforms for protein detection

Array-based devices have also been used for protein detection. In one recent study, a microfluidic protein chip was developed for an ultrasensitive and multiplexed assay of cancer biomarkers [87]. Aqueous-phase synthesized quantum dots were employed as fluorescent signal amplifiers to improve the detection sensitivity. The device possessed ultrahigh femtomolar sensitivity for cancer biomarkers and could be used directly in serum.

2.7 Expert commentary & five-year view

The development of miniaturized droplet-based systems for biomarker analysis is rapidly expanding. Several droplet-based and array technologies have been commercialized and served as important tools in impactful biomarker studies. Such highly sensitive and quantitative droplet-based platforms afford researchers the opportunity to explore complex landscapes of genetic interactions. In the future, disease associations may be discovered and elucidated as a result of these new droplet-based technologies. The three different branches of droplet-based analysis – microfluidic droplets, surface-based droplet platforms and array-based technologies – are indicated for use in different applications. Microfluidic droplet-based devices boast extremely high-throughput – millions of discretized droplets originating from a single sample can be analyzed on a microfluidic droplet device – allowing the identification of rare alleles and alleviating the need to run multiple titrations for quantitation. Furthermore, by integrating valves, these platforms can perform true combinatorial screening that is necessary for many applications like genotyping. In addition, researchers have demonstrated the ability to characterize single cells. In contrast to microemulsions, surface-based droplet platforms generally deal with larger volumes and provide an opportunity to develop highly automated, miniaturized diagnostic systems. These platforms may function as

portable bench-top environments that dramatically shorten the transition of a bench-top assay into a point-of-care format. Finally, array-based devices afford relatively high-throughput but the number of reactions is limited by the number of compartments on a single device. One distinct advantage is that array-based devices allow real-time monitoring of biological reactions. In the future, droplet-based devices may become essential in the area of biomarker detection and personalized medicine.

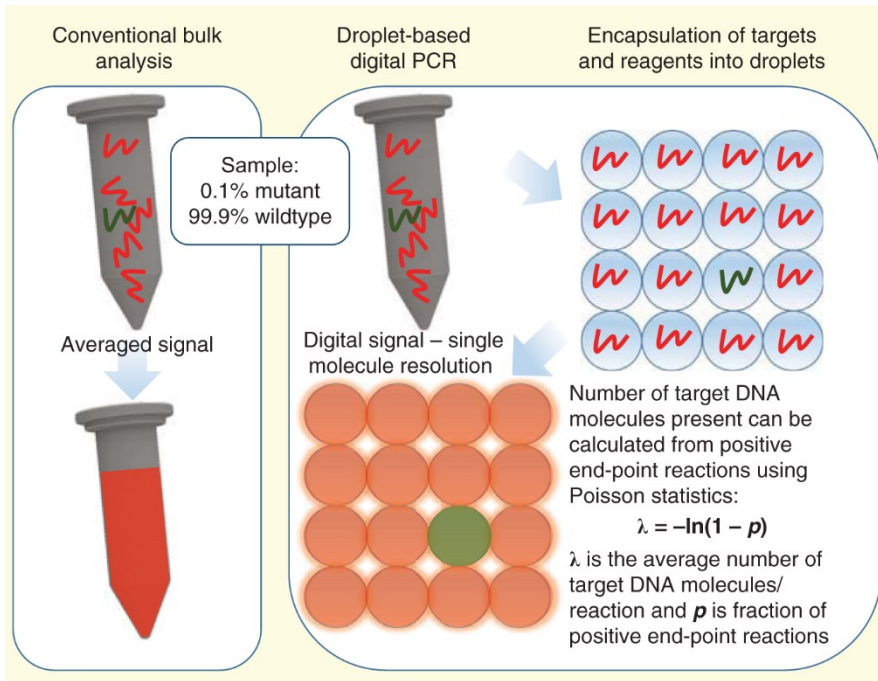


Figure 2.1. Schematic of digital PCR.

Conventional bulk analysis (left panel): if a rare target is present among an excess of competing 'normal' targets, an averaged signal will be acquired. In contrast, droplet-based PCR (right panel) is more quantitative and allows encapsulation of targets and reagents into droplets. The number of target DNA molecules can be calculated using Poisson statistics. This concept of limiting dilution in a miniaturized droplet format leads to single-molecule resolution.

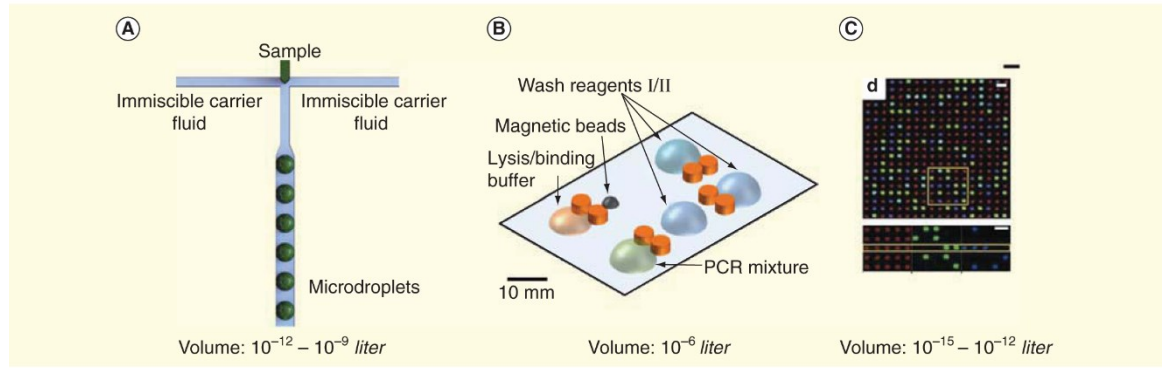


Figure 2.2. A conceptual diagram of droplet microfluidics, surface droplet platforms and static droplet arrays.

Droplet microfluidics: emulsions of water-in-oil droplets are formed. Droplets can be generated by shearing water-in-oil to form droplets in a method called flow focusing (A). Surface droplet platforms: in this approach, aqueous reservoirs in the nanoliter-to-microliter range are manipulated individually on an open planar substrate rather than inside the microchannels (B). Static droplet arrays: droplets may also be spatially indexed in 2D arrays (C). These highly miniaturized, parallel reactors can be monitored in real time. Reproduced by permission from [51] Macmillan Publishers Ltd (2011).

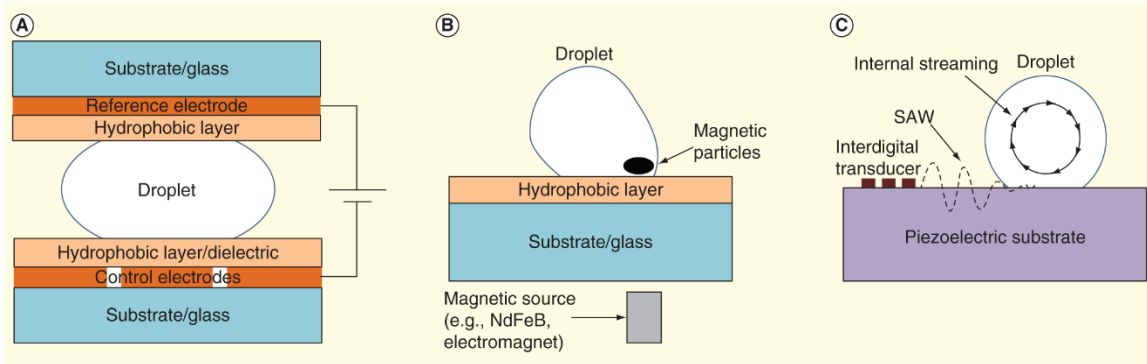


Figure 2.3. Schematics illustrating various modes of droplet actuation on surface.

(A) Electrowetting-on-dielectric in a two-layer configuration, with a reference electrode on top and an array of control electrodes on the bottom. (B) Magnetofluidic actuation performed using a permanent magnet, which exerts force on magnetic particles contained inside a droplet and induces droplet transport or particle extraction. (C) Surface acoustic wave actuation (SAW) utilizes interdigital transducer patterned on a piezoelectric substrate, which generates acoustic waves along the substrate surface. When a droplet is placed on the surface, energy transported through SAW is absorbed by the droplet and generates internal streaming that facilitates mixing, transport or fission depending on the wave amplitude.

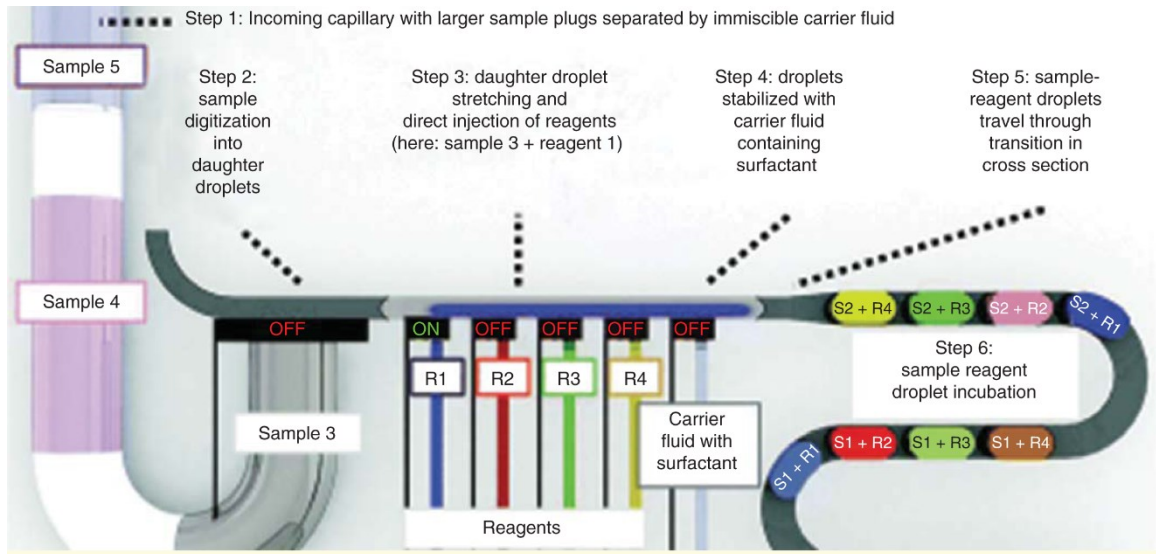


Figure 2.4. Droplet platform for on-demand generation of combinatorial mixtures of samples and reagents.

In this platform, the use of valves to create droplets facilitates control over the precise composition of the droplet. Using this technique, the ability to generate highly combinatorial mixtures was demonstrated. Step 1: a capillary attached to the microfluidic device injects sample plugs separated by immiscible carrier fluid. Step 2: a pneumatic valve chops these plugs (~200 nl) into smaller daughter droplets (~20 nl). Step 3: daughter droplets are stretched in the fusion zone and reagents are injected directly into the droplets. Step 4: the hybrid sample–reagent droplets are stabilized with carrier fluid containing surfactant. Step 5: sample–reagent droplets travel through a transition in cross section. Step 6: finally, sample–reagent droplets are incubated in the incubations zone. Reproduced with permission from [62], The Royal Society of Chemistry (2012).

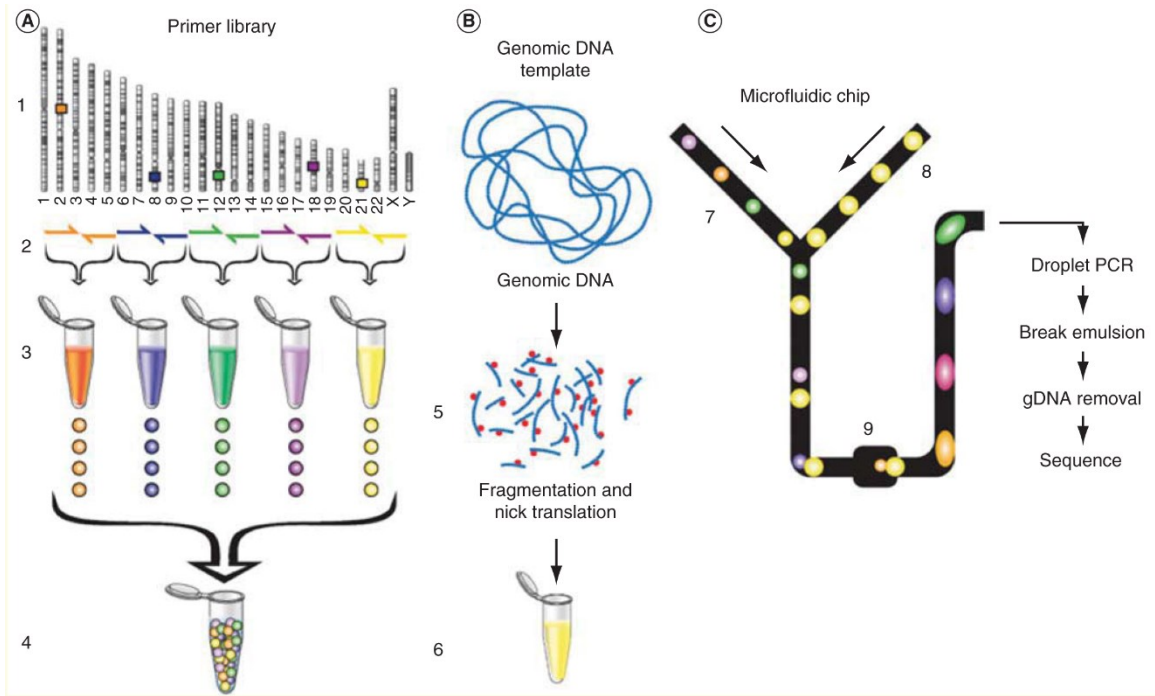


Figure 2.5. Microdroplet PCR workflow.

(A) Here, a primer library is generated by emulsifying different primers and collecting them in a single tube. (B) Genomic DNA is processed and collected. (C) Primer droplets and DNA droplets are reinjected on to a chip for fusion. (A) Here, a primer library is generated by emulsifying different primers and collecting them in a single tube. (B) Genomic DNA is processed and collected. (C) Primer droplets and DNA droplets are reinjected on to a chip for fusion. Droplets are then collected into an Eppendorf tube and then incubated offline. The emulsion is then broken and amplified targets are sequenced. Reproduced with permission from [63] Macmillan Publishers Ltd (2009).

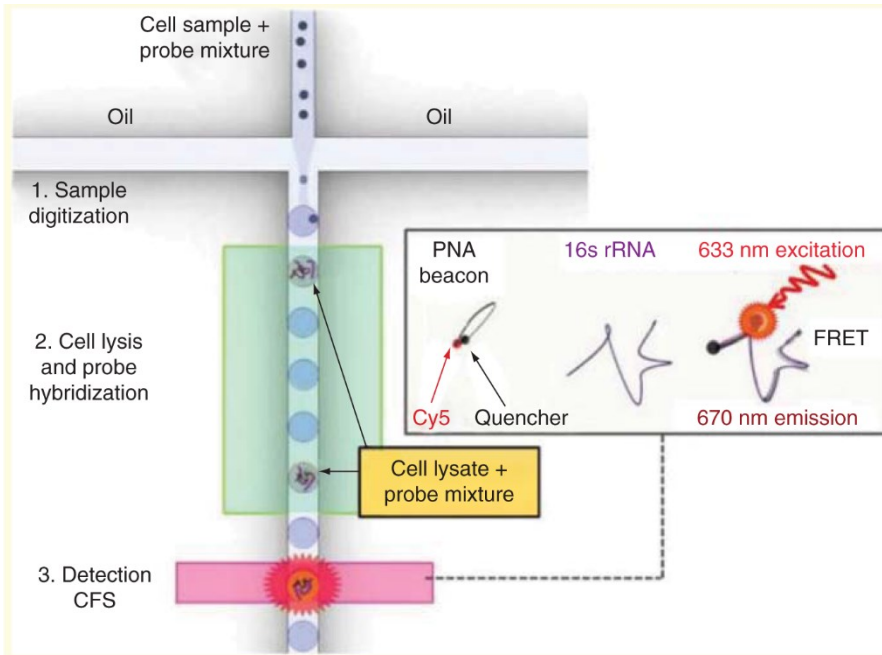


Figure 2.6. Amplification-free genetic detection of single pathogenic cells on a droplet-based microfluidic device. Droplets are generated by shearing water-in-oil to form droplets in a method called flow focusing. In this example, pathogenic cells are encapsulated within droplets, lysed and then detected inline [71]. A peptide nucleic acid fluorescence resonance energy transfer probe (PNA beacon) is used to detect 16S rRNA present in pathogenic cells. The microfluidic platform was coupled with highly sensitive confocal fluorescence spectroscopy for sensitive detection of target biomolecules from individual droplets. Reproduced with permission from [71] The Royal Society of Chemistry (2012).

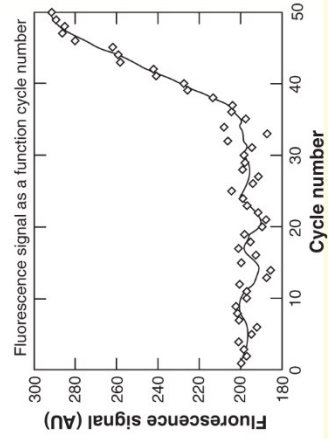
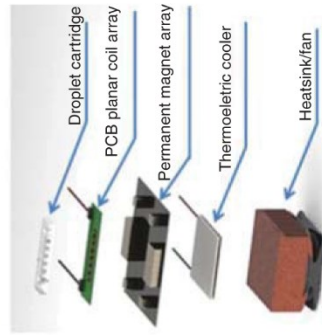
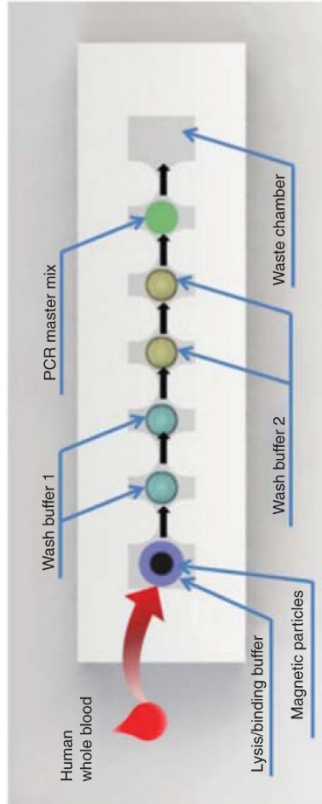
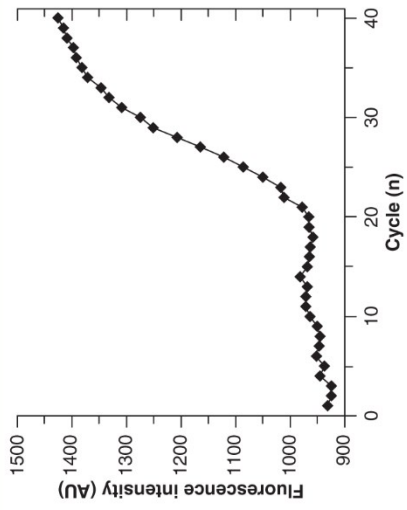
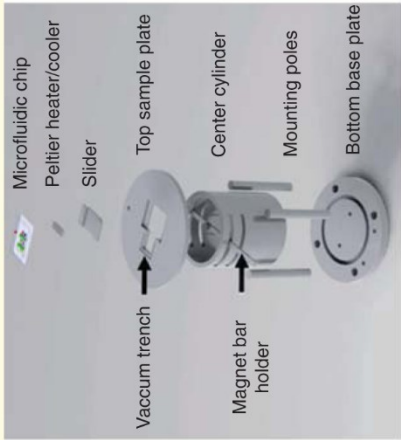
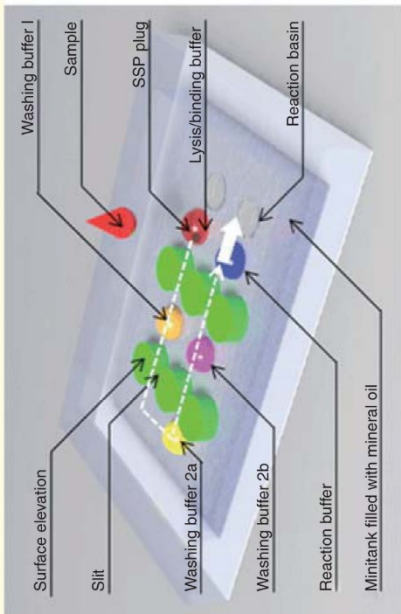


Figure 2.7. Real-time PCR droplet platforms for integrated sample processing and detection.

Zhang et al. (top panel) demonstrate amplification of the 16S ribosomal RNA gene from *Escherichia coli* using a TaqMan real-time PCR assay [31]. Chiou et al. (bottom panel) demonstrate real-time amplification of the KRAS oncogene target from genomic DNA that was extracted on chip directly from human whole blood [40]. Reproduced with permission from [31] The Royal Society of Chemistry (2011). Reproduced with permission from [40] Elsevier (2013).

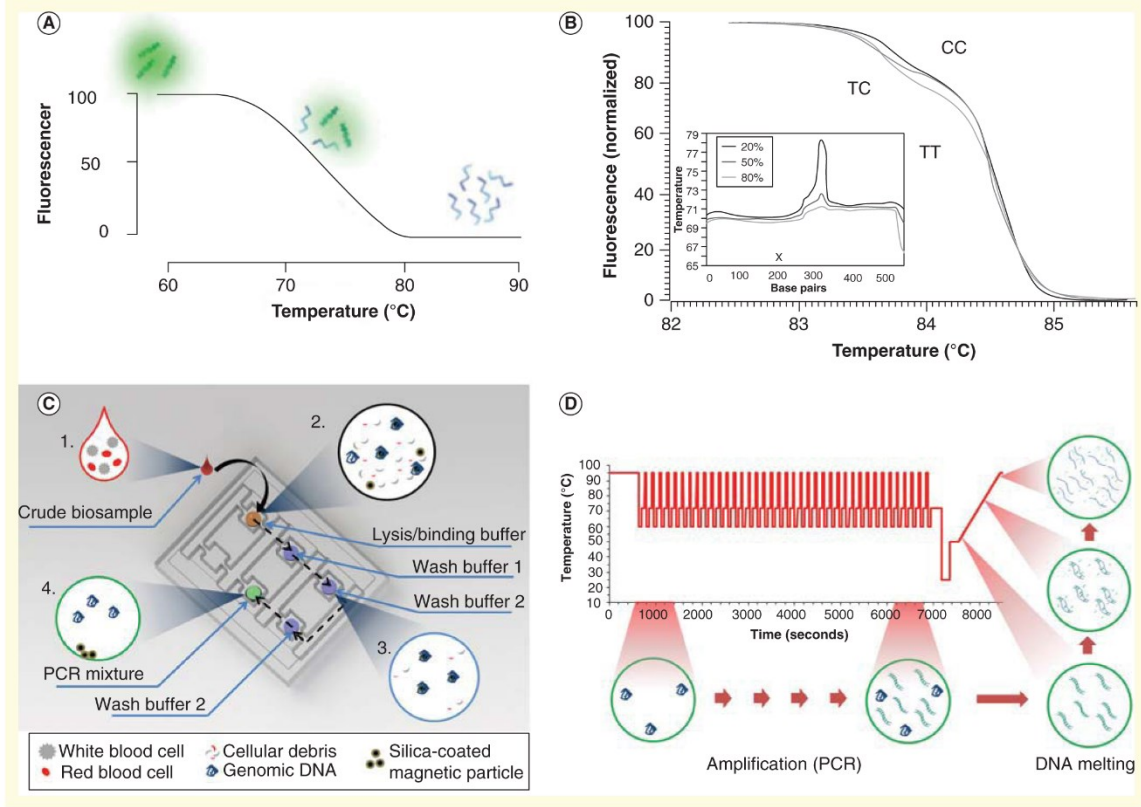


Figure 2.8. Melting curve analysis for genetic mutation detection using an integrated droplet platform.

(A) Shows the principles of melting curve analysis. As the temperature is increased, duplex DNA is dissociated along with double-stranded DNA binding dyes, resulting in a decrease in fluorescence. (B) Shows an example of melting curve analysis for identification of a single-nucleotide polymorphism within a 544-bp fragment of the HTR2A gene. Bottom panel (C) Shows the layout of magnetically actuated droplet cartridge for performing genomic DNA isolation, PCR and melting curve analysis from biological sample. (D) Shows temperature profile achieved at the incubation chamber, including the initial PCR amplification and thermal ramp for melting curve acquisition. Adapted from [76] and [32]. Reproduced with permission from [76]. American Association for Clinical Chemistry (2003). Reproduced with kind permission from [32] Springer Science and Business Media (2014).

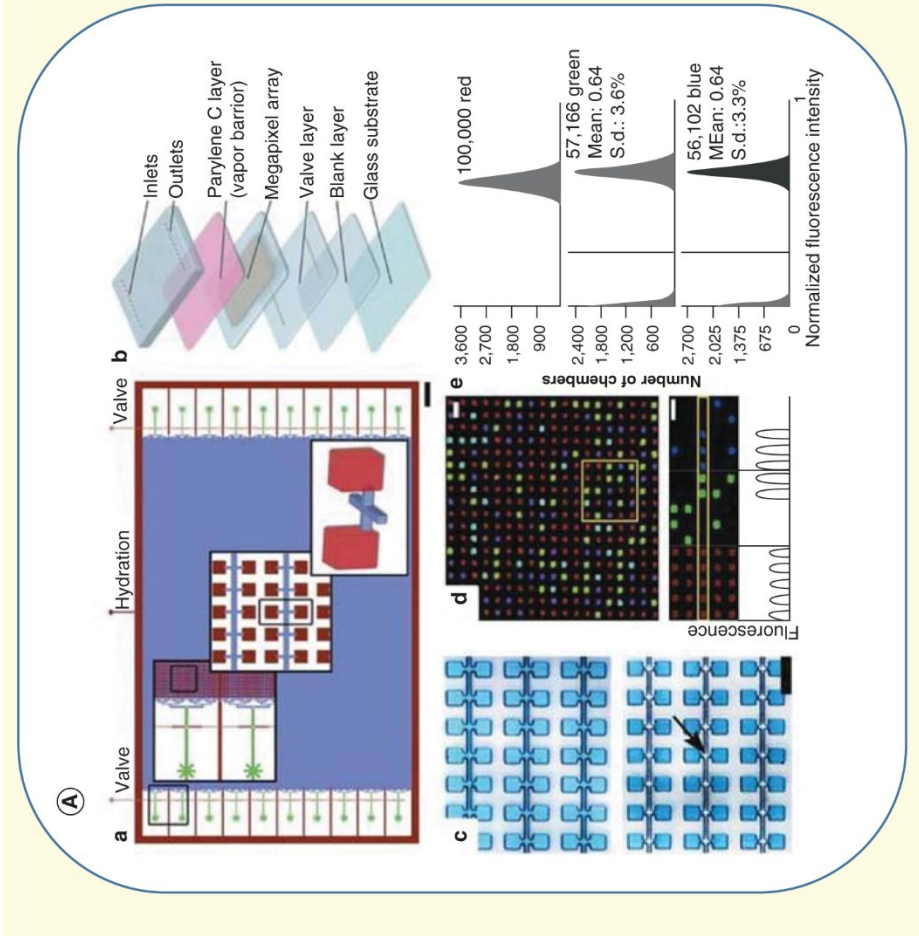
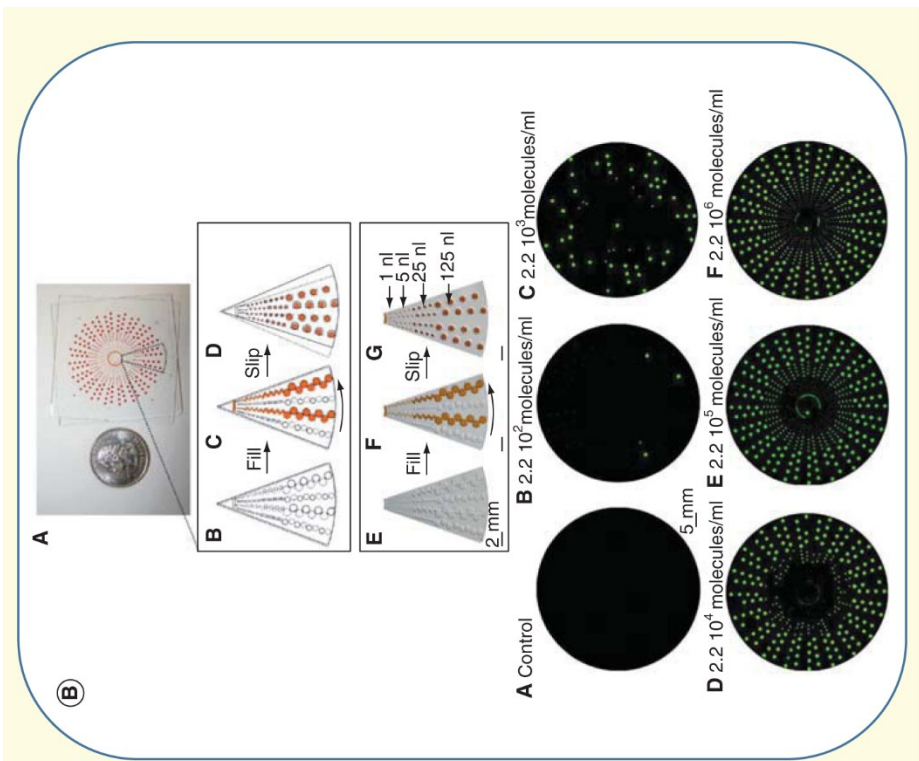


Figure 2.9. Megapixel digital PCR and SlipChip.

Megapixel digital PCR (left panel). (A) Schematic of megapixel digital PCR device. This device performs digital PCR of a single sample in 1 million small reactors. The total number of positive counts and negative counts can be precisely quantified. SlipChip (right panel). Rotational multivolume SlipChip well volumes: 1, 5, 25 and 125 nL). Bottom panel: fluorescent photograph of a multiplexed digital RT-PCR detection panel: i) measurement of internal control of 906 nt RNA template in HCV sample; ii) HCV control viral RNA measurement; iii) negative control for HIV (HIV primers with no loaded HIV RNA template); iv) HIV viral RNA measurement; v) negative control for HCV (HCV primers with no loaded HCV RNA template). Inset shows an amplified area from HCV viral load test. A) Adapted from [51] and [84]. Reproduced with permission from [51] Macmillan Publishers Ltd (2011). B) Reproduced with permission from [84] American Chemical Society (2011).

3

Microfluidic platform for on-demand generation of spatially indexed combinatorial droplets

Zec, Helena, Tushar D. Rane, and Tza-Huei Wang. "Microfluidic platform for on-demand generation of spatially indexed combinatorial droplets." Lab on a Chip 12.17 (2012): 3055-3062. Reproduced with permission from The Royal Society of Chemistry.

We propose a highly versatile and programmable nanolitre droplet-based platform that accepts an unlimited number of sample plugs from a multi-well plate, performs digitization of these sample plugs into smaller daughter droplets and subsequent synchronization-free, robust injection of multiple reagents into the sample daughter droplets on-demand. This platform combines excellent control of valve-based microfluidics with the high-throughput capability of droplet microfluidics. We demonstrate the functioning of a proof-of-concept device which generates combinatorial mixture droplets from a linear array of sample plugs and four different reagents, using food dyes to mimic samples and reagents. Generation of a one dimensional array of the combinatorial mixture droplets on the device leads to automatic spatial indexing of these droplets, precluding the need to include a barcode in each droplet to identify its contents. We expect this platform to further expand the range of applications of droplet microfluidics to include applications requiring a high degree of multiplexing as well as high throughput analysis of multiple samples.

3.1 Introduction

Droplet microfluidic platforms are in the early stages of revolutionizing high throughput and combinatorial sample screening for bioanalytical applications [88-91]. Droplet-based systems have many advantages over conventional microtiter techniques for

combinatorial screening applications. Microfluidic droplets function as miniaturized reaction containers consist of pico or nanolitre volumes, thereby facilitating reduced reagent consumption and background noise [91]. Furthermore, carrier fluid shields each droplet, mitigating the problems of absorption onto solid surfaces and contamination. The high surface area to volume ratio of droplets also facilitates shorter heat and mass transfer times, leading faster reaction kinetics in droplets [89, 92].

Recent publications in the microfluidic domain boast high throughput capability of their respective droplet-based platforms. Compartmentalization of many small droplets allows isolation of interfering molecules into separate volumes, thereby facilitating digital analysis of biological entities. Several examples have been demonstrated including: droplet platforms for high throughput single copy DNA amplification [93-95], droplet platforms for high throughput single cell screening [66, 96, 97] as well as droplet platforms for single organism screening [98, 99]. These droplet platforms are capable of high resolution screening of the biological contents at the level of the fundamental unit. However, they are limited to the analysis of a single sample under a homogeneous reagent condition.

The aforementioned droplet platforms are incapable of addressing the needs of numerous applications which require high degrees of multiplexing as well as high-throughput analysis of multiple samples. Some examples include genetic fingerprinting for forensics [100], single nucleotide polymorphism (SNP) analysis for crop improvement and domestication [101], genotyping required for identification of genes associated with common diseases [102] and generation of a blood donor genotype database for better matching between recipient and donor to prevent adverse transfusion reactions [103]. All these applications require multiplexed screening of a single sample with a panel of reagents (or markers) and rapid screening of a large number of samples to generate the required databases.

In recent years, there have been attempts to expand the capacity of droplet platforms for the analysis of a biological or chemical sample with multiple reagents. One of the well-tested platforms has been the droplet platform developed by RainDance Technologies, for massively parallel PCR enrichment for DNA sequencing [63]. This platform involves a multistep approach with generation of a large library of PCR reagent

droplets by a microchip, followed by merging of these reagent droplets with sample droplets generated from a DNA sample on a second device. These sample-reagent hybrid droplets are then collected in standard PCR tubes for thermocycling, followed by fluorescence detection and sequencing. In this platform, the content of each individual droplet is unknown and is decoded only by offline nucleic acid sequencing. Therefore, it cannot be applied to other applications that require real-time detection [91]. A solution to this problem is to associate a unique optical-code with each reagent prior to mixing with the sample. However, an optical-coding scheme based on fluorescence intensity is practically limited to a small number of 'codes' due to the small allowable number of fluorophores without spectral crosstalk and the limited dynamic range of the optical detection setup being used [91]. Furthermore, the electrocoalescence technique used in such platforms for droplet merging is susceptible to errors of no fusion caused by an excess of droplets of a reagent or unintended fusion of more than two droplets due to highly stringent synchronization requirements [104]. A recent article demonstrated a picoinjector which can overcome this problem and be used to add controlled volumes of multiple reagents to sample droplets using electromicrofluidics [105]. However, similar to droplet platforms discussed earlier, the content of each individual droplet is unknown unless a barcode is included in each individual droplet.

Alternatively, a series of articles adopted a cartridge technique for increasing the throughput of the droplet platform [106]. This technique involves generation of an array of reagent plugs in a capillary (cartridge), which are sequentially introduced to a simple microfluidic device for merging with a single substrate. The reagent plugs can be further digitized into smaller droplets prior to merging with the sample. As the length of the capillary can be very long, the number of reagents to screen against the sample is virtually limitless. This technique has been applied to many applications including protein crystallization and study of bacterial susceptibility to antibiotics [107]. Although the aforementioned droplet and cartridge platforms are capable of high throughput and multiplexed analysis, they are still limited to screening of a single sample at a time. Recently, a microfluidic platform was proposed for combinatorial chemical synthesis in picolitre droplets, where droplets of one library of reagents were fused at random with droplets containing a different set of reagents [104]. This platform has the potential of

generating a large set of possible combinations of different reagents. However, as aforementioned, the unknown identity of the compounds within individual droplets precludes its use for many screening applications that require real-time detection.

Here we present a droplet platform capable of on-demand generation of nanolitre droplets of combinational mixtures of samples and reagents, needed for biochemical screening applications that require multiplexing and high-throughput capability. On-demand droplet generation and manipulation using pneumatic valves has been demonstrated by other groups in the past [108-110]. However, these platforms have focused on generating multiple reagent combinations using fixed number of inputs to the device, severely limiting the number of possible sample-reagent combinations being generated on the device. The droplet platform reported in this article uses a linear array of sample plugs as an input to the device, removing the limitation imposed by the number of inputs to the device. Initially, a preformed linear array of sample plugs separated by a carrier fluid is flowed from the cartridge into the microfluidic device, wherein each plug is digitized by a pneumatic valve into smaller sample daughter droplets. The volume of the resulting daughter droplet can be precisely controlled by varying the valve opening time and the back pressure on the cartridge containing sample plugs. The daughter droplets are then directly injected with reagents in a synchronization-free manner. The microfluidic design features a robust fusion module which exploits local channel geometry for synchronization-free injection of reagents into each sample daughter droplet. After reagent injection into a sample droplet, our microfluidic device introduces additional carrier fluid containing surfactant to the channel containing the sample-reagent hybrid droplet array to prevent unwanted merging of these droplets on the device. In the proposed microfluidic device, droplets are indexed by their layout in a 1D array, enabling the identification of the contents of each droplet by spatial indexing. Spatial indexing as a means for identification of droplet content obviates the need for a limiting optical barcoding scheme.

3.2 *Materials and Methods*

3.2.1 Serial Sampling Loading System

The sample library was generated using a custom-designed Serial Sample Loading System (SSL). Fig 6.2 is a schematic illustrating the functioning of the SSL system. Briefly, the SSL system was designed to be compatible with Costar 96-well plates (Corning). Initially the wells on a Costar 96-well plate are filled with the samples and the carrier fluid to be used for generating the sample plug array. An Aquapel (PPG Industries) treated silica capillary is then attached to a capillary adapter on the SSL system, which is also connected to a positive pressure input. A sample well is then interfaced with the capillary through the capillary adapter. Application of positive pressure to the sealed sample well for a controlled amount of time is then used to drive a sample plug from the well into the capillary. This sequence of steps is then repeated to load alternating sample and carrier fluid plugs into the capillary (Fig. 6.2b). More detailed information on the structure and operation of different components of the SSL system can be found in the section 6.5.4.

3.2.2 Fabrication of the Master Molds for the Microfluidic Device

The fluidic layer on the microfluidic device features five different heights of microfluidic channels (Fig. 6.3b and c). As a result, the fluidic mold consists of five different layers of photoresist. The fluidic channel heights in these five different photoresist layers were expected to be 25 μm , 50 μm , 100 μm , 200 μm and 360 μm . The photoresist used for the 25 μm layer was SPR 220-7.0 (Rohm & Haas), while the rest of the layers were fabricated using SU-8 3050 (MicroChem). Fabrication was performed using standard photolithography techniques. Briefly, a SPR 220-7.0 layer was spin coated on a 4 inch silicon wafer. This layer was patterned using photolithography and hard baked to generate a rounded channel cross section, required for effective valve closure, as has been described earlier [111]. For all other layers, SU-8 3050 was spin-coated on the wafer and patterned using standard photolithography, excluding the developing step. This technique was found to be very effective in preventing generation of bubbles and non-uniform coating of photoresist on the wafer due to the presence of features from earlier layers on the wafer. A single developing step for all four SU-8 3050 layers was used to remove excess photoresist on the wafer (Fig 6.7). The control layer for the microfluidic

device on the other hand consisted of microfluidic channels of a single height. As a result, the mold fabrication for the control layer was relatively simpler, with a single layer of SU-8 3050 photoresist, 50 μm in height.

3.2.3 Microfluidic Device Fabrication

The microfluidic devices were fabricated using multilayer soft lithography techniques [111]. The protocol differed slightly from our standard protocol [112-114] due to the need for proper functioning of push-down valves(103) while accommodating tall features (up to 360 μm) on the fluidic layer. The thickness of the polydimethylsiloxane (PDMS) membrane separating the control layer and the fluidic layer in a microfluidic device needs to be less than ~ 50 μm , for complete valve closure at reasonable pressure (~ 30 PSI). However, the presence of fluidic regions as tall as 360 μm on the fluidic layer mold precluded the possibility of covering the entire fluidic layer mold with PDMS, while maintaining the thickness of the PDMS layer to a value less than 50 μm in the regions of the device containing valves. To overcome this problem, a modified three-layer fabrication process was developed. Detailed description of the fabrication process is included in section 6.5.2.

3.2.4 Capillary-to-Chip Interface

Following the microfluidic device fabrication, a silica capillary was attached to the ‘capillary inlet’ on the microfluidic device (Fig. 6.3b). The 360 μm tall channel region at the capillary inlet accommodates a silica capillary with an OD of 360 μm . A 10 mm section of silica capillary is inserted horizontally into this tall channel on the device until it is flush with the 200 μm tall fluidic channel on the device. To seal the capillary to the chip and prevent leakage, PDMS was dispensed around the capillary at the interface between the capillary and the device. The PDMS tended to crawl into the 360 μm channel and surround the capillary, effectively sealing the capillary-to-chip connection. The final assembly was baked for at least 2 hours at 80°C before usage.

3.2.5 Device control

All the inputs on the device were kept under constant pressure, with independent input pressure for 1) carrier fluid input, 2) all four reagent inputs and 3) carrier fluid with surfactant input. The pressure applied to the capillary input was controlled directly by the pressure controller used for the SSL system. All the valves on the device were controlled by an array of off-chip solenoid valves, as has been demonstrated earlier(34). We developed Matlab (Mathworks, Natick MA) software for computer control of the valve array. This software allowed us to execute a predetermined sequence of valve actuation with independent time control for each actuation. The opening of a valve corresponding to an input on the device led to the release of a droplet of fluid from that inlet into a central channel on the device. The volume of this droplet could be controlled through variation of the opening time of the valve.

3.2.6 Reagents

All the devices and capillaries were treated with Aquapel to render their surface hydrophobic. The testing of our platform was performed using food dyes (Ateco, Glen Cove, NY) to mimic different samples and reagents for easy visualization. The carrier fluid used to maintain the separation between sample plugs consisted of a perfluorocarbon (FC-3283) and a non-ionic fluorosoluble surfactant (1H,1H,2H,2H-Perfluoro-1-octanol) mixed in a ratio of 8:1 by volume. The carrier fluid with surfactant consisted of FC-40 (3M) and 2% 'EA' surfactant (Raindance Technologies) by weight.

3.2.7 Sample plug and droplet volume estimation

We estimated the volume of sample plugs and sample droplets generated using the SSL system and the microfluidic device respectively. This volume estimation was performed by processing the images of these sample plugs or droplets using the software ImageJ(104). Specifically, for sample plug volume estimation, a series of sample (blue food dye) plugs were generated in a silica capillary using the SSL system. A colour image of these plugs was taken against the white background of a 'letter' sized sheet of

paper using a standard Digital Single-Lens Reflex (DSLR) camera. This image was imported in ImageJ and the length scale was set to true length using the known length of the letter sized paper in the image. The lengths of the sample plugs were then manually measured for each plug using the ‘Measure’ function in ImageJ. The plug lengths could be converted to plug volumes with the known cross sectional area of the capillary. For sample droplet volume estimation, we generated droplets made of blue food dye using one of the four reagent inlets on the mi whole device was then imaged using a DSLR camera. The image was imported in ImageJ and cropped to obtain an image of the incubation region on the device. This image was then converted to a binary image using colour thresholding to identify droplets over the background image. An estimate of the droplet area for each droplet in the image was then obtained using the ‘Analyze Particles’ function. This analysis was limited to particle areas larger than a lower threshold to exclude any particles and occasional satellite droplets from the analysis. The droplet areas thus estimated were then converted to droplet volume using the known depth of the incubation channel region (200 μm).

3.3 *Results and Discussion*

3.3.1 **Overall Work Flow**

Fig 6.1 is a schematic illustrating the functioning of the platform. Initially a cartridge (capillary) is loaded with a library of sample plugs forming a serial sample plug array: plugs are separated from each other by an immiscible carrier fluid. This cartridge is interfaced with a microfluidic device featuring multichannel architecture and pneumatic microvalves. The microfluidic device digitizes sample plugs into smaller daughter droplets on. Each sample daughter droplet then moves to the downstream fusion region where a specific reagent is injected into the sample daughter droplet. The reagent droplets are injected into the sample daughter droplet through controlled actuation of valves corresponding to the reagent inlets. Supp. Video 6 shows this sequence of events. No strict synchronization or droplet detection module is necessary for fusion of sample and reagent to occur as the sample droplet is elongated in the fusion area (Supp. Video 7), exploiting the local channel geometry. The resulting sample-reagent droplet undergoes

mixing and travels downstream to the incubation region on the device. After reagent injection, additional carrier fluid containing surfactant is released into the central channel on the device to stabilize sample-reagent hybrid droplets. The sequence of droplets is maintained throughout the device, precluding the need for a complicated barcoding scheme to identify the contents of each individual droplet.

3.3.2 Capillary-to-Chip Interface

Our prototype platform necessitated the capillary-to-chip interface design to allow for sample plug introduction on chip. This objective presented a unique challenge, since proper functioning of the platform requires smooth transition of sample plugs from the large ID of the capillary to shallow channels on the device in the valve regions. There have been demonstrations of capillary-to-chip interfaces in the past for introducing sample plugs from a capillary to a microfluidic device. However, the devices used don't face this problem as they typically feature large channels with a valve-less design(25, 99). The capillary interface we designed (Fig. 6.3b and c) between the capillary and microfluidic chip was found to be effective in minimizing plug break up as plugs moved from the high ID (200 μm) of the capillary to the shallow channels on chip (25 μm). This transition consisted of 5 different channel sections with gradually reducing channel heights of 360 μm , 200 μm , 100 μm , 50 μm and 25 μm . This gradual transition minimizes the shear stress on the sample plug as it traverses from a capillary to the shallow channels on the chip, preventing its breakup in transit.

3.3.3 Droplet uniformity using mechanical valve based droplet generation

We examined the performance of the mechanical valves on our microfluidic device for their capability to control the droplet size generated. To conduct this experiment, we primed the incubation channel on the device with the carrier fluid. We then used one of the reagent inlets on the device for generating droplets made of blue-colored food dye into the incubation channel region. The two parameters which could be used to control the droplet size generated from a reagent inlet are 1) Input pressure to the reagent inlet (Preagent) and 2) The opening time of the valve corresponding to the reagent inlet (Topen). Initially, we fixed the value of Preagent and generated droplets on the device for different values of Topen. Droplet generation was continued for each condition tested,

until the incubation region on the device was completely full of droplets. We then estimated the volume for all these droplets using the image processing technique discussed in the ‘Materials and Methods’ section. The mean and standard deviation of fifty droplets generated for each condition was plotted against T_{open} in Fig. 6.4b. This experiment was repeated for three different fixed values of Preagent. As expected, the linear relationship between droplet volume and T_{open} indicates excellent and predictable control of the device over droplet volume. Small standard deviation observed on the droplet volume also indicates excellent droplet uniformity for identical droplet generation conditions. This result is very important to ensure the capability of the device to generate droplets of various compositions on-demand.

3.3.4 Sample Digitization

We examined the capability of our device to digitize a set of sample plugs being supplied to the device into smaller sample daughter droplets. To conduct this experiment, we generated a set of sample plugs into a silica capillary using the SSL system. These sample plugs were delivered to the microfluidic device through the capillary inlet, under pressure provided by the pressure controller on the SSL system. For this experiment, the repeating sequence of steps executed on the device was as following: 1) Generate small droplet from a sample plug in the central channel, 2) Move the droplet towards incubation region with carrier fluid 3) Release small amount of carrier fluid with surfactant in the central channel. Repeating this set of steps led to generation of an array of sample droplets generated through digitization of sample plugs on the device. Examples of unmerged sample daughter droplets are shown in Fig. 6.6a (Sample droplets A, B, C and D). The order of the sample plugs in the capillary is consistently maintained on the device, even after the digitization operation. One shortcoming of this operation is the generation of non-uniform droplets towards the beginning and the end of the sample plugs. This is because the valve actuation sequence is continuously executed without any sensing of sample plug arrival on the device. However, the sample droplet uniformity is maintained throughout the rest of the sample plug. As the droplets generated on the

device are stabilized with surfactant, undesirable merging of non-uniform droplets originating from the front- or back-end of plugs is avoided on the device.

3.3.5 Generation of droplets of combinatorial mixtures

In this section we demonstrate proof-of-concept generation of combinatorial mixtures from sample plugs and reagent droplets on our device. For discernibility, we chose to use different food dye solutions to simulate different samples and reagents. Fig. 6.5 shows how reagent injection operations are performed in the fusion region on our device (also shown in Supp. Video 6). First, a sample plug travels from the capillary on to the microfluidic device. This plug is then chopped into a smaller sample daughter droplet. This droplet is then moved to the downstream fusion zone through release of carrier fluid in the central channel on the device. As every single input on the device is controlled with an individual valve, the device functions like an assembly line with complete temporal and spatial control over every single operation, as against typical droplet generating devices where the carried fluid flow is continuous. This level of control also implies that the operation of the device can be paused and resumed with a completely new valve actuation sequence, on demand without affecting the existing droplets on the device. None of the droplet devices reported in literature so far has this capability to the best of our knowledge. A reagent droplet is then injected directly into the sample daughter droplet (Fig. 6.5a). The volume of reagent solution injected into the sample droplet can be controlled through variation of the opening time for the valve corresponding to the reagent inlet. Supp. Video 7 provides a close-up view to how reagent injection is performed. The fusion zone is designed such that the sample daughter droplet is sufficiently elongated within a region, which overlaps with all the injection ports of the interrogating reagents. This elongated droplet state removes the need for strict positioning accuracy requirements on the sample droplet for reliable injection of reagent into the sample droplet. In addition to demonstrating injection of a single reagent in a sample droplet, we have demonstrated injection of up to four reagents into a single sample droplet as shown in Fig. 6.5b. The concept of droplet elongation to aid reagent injection can be easily scaled to accommodate tens of reagent inlets, if desired.

After reagent injection, the sample-reagent droplet is driven further downstream with the help of carrier fluid. Following this, a small plug of carrier fluid with surfactant is released in the central channel for stabilizing the droplets in the incubation region. Using this scheme we can simultaneously take advantage of a surfactant-free zone in one area of the chip to promote sample-reagent merging while deliberately using surfactant in another area to increase droplet stability and prevent unwanted droplet merging.

Fig. 6.6 demonstrates the reliability of the fusion mechanism on our device. Fig. 6.6a is a table of 16 different sample-reagent combinations generated on a single chip through all possible merging combinations of four different sample daughter droplets (A: blue, B: yellow, C: green, D: water) with four different reagents (Reagent 1: orange, Reagent 2: water, Reagent 3: blue, Reagent 4: yellow) with the condition of merging exactly one sample with one reagent.

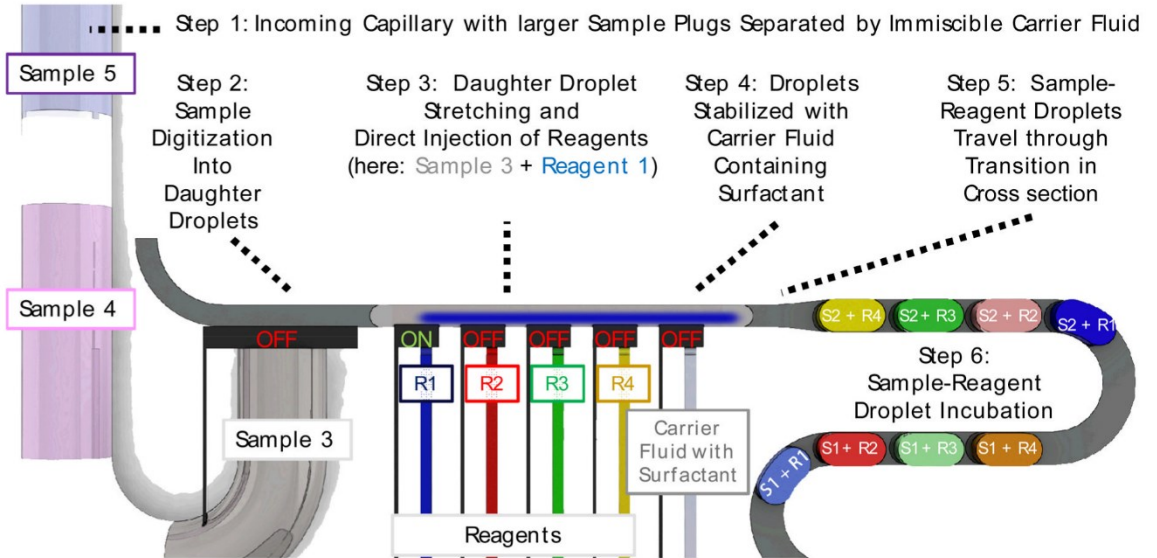
The micrographs in Fig. 6.6b show a repeating sequence of the sample-reagent hybrid droplets in the incubation region of the chip. The chip is operated such that the sample daughter droplets are merged with a repeating sequence of four different reagents. As a result a repeating sequence of four possible combinations generated through mixing a single sample with four different reagents can be seen in each individual micrograph. Once a sample plug is exhausted, the sample daughter droplets generated from the next incoming sample plug start merging with the same repeating sequence of reagents generating a repeating sequence of a new set of four different sample-reagent combinations in the incubation region on the chip. The droplet monodispersity as well as the uniform spacing between droplets is clearly visible in these micrographs. The inset in Fig. 6.6b displays zoomed-in view of these micrographs of the incubation region illustrating two repeats of each sequence in the incubation region. These images also demonstrate the capability of the device to maintain the order in which droplets are generated, throughout the incubation region on the device. We have demonstrated 16 combinations in this instance, but by employing multiple (2, 3 or 4) reagent merging with sample daughter droplets, as demonstrated in Fig. 6.5b, many more combinations can be generated using our prototype device.

3.4 *Conclusion*

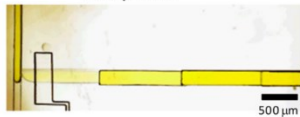
In summary, we have demonstrated a platform capable of preparing droplets from combinational mixtures of a large number of samples and reagents. This is accomplished by synchronization-free and detection-free fusion of sample daughter droplets and reagents. A key benefit of this architecture is the ability to scale this device to analyze N samples against M reagents ($N \times M$) where N can range from hundreds to thousands without accompanying increase in device complexity. Additional reagent set multiplexing can be accomplished analogously by introducing linear arrays of reagent set plugs similar to sample introduction. Furthermore, this design allows for spatial indexing, by maintaining the sequence of droplets from generation throughout incubation, precluding the need for barcoding.

This platform presents a novel design with several important components: a unique SSL system which uses pressure to inject uniform volumes of sample into a capillary directly from an industry standard multi-well plate. This capillary is then interfaced with a microfluidic device using a novel capillary-to-chip connection. The microfluidic device is capable of combinatorial screening operations. Robust synchronization-free reagent injection is performed on the device based on a design which capitalizes on droplet elongation in the fusion zone on the device. In our prototype design up to 4 reagent droplets can be fused with a single sample droplet. However, by employing the same concept many more reagent inlets can be introduced on chip to perform merging operations. In addition, we have demonstrated a technique for reagent injection in droplets that capitalizes on controlling droplet surface chemistry by controlling surfactant concentration at different regions on the chip. That is, we have demonstrated a surfactant-free environment in the fusion zone on the device, thereby promoting reagent injection in sample droplets while the droplets are stabilized by surfactant in the incubation region. For the microfluidic chip design, several areas can be explored to further enhance the operation of the chip. To make the transition of sample plugs from a capillary to the microfluidic device more gradual a photolithography process employing a grayscale mask could be used. This approach can generate very gradual reduction in channel cross section from a large capillary to shallow microfluidic channels on the device as against the 5 step reduction demonstrated in the current version of the device. Furthermore, reagents may be loaded in cartridge format to further enhance multiplexing capabilities.

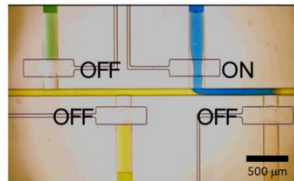
We expect the platform described here to be a promising candidate for combinatorial screening applications using droplet microfluidics.



Step 2: Sample Digitization (Yellow) into Daughter Droplets



Step 3: Sample Daughter Droplet (Yellow) Stretching And Injection of Reagent (Blue)



Step 5: Sample-Reagent Droplet (Green) Travels through Transition

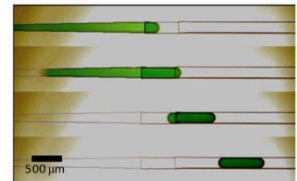


Figure 3.1. A schematic of the sample screening platform.

Step 1: A cartridge is loaded with a library of sample plugs separated by an immiscible carrier fluid. This cartridge is interfaced with a microfluidic device. Step 2: On-demand digitization of incoming sample plugs into smaller daughter droplets. The volume of individual daughter droplets can be controlled by valve opening time and back pressure on the cartridge. Step 3: By exploiting the cross sectional area of the central channel, the sample daughter droplet is stretched in the “Fusion Region”. This approach allows for robust, synchronization-free injection of up to four reagents simultaneously directly into the daughter droplet. The volume of reagent injected is controlled through modulation of back pressure and valve opening time corresponding to the reagent inlet. Step 4: Once sample and reagent have been combined into one droplet, the droplets are stabilized with carrier fluid containing surfactant to prevent unwanted droplet coalescence downstream. Step 5: Sample–reagent droplets travel to an incubation channel. Step 6: The sample–reagent droplets are incubated while maintaining their sequence in downstream incubation channels. This approach allows for droplet identification through spatial indexing in a 1-dimensional array.

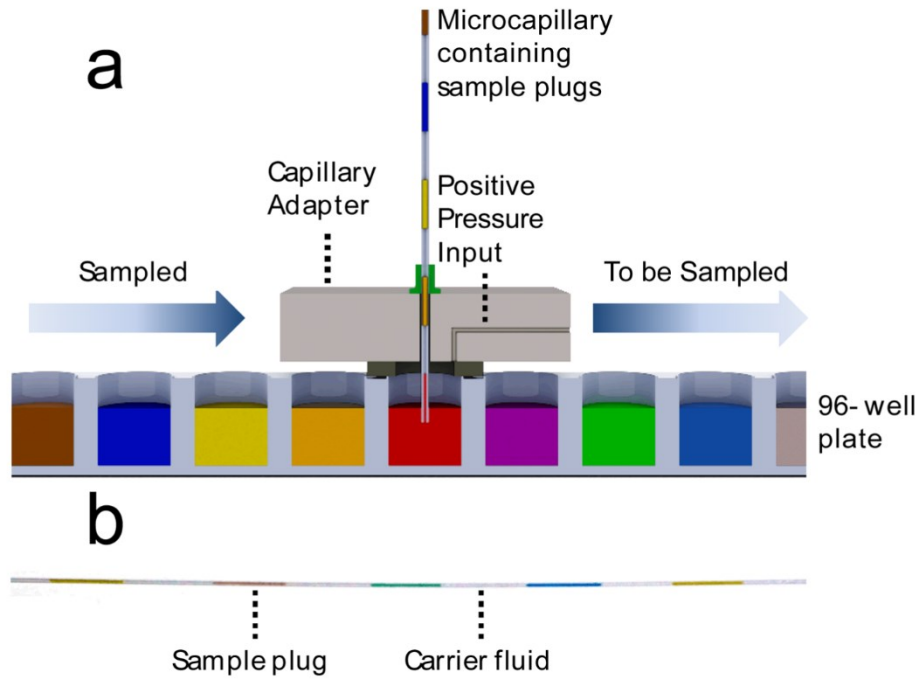
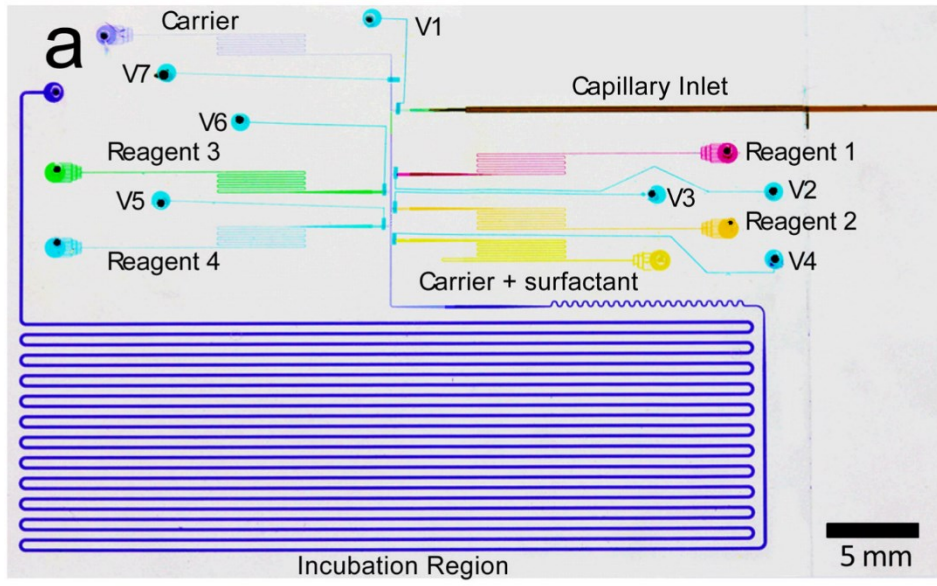


Figure 3.2. The Serial Sample Loading (SSL) system.

A custom SSL system was designed which employs positive pressure to inject a sample plug into a microcapillary from a standard multi-well plate. A custom capillary adapter in the SSL system provides an interface between a microcapillary and a multi-well plate. This adapter can seal a well on the multi-well plate, thus generating a temporary pressure chamber inside the sample well. A pressure input on the adapter can then be used to apply controlled pressure to the fluid inside the sample well. This positive pressure drives a small plug of sample from the well into the microcapillary. Following this, the seal is broken and the multi-well plate is moved to seal another sample well with the capillary adapter. This sequence of steps is repeated to generate a sample library into the microcapillary. b) An image of a food dye sample plug array generated using the SSL system. Each sample plug is separated from each other by an immiscible carrier fluid.



b



Figure 3.3. Microfluidic Device Design.

a) Photograph of a prototype device. The microfluidic device has a multichannel architecture: 1) The central channel with fusion region and incubation region (purple), 2) Capillary inlet, 3) Reagent inlets: reagent 1 (pink), reagent 2 (orange), reagent 3 (green), reagent 4 (turquoise) and surfactant oil inlet (yellow). The valves on the device (V1–V7) are indicated by a turquoise dye. b) A scan of the capillary inlet region, indicating the height difference between different sections of the capillary inlet to facilitate smooth sample plug transition from the large ID of the capillary to the shallow channels on the microfluidic device.

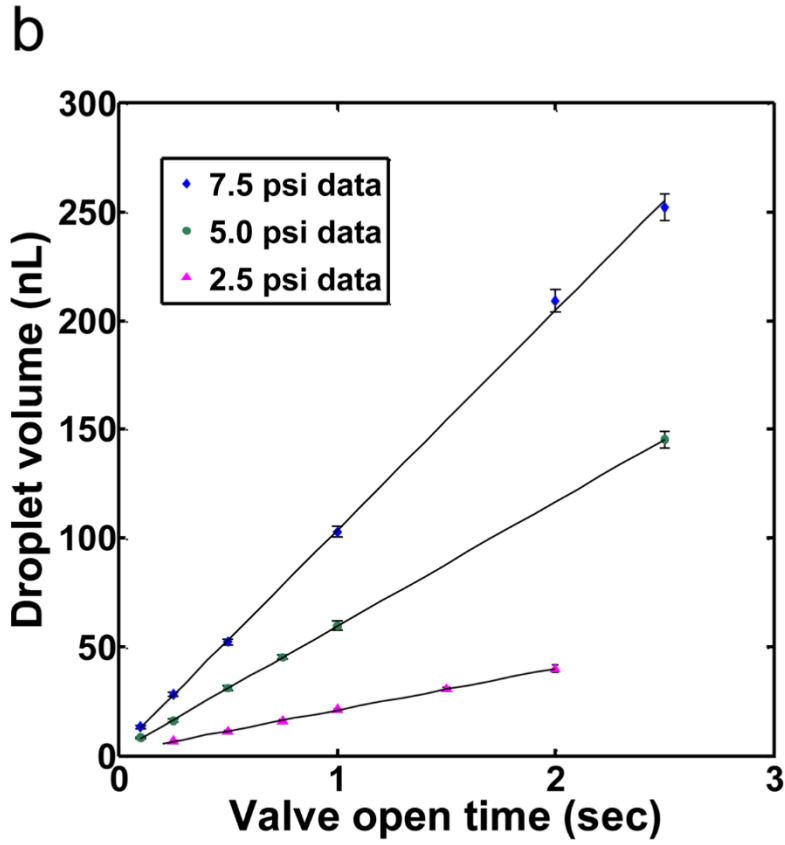
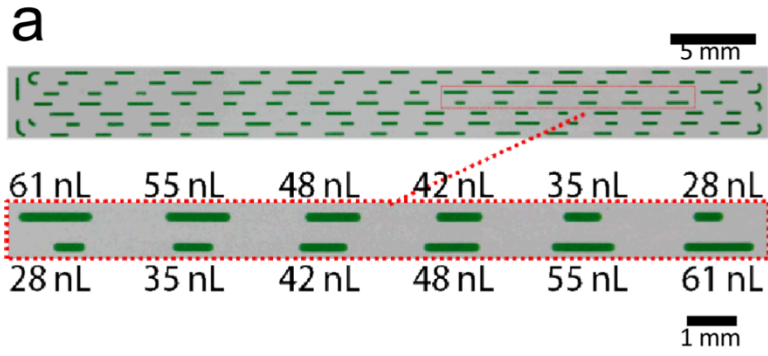


Figure 3.4. Control of droplet volume and droplet uniformity using mechanical valve based droplet generation.

a) Micrograph of the incubation region on the microfluidic device filled with reagent droplets generated using sequentially increasing valve opening times ($T_{\text{on}} = 0.3, 0.4, 0.5, 0.6, 0.7, 0.8$ s) for a fixed back pressure on the reagent inlet ($P_{\text{reagent}} = 5$ psi). This resulted in a linear array of repeats of a sequence of six droplets, with each droplet increasing in volume. b) A plot of droplet volume *versus* the valve opening time (T_{open}) for a valve corresponding to a reagent inlet for three different values of back pressures applied to the reagent inlet ($P_{\text{reagent}} = 2.5, 5$ and 7.5 psi). The droplet volumes plotted are an average of volumes estimated from 50 droplets for each condition. The error bars in the volume data are too small to be seen on the plot.

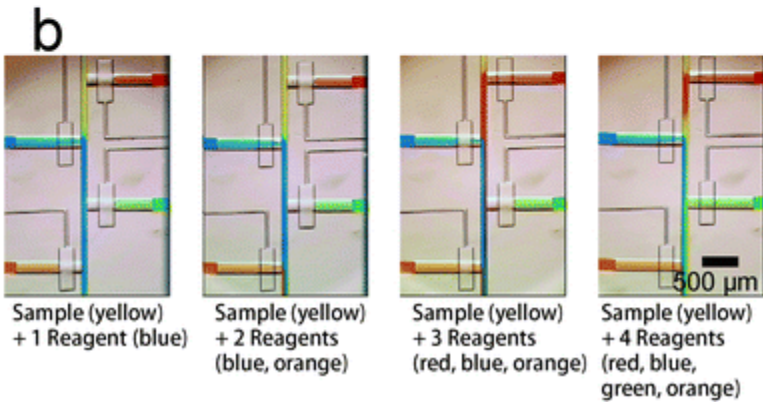
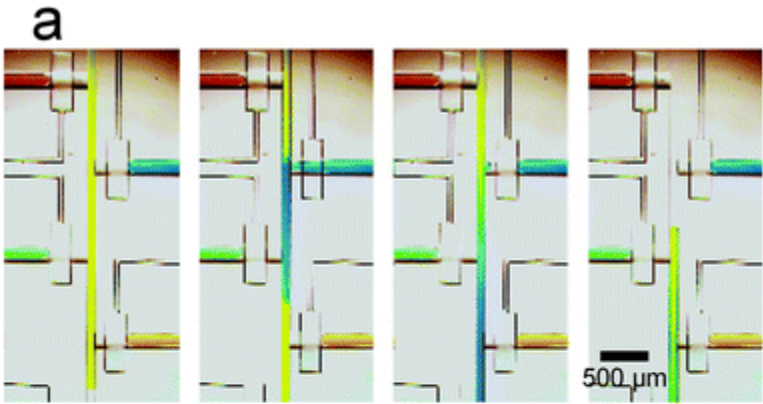


Figure 3.5. Demonstration of reagent injection in sample daughter droplets.

- a) Time series of images indicating reagent injection into sample daughter droplets at the 'Fusion zone' on the device. A sample daughter droplet (yellow) is released from the capillary inlet and is halted in the 'Fusion zone' by actuating a valve upstream which controls carrier fluid injection into the central channel on the device. A reagent (blue) is released and injected directly into the sample droplet. The elongated configuration of the sample daughter droplet in the 'Fusion zone' ensures robust reagent injection operation on the device without the need for precise sample droplet positioning.
- b) A series of photographs demonstrating injection of different numbers of reagents into a sample daughter droplet simultaneously.

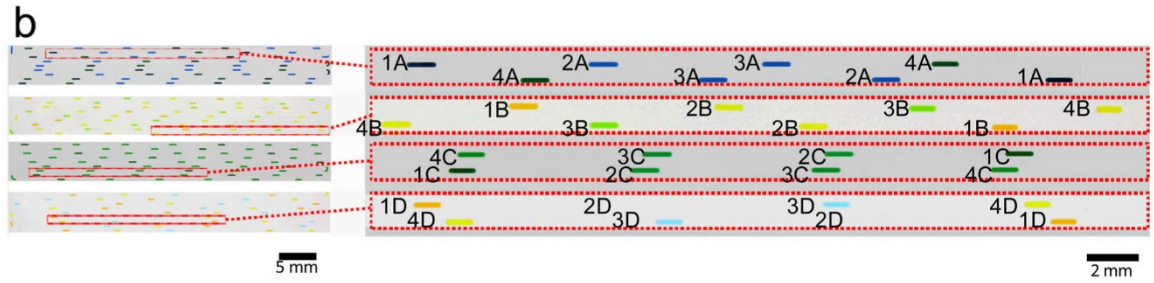
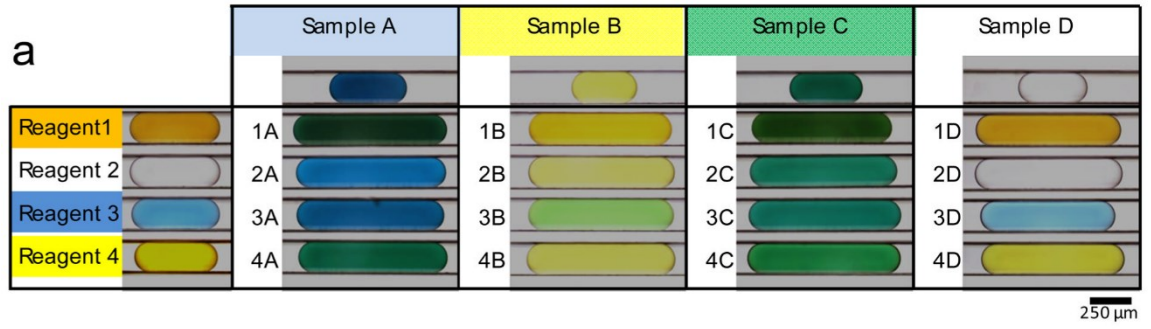


Figure 3.6. Photographs of the incubation region indicating the multiplexing capability of the device.

a) Table with micrographs indicating combinatorial mixture droplets generated on the device using four different samples [Sample A (blue), Sample B (yellow), Sample C (green), Sample D (water)] and four different reagents [Reagent 1 (orange), Reagent 2 (water), Reagent 3 (light blue), Reagent 4 (yellow)]. Droplets 1A–4A, 1B–4B, 1C–4C, and 1D–4D are each generated from a combination of the sample and reagent in the corresponding column and row, respectively. For example, Droplet 1A is the combination of sample A with reagent 1. b) The left panel shows four different micrographs showing repeating sequences of sample daughter droplets generated from a single sample plug merged with four different reagents on a single device. The right panel shows a zoomed in version of a small section of the micrographs from the left panel for easy visualization of the droplet sequence. The droplet identification codes in this panel are the same as those used in subfigure a. Note: The sequence of droplets seems to be going in the opposite direction in alternate channels due to the changing direction of flow in serpentine channels.

3.5 *Supplementary section*

3.5.1 **Mold Fabrication**

The work flow used for fabricating the fluidic layer mold is illustrated in Fig 6.7. The mold consists of five different layers of photoresist with heights of 25 μm , 50 μm , 100 μm , 200 μm and 360 μm . The photoresist used for the 25 μm layer was SPR 220-7.0 (Rohm & Haas), while the rest of the layers were fabricated using SU-8 3050 (MicroChem). Initially a 25 μm tall SPR 220-7.0 layer was spin coated on a silicon wafer. This layer was patterned using photolithography and hard baked to generate a rounded channel cross section, required for effective valve closure. Rest of the layers were fabricated by stacking and patterning multiple layers of SU-8 3050 on the wafer. All the steps required for standard photolithography (Soft Bake, Exposure and Post Exposure Bake) are conducted for each layer of SU-8 3050, except the developing step. This step is conducted in common for all layers after the last SU-8 layer is patterned to remove excess unexposed photoresist from the wafer (Fig 6.7). This technique was found to be very effective in preventing generation of bubbles and non-uniform coating of photoresist on the wafer due to the presence of features from earlier layers on the wafer.

3.5.2 **Device Fabrication and Operation**

The microfluidic device for our experiments was fabricated using multilayer soft lithography technique. Standard dual layer microfluidic devices with push-down valves fabricated using polydimethylsiloxane (PDMS) require shallow fluidic channels to make sure the layer of PDMS between the fluidic and control layer is sufficiently thin ($\sim 50\mu\text{m}$) for complete closure of valves at low pressures ($<30\text{psi}$). The requirement of shallow fluidic channels is incompatible with our chip design. So we developed a modified fabrication process for our device. This modified soft lithography process is outlined in Fig 6.8. For this modified fabrication process, three different batches of PDMS were mixed. These varied in composition, and base to crosslinking agent ratios of 15:1, 10:1 and 6:1 were used, respectively. These batches were thoroughly mixed and degassed prior to use for device fabrication. The control layer mold was spin coated with a thick layer ($\sim 1\text{ mm}$) of 6:1 PDMS and baked at 80°C for 7 mins. A thin layer of 15:1 PDMS

was spin coated on the fluidic layer mold. The device was designed such that the valve regions on the device were placed in areas surrounded by shallow fluidic channels, ensuring uniform coverage of these regions with a thin layer of PDMS. The PDMS on the fluidic layer mold was then baked at 80°C for 6 minutes. The PDMS was removed from the control layer mold and the control layer was cut to the exact size of the valve regions on the device, while not covering any channels higher than 50 μm on the device (Fig 6.8). The control layer PDMS pieces were aligned with baked PDMS layer on the fluidic layer mold under a stereoscope. The fluidic layer mold with the aligned control layer was baked at 80°C for 20 mins to promote adhesion between the control layer and the fluidic layer. Following this, 49.5 g of 10:1 PDMS was poured on the fluidic layer mold, covering all features on the fluidic layer mold with a 3-4 mm thick layer of PDMS. The fluidic layer mold was then baked for at least 30 minutes at 80°C. Following this, the PDMS was removed from the fluidic layer mold and individual devices were cut. Fluidic access holes were then punched into the device and the device was bonded to a coverglass through oxygen plasma treatment.

3.5.3 Fusion Zone design

An important aspect of our microfluidic device is the robust synchronization-free fusion mechanism. This mechanism utilizes the cross-sectional area of the central channel on the microfluidic device for the merging operation. Fig 6.9 demonstrates the design criteria of the fusion region on our device. In our current design, the dimensions of the fusion zone, defined as the distance between the first and last reagent inlet (3800 μm), height (50 μm) and width (100 μm) of the central channel determine the volume of the fusion zone (19 nL). This volume of the fusion zone corresponds to the minimum volume of the sample daughter droplet, such that the droplet spans the entire length of all the reagent injection sites on the chip. As a result, the sample daughter droplet position doesn't need to be finely controlled to inject different reagents in it. If there is a need for smaller reaction volumes, the cross-sectional area of the central channel can be modified to reduce the minimum volume of the sample daughter droplet required. For instance, reducing the fusion zone channel height from 50 μm to 10 μm will result in reduction

in minimum required droplet volume from 19 nL to 3.8 nL (Fig 6.9). A similar approach can be used to accommodate more than four reagent inlets on the chip.

3.5.4 Serial Sample Loading System

3.5.4.1 Background

High throughput sample processing is a critical requirement for a large number of industries. Some examples include the agricultural, pharmaceutical and biotechnological industries(105). As a result, there is a constant drive for innovation in sample processing techniques, supporting these industries. One major breakthrough in this domain has been the application of various robotic sample handling techniques, to improve the speed of sample processing as well as to reduce the volume of reagents used per reaction. Although the robotic systems have become incredibly fast at sample processing operations, they are typically limited to operating with standard multi-well (96, 384 and 1536 well) plates. As a result, the typical sample volume consumption is on the order of microliters per reaction for such systems(105). Recent advances in the microfluidic domain show promise in overcoming this limitation of the robotic systems. Droplet-based microfluidic systems have been shown to be capable of performing biomolecular screening with sample volumes as low as picoliters(1, 5, 8, 48, 69). However, introducing a large number of samples on a miniature microfluidic device is difficult since it is impractical to have hundreds to thousands of sample inlets to a single microfluidic device. Furthermore, the tubing used for supplying the samples to such a microfluidic device would already consume orders of magnitude more sample than is required for the actual analysis on the microfluidic device. So, there is a need for an efficient way to transport a large number of samples to a microfluidic device. Ideally such a sample transport system would be flexible enough to supply variable number of samples to a microfluidic device without any modifications in the transport system or the device.

The ‘plug-in cartridge’ technique developed by the Whitesides group(106) provides an elegant solution to the problem of introducing a large number of reagents on a microfluidic device through a single inlet. Under this approach, a series of sample plugs are loaded into a capillary, with air bubbles present between sample plugs acting as spacers. This capillary is connected to a microfluidic device, for serial delivery of these

sample plugs. However, in this approach, the sample plugs are constantly in contact with the capillary inner surface, leading to the problem of cross contamination between plugs(106). Another modification of this approach developed by the Ismagilov group(107) utilizes an immiscible carrier fluid instead of an air bubble to act as a spacer between sample plugs. The carrier fluid in this approach preferentially wets the inner surface of the capillary, thus preventing direct contact between sample plugs and the capillary surface. As a result, the problem of cross contamination between sample plugs is eliminated. The carrier fluids typically used for generating these sample plug arrays are fluorinated oils, which also reduce the problem of reagents leaking from sample plugs into the carrier fluid due to their low solubility for most reagents(107).

Although this approach is promising, the current techniques used under this approach for generating the ‘sample plug cartridges’ have some issues which need to be resolved. The common technique of using a syringe pump for aspirating sample plugs from a sample well(99, 108, 109) in a multi-well plate can be extremely slow. Another technique of using vacuum for aspirating a sample plug can be much faster(106). However, this technique can only provide a maximum driving pressure of 1 atm (~15 psi). As a result, the driving force may not be sufficient to load large numbers of sample plugs into a capillary due to the increasing fluidic resistance of the capillary with the introduction of sample plugs. Furthermore, both these techniques require the free end of the capillary to be attached to either a syringe or a vacuum source, thus excluding the possibility of operating this sample loading system in sync with the operations on a downstream microfluidic device. This can be a major setback to throughput as the possibility of conducting assays in continuous flow manner on microfluidic devices, as has been demonstrated earlier(110), is precluded.

To overcome these issues, we conceptualized and fabricated a sample plug loading system, which utilizes positive pressure for loading sample plugs from an industry standard multi-well plate to a capillary. Fig 6.10 shows a schematic illustrating the working principle of this system. A critical component of this system is a ‘capillary adapter’ which acts as an interface between a capillary, to be used for holding the sample plug array, and a multi-well plate used for holding samples. As shown in the schematic, the capillary adapter can be sealed with a sample well on the multi-well plate, creating a

temporary pressure chamber in the sample well. In this sealed mode, the capillary attached to the capillary adapter is immersed in the sample present in the well. The pressure input on the capillary adapter can then be used to apply pressure to the sample in the well for a controlled amount of time. As a result, a small plug of sample is pushed from the well into the capillary. The size of this plug can be controlled by varying the input pressure and the pressure application time. Repeating this process with multiple sample wells can be used to generate an array of sample plugs in the capillary. As is clear from Fig 6.10, this whole sample plug loading process only requires one end of the capillary to be engaged, while the other end of the capillary is free to be interfaced with a downstream microfluidic device, where further operations can be carried out with the sample plug array.

Fig 6.11 shows a detailed model of the capillary adapter we designed in the CAD software ‘Solidworks’ (Solidworks Corp.). The wider backside of the adapter with the three large holes is used to bolt the capillary adapter to a stable support. The narrower front side is the actual functioning head of the capillary adapter. The functioning head consists of three disc shaped recesses on three sides (top, left and right), which are used to seat three NanoPorts (Idex Health and Science). The NanoPorts can be used to make a leak free connection with different types of tubing. The NanoPort on the top side is used to attach the capillary to the capillary adapter. The NanoPort on left side is used to attach the pressure supply line to the capillary adapter, while the NanoPort on the right side can be used to gauge pressure in the sample well, if required. All these NanoPorts holding locations on the capillary adapter have holes drilled in the center and routed to the bottom of the capillary adapter, as shown in the bottom view (Fig 6.11). When in use, the capillary goes through the straight hole drilled from the top of the capillary adapter to the bottom side. The bottom side of the capillary adapter has a disc shaped recess and a protruding circle. The disc shaped recess holds a silicone sealing ring, which is used to temporarily seal the capillary adapter with a sample well on a 96-well plate. The protruding circle acts as a centering feature, which is used for centering the capillary adapter into a sample well.

Our assembled Serial Sample Loading (SSL) platform is shown in Fig 6.12. All the components of the SSL platform are attached to an aluminum breadboard for support. A

vertical stainless steel post bolted to the aluminum breadboard provides strong support structure for the capillary adapter. The capillary adapter is bolted to an angle bracket, which can slide on the post. This assembly allows us to manipulate the height of the capillary adapter from the aluminum base, as required. The capillary adapter is fixed at a suitable height to leave sufficient space for an assembly for XYZ motion of a 96-well plate below it. To control the cost of the pilot system, we chose to keep the motion of the 96-well plate in the XY plane manual by using simple rails. However, these rails can be easily replaced with a motorized XY stage for automated motion of the 96-well plate. Controlled motion of the 96-well plate in the Z dimension, however, is critical for providing a reproducible seal between the capillary adapter and a sample well. So the motion in the Z-dimension was motorized. Typical linear translation stages are ill-suited for this application due to the limitation on the load supported by these stages along the direction of travel. Hence, a Motorized Lab Jack was used for automated motion of the 96-well plate in the Z dimension. Fig 6.12 also shows an Electronic Pressure Controller, which can control the pressure applied to a sample well through the capillary adapter.

3.5.4.2 Materials and Methods

The capillary adapter was designed in Solidworks (Solidworks Corp.) and then fabricated at the Physical Sciences Machine Shop at Johns Hopkins University. The capillary adapter was fabricated using stainless steel as substrate, to prevent corrosion due to contact with biological samples and buffers. All other structural components for the SSL system were purchased from Thorlabs (Newton, NJ). A Motorized Lab Jack (L490MZ/M, Thorlabs) was purchased to use for computer controlled vertical motion of the 96-well plate in the SSL system. The electronic pressure controller used with the SSL system was purchased from Alicat Scientific Inc. (Tucson, AZ). The pressure controller used is a dual valve pressure controller (PCD-100PSIG-D-PCV03), which eliminates the need for bleed ports and relief valves typically required for pressure control in a closed volume. NanoPorts (N-124H, N-333 and N-125H IDEX Health and Science) were bonded to the capillary adapter at the three ports according to the instructions provided by IDEX. The sealing ring attached to the bottom of the capillary adapter was fabricated using a silicone septum (Corning). The ring shape was punched out of the silicone septum using

hole punches (3/8" and 13/64" hole diameter, McMaster). The capillary adapter was designed to be compatible with Costar 96-well plates (Corning). The Motorized Lab Jack and the Electronic Pressure Controller were interfaced with a computer through USB ports. Custom software written in LabVIEW (National Instruments), allowed us to control the motion of the 96 well-plate in the vertical direction, as well as the pressure applied to a sample well through the capillary adapter.

The sample loading experiments were conducted using Silica Capillary Tubing (Polymicro Technologies). The capillaries were treated with Aquapel™ (PPG Industries) before an experiment, to render the inner surface of the capillary hydrophobic. The samples used for most experiments were food dyes (Ateco, Glen Cove, NY), unless specified otherwise. The carrier fluid used for separating sample plugs from each other was a mixture of FC-3283 (3M) and 1H,1H,2H,2H-Perfluoro-1-octanol (Sigma-Aldrich Co.) in the ratio of 8:1 by volume. For these experiments, the Aquapel treated capillary was completely filled with the carrier fluid first. Following this, a sample well on the 96-well plate was manually aligned with the capillary adapter. The LabVIEW software then raised the 96-well plate in vertical direction, to seal the sample well with the capillary adapter. The same software was then used to apply the desired pressure profile to the sample well for the desired amount of time. Following this, the 96-well plate was lowered by the LabVIEW software. We then manually aligned another well containing the carrier fluid with the capillary adapter. The same sample plug loading steps were then used to load a carrier fluid plug into the capillary. This alternating sequence of sample and carrier fluid plug loading was repeated until the desired number of sample plugs was loaded into the capillary. For the experiments which required sample plug volume estimation, we used a 1 m long silica capillary with a 200 µm inner diameter (ID). The sample used for these experiments was a single food dye. A series of 12 sample plugs separated by carrier fluid was loaded into the capillary using the steps described above. This capillary was then placed on the white background of a 'letter' sized sheet of paper and imaged using a Digital Single-Lens Reflex (DSLR) camera. The camera was placed such that the whole letter sized paper was included in the camera's field of view. The image was then imported in ImageJ (104) for plug volume estimation. Length scale was set in the image using the known length of the letter sized sheet of paper. Following this, the length of

each sample plug was measured by manually drawing a line marking the length of the plug in ImageJ. This measured length, along with the known cross sectional area of the capillary was then used to estimate the plug volume for each sample plug. The plug volume data from the last 10 sample plugs for each loading condition was then used for the data analysis.

3.5.4.3 Results

One of the first critical tests of our SSL platform was to determine its capability to provide significantly higher driving pressure than vacuum (~15 psi) for sample plug loading in a capillary. To conduct this test, we first attached a silicone sealing ring to the capillary adapter, as described in the 'Materials and Methods' section. The NanoPorts for the capillary and pressure gauge on the capillary adapter were plugged using plugs (IDEX Health and Science). The electronic pressure controller was connected to an input pressure supply of 95 psi from a Nitrogen cylinder. A sample well on a Costar 96-well plate, was then sealed with the capillary adapter using the SSL system. The LabVIEW software was then used to raise the pressure in the sealed sample well to different peak pressure values (10, 20, 30, 40 and 50 psi). Fig 6.13 shows a plot of the pressure in the sample well, sensed by the pressure controller, for these 5 different tests. The pressure plot for each test consists of 3 distinct regions: Rising phase (the pressure in the sample well is raised from zero to peak value during this phase), Peak pressure phase (pressure in the sample well is maintained at peak value during this phase) and Decline phase (pressure in the sample well is reduced from peak to zero psi during this phase). The duration of each of these phases can be controlled using the LabVIEW software. All these phases were fixed at duration of 5 sec each for the plots shown in Fig 6.13. The pressure plots demonstrate that the pressure controller can easily maintain a peak pressure of 50 psi in the sealed sample well as commanded. Thus, proving that our SSL system can provide substantially higher driving pressures than a vacuum based system for sample plug loading in a capillary. The pressure controller we used was factory calibrated to a maximum pressure of 50 psi. Hence, we couldn't test the SSL system for pressures higher than 50 psi. Furthermore, Fig 6.13 also demonstrates that the pressure controller can control the timing of the 'Rising' and 'Peak pressure' phases very precisely. The

duration of the 'Decline' phase, however, being a passive process driven by the pressure difference between the sealed sample well and the atmosphere, depends to some extent on the peak pressure value.

We then tested the capability of the SSL system to load a series of sample plugs into a capillary. Initial testing was conducted using food dyes as samples for easy visibility. A silica capillary was loaded with alternate plugs of different food dyes and carrier fluid using the SSL system. Fig. 6.14a shows a micrograph of the silica microcapillary with a few food dye sample plugs. The micrograph shows excellent uniformity of plugs, the ability of the SSL system to keep sample plugs separate from each other, as well as the capability to load sample plugs without breakup into the capillary. We then tested the sample plug loading scheme with a biologically relevant sample in the form of a 'PicoGreen' (Life Technologies) stained Lambda DNA (Promega) sample. The Lambda DNA was present at a concentration of 2 μ g/ml concentration in the sample. Biological samples provide additional challenge to the sample plug loading process due to the lack of any visual feedback during sample plug loading. Food dyes are easily visible and their plug uniformity can be easily discerned during the loading process. However, most biological samples being transparent, it is difficult to differentiate them from the transparent carrier fluid. The variation in plug size is solely dependent on the repeatability of the SSL system. We thus loaded these Lambda DNA sample plugs into a silica capillary essentially blindly and then obtained a fluorescence image (Fig. 6.14b) of the silica capillary using a Typhoon 9410 Variable Mode Imager (GE Healthcare). The fluorescent Lambda DNA plugs can be clearly seen over the dark background of the interspersed carrier fluid plugs. Excellent uniformity of plug loading, despite lack of visual feedback is also clearly evident from this image. The ultimate purpose of the SSL system is delivery of a large array of sample plugs to a microfluidic device for further processing. So, as a proof of principle, we also demonstrated interfacing of a capillary with a simple microfluidic device (Fig. 6.14c). A series of sample plugs made from food dye using the SSL system, were then delivered from the capillary to the microfluidic device. Excellent transition of sample plugs from the capillary to the microfluidic device without break-up can be clearly seen from the image in Fig. 6.14c.

We then conducted more rigorous testing of the SSL platform to determine its capability to maintain sample plug uniformity, as well as control the sample plug size as desired. To conduct these experiments, we loaded a series of twelve sample plugs made of the same food dye into a 1m long silica capillary for each set of sample plug loading conditions, as described in the ‘Materials and Methods’ section. The sample plug volume estimated from the last ten sample plugs was used to estimate the mean and standard deviation of the plug volume for each loading condition. These values were then used for the plots shown in Fig. 6.15 and 6.16. The sample plug volume depends on a few factors: 1) Peak pressure (P_{peak}) applied, 2) duration of the ‘Rising’ and ‘Decline’ phases of pressure application and 3) the duration (T_{peak}) of the Peak pressure phase. All these parameters can be precisely controlled in the SSL system with our LabVIEW software. We decided to vary the intuitive factors like P_{peak} and T_{peak} to control the sample plug volume. Initially, we held P_{peak} constant and varied T_{peak} to estimate the sample plug volume generated for different T_{peak} values. This experiment had two objectives: First to estimate the variation in plug volume for a fixed set of loading conditions and second to estimate the relationship between plug volume and T_{peak} for a fixed value of P_{peak} . Fig. 6.15 shows a plot of sample plug volume vs T_{peak} for three different values of P_{peak} (0.5, 1 and 1.5 psi). The linear relation between plug volume and T_{peak} for each individual P_{peak} value demonstrates the capability of the SSL system to precisely control the plug volume in a predictable manner, through the variation of the duration of the ‘Peak pressure’ phase. Furthermore, the plug size variation indicated by the error bars is fairly low with a maximum coefficient of variation of approx. 7% for all but two smallest plug volumes generated, where we were approaching the lower limit of the operation of the electronic pressure controller. We expect the system performance, in terms of plug volume variability, to improve as the motion of the 96 well plate is automated in the horizontal plane too, as the overlap of the sample well wall with the sealing ring of the capillary adapter can be reproduced across the area of the 96 well plate, providing a reproducible seal for every single sample plug loading step.

Varying T_{peak} to control plug volume can be beneficial for smaller plug volumes. However, as the plug volume increases, T_{peak} can quickly increase, reducing the speed at which sample plugs can be loaded in a capillary. For larger plug volumes, it would be

beneficial to raise the peak pressure, to achieve larger plug volume in the same amount of time. Fig 6.16 shows a plot of the sample plug volume vs P_{peak} for a fixed value of T_{peak} (1 sec). This plot shows another linear relationship between sample plug volume and P_{peak} , providing an alternative predictable way to vary the sample plug volume through variation of the peak pressure applied to the sample well. The value of P_{peak} here is only limited by the pressure at which the seal between the sample well and the capillary adapter breaks down. This result, thus illustrates a limitation of applying vacuum to load sample plugs in a capillary, which can be overcome with the use of the SSL system. Although, the vacuum level can be controlled with a regulator, the driving pressure cannot be greater than 1 atm (~15psi), limiting the speed at which large sample plugs can be loaded in a capillary.

One limitation of the SSL system is its dependence on the fluidic resistance of the capillary for maintaining the uniformity of sample plug volume for the same sample plug loading conditions. However, as more and more sample plugs are loaded into the capillary, the fluidic resistance of the capillary increases, gradually reducing the sample plug volume over the course of loading of sample plugs. This effect is illustrated in Fig 6.17a. In this figure, the sample plug volume data is normalized by the plug volume of the first sample plug generated for each loading condition. The normalized sample plug volume is then plotted against the sample plug number in the loading sequence. As seen from the plot, for three independent loading conditions (P_{peak} : 1 psi, T_{peak} : 1.5, 2 and 2.5 sec), we observe a consistent gradual reduction in the sample plug volume as the number of sample plugs in the capillary increases.

This problem can be avoided through pressure compensation for the changing fluidic resistance of the capillary. We observed the sample plug volume reduce by approx. 15% for the 10th sample plug loaded into a capillary for all the three conditions shown in Fig 6.17a. So we did simple linear peak pressure (P_{peak}) increase for each sample plug in the loading sequence to compensate for the 17% ($1/0.85$) increase in the fluidic resistance over the course of loading 10 sample plugs in the capillary. The normalized sample plug volumes for this modified loading scheme with the same starting point as the three conditions shown in Fig 6.17a, are plotted in Fig 6.17b. These plots demonstrate that a simple compensation scheme can avoid gradual reduction in sample plug volume with

increasing number of sample plugs, further improving the sample plug uniformity of the SSL system. In the future versions of the SSL system, the compensation scheme can be further improved by devising a mathematical model of the changing fluidic resistance in the capillary and incorporating it in the LabVIEW software, to automatically compensate for the changing fluidic resistance by varying the peak pressure (P_{peak}) applied to the sample well for each consecutive sample plug being loaded into the capillary. Alternatively, an imaging based technique can be used to detect the appearance of the edge between a sample plug and the carrier fluid at a particular distance from the end of capillary immersed in the sample solution, to provide feedback for computer control of the pressure controller. This approach can enable very accurate metering of sample plug volume for each sample plug despite changing fluidic resistance in the capillary.

3.5.4.4 Discussion

In conclusion, we have devised a new technique for serial delivery of a large number of samples to a microfluidic device, directly from a standard multi-well plate. Our SSL system differs from similar techniques developed by other research groups in the past, in the application of positive pressure as a driving force for the loading of a series of sample plugs into a capillary for direct delivery to a microfluidic device. The SSL system can be used for rapid sample plug loading into a capillary with the only rate limiting step being movement of the multi-well plate, to load samples from different sample wells. We demonstrated the functioning of the SSL system as well as its capability to precisely control the sample plug volume. Since the SSL system engages only one end of the capillary in sample plug loading, it can be directly interfaced with a downstream microfluidic device for its operation in synchronization with the microfluidic device. In its current form, the SSL system was designed for loading sample plugs into a single capillary. However, the design can be easily extrapolated for simultaneous loading of sample plugs in multiple capillaries from a row of sample wells. We expect the SSL system to be instrumental in further improvement in the throughput of droplet-based microfluidic devices in future.

4 *Enhancing Throughput of Combinatorial Droplet Devices via Droplet Bifurcation, Parallelized Droplet Fusion, and Parallelized Detection*

Combinatorial droplet microfluidic devices with programmable microfluidic valves have recently emerged as a viable approach for performing multiplexed experiments in microfluidic droplets. However, the serial operation in these devices restricts their throughput. To address this limitation, we present a parallelized combinatorial droplet device that enhances device throughput via droplet bifurcation, parallelized droplet fusion, and parallelized droplet detection. In this device, sample droplets split evenly at bifurcating Y-junctions before multiple independent reagent droplets are injected directly into the split sample droplets for robust droplet fusion. Finally, the fused sample and reagent droplets can be imaged in parallel via microscopy. The combination of these approaches enabled us to enhance the throughput by 16-fold – with ready potential for further enhancement – compared to traditional, serially-operated combinatorial droplet devices. Given its current performance and prospect for future improvements, we believe the parallelized combinatorial droplet device has the potential to meet the demand as a flexible and cost-effective tool that can perform high throughput screening applications.

4.1 *Introduction*

Recent years have seen the emergence of microfluidic droplet technology in a variety of chemical and biochemical applications [115] ranging from single-cell analysis [70, 116, 117] to enzyme kinetics measurements [118, 119] and even nanoparticle synthesis [120, 121]. In particular, microfluidic droplets have proven pivotal in digital analysis of individual biological samples at the single-molecule level [59, 67, 122, 123]. While this technology offers the capacity to divide a homogeneous reaction (i.e., one sample against one set of reagents) into a large number of reactions in droplets, it nevertheless faces challenges in generating a large combination of sample-reagent mixtures in a multiplexed manner. And although approaches such as integrated picoinjectors [105, 124], segregated microfluidic plugs in tubing [104, 106, 107, 125], and multiple devices [69] have been demonstrated to improve the multiplexing capacity of microfluidic droplet platforms, there remains a critical need for alternative approaches that facilitate multiplexed experiments in droplets.

As a promising alternative, droplet microfluidic devices that utilize programmable microfluidic valves to mix combinations of samples and reagents on-demand [62, 108, 126-130] presents a viable approach to performing multiplexed experiments in microfluidic droplets. For example, such devices have been employed to demonstrate multiplexed experiments such as the detection of DNA [128, 130] and characterization of matrix metalloproteases [127, 130]. Importantly, in some of these devices, the conservation of positional order of each droplet after combinatorial assembly enables spatial indexing as an effective means to track droplets [62, 130]. Unfortunately, a key limitation to this platform is its throughput. Because the combinatorial droplets are generated sequentially and serially, the rate of analysis is limited by the rate at which droplets can be assembled and detected in the order of assembly (Figure 1A). A design that can increase the throughput of such microvalve-based combinatorial droplet devices is therefore needed.

To address this limitation, we have developed a parallelized combinatorial droplet device design. This design is achieved via droplet splitting [131-137], parallelized droplet fusion, and parallelized droplet detection (Figure 1B). Specifically, each sample droplet first travels through bifurcating Y-junctions (two stages as shown here) and split into identical daughter droplets (four as shown here) before each daughter droplet is fused

with its designated reagent. Importantly, the reagents can be simultaneously injected into the daughter droplets, thereby facilitating improved throughput. Finally, the entire group of fused sample-reagent droplets originating from the single sample droplet can be detected in parallel, further enhancing the throughput. To demonstrate this concept, we designed and fabricated a parallelized combinatorial droplet device and showed that the new design can improve the device throughput by 16-fold – with ready potential for further enhancement – when compared to a traditional, single-channel design.

4.2 *Experimental Section*

4.2.1 **Mask Design and Printing**

Fluidic and valve layer masks were designed in L-Edit v16.0 (Tanner EDA, Monrovia, CA). To account for polydimethylsiloxane (PDMS) shrinkage during the soft lithographic molding step (see Master Mold Microfabrication section), features on the valve layer mask were expanded by 1.5% in both dimensions. Mask patterns were printed onto high-quality transparencies at 20000 dpi by CAD/Art Services, Inc. (Bandon, OR). Transparency masks were mounted on five-inch soda lime glass mask holders (HTA Enterprises, San Jose, CA) and stored in clean room environment prior to use.

4.2.2 **Master Mold Microfabrication**

Master molds for both fluidic and valve layers of the PDMS chip were microfabricated via standard photolithography techniques. Fluidic and control layer molds were fabricated on four-inch silicon wafers (Polishing Corporation of America, Santa Clara, CA). Prior to processing, all wafers underwent a dehydration bake at 200 °C for at least two hours. Our device design involves regions with two different channel heights. Shallow channels fabricated with SPR-220-7 (positive photoresist; Microchem Corp., Newton, MA) are incorporated near the sample introduction region and reagent inlets to allow for valve actuation. The height of these channels is ~25 μm and these can be collapsed by applying pressure to the control layer. This layer was patterned using photolithography and hard baked to generate a rounded channel cross section, as required for effective valve closure [138]. This was followed by patterning of SU8-3025

(Microchem Corp., Newton, MA) to generate the rest of the fluidic channel network (height was $\sim 45\ \mu\text{m}$) on the fluidic mold. For the valve control mold, a single layer of SU8-3025 was patterned on the wafer (height was $\sim 45\ \mu\text{m}$).

4.2.3 Microfluidic Chip Fabrication

The microfluidic devices were fabricated using multilayer soft lithography techniques [139]. A modified three-layer fabrication process was developed [62, 127]. We used SYLGARD 184 Silicone Elastomer Kit (Dow Corning, Midland, MI) for fabricating our chips. Prior to use, fluidic layer molds were silanized using vapor deposition of chlorotrimethylsilane (Sigma-Aldrich, St. Louis, MO) for at least 15 minutes to minimize adhesion between PDMS and the patterned structures on the wafer. For this modified fabrication process, three different batches of PDMS were mixed. These varied in composition, and base to crosslinking agent ratios of 15:1, 10:1 and 6:1 were used, respectively. PDMS was degassed for approximately 30 minutes before pouring on the respective molds. The control layer mold was spin coated with a thick layer ($\sim 1\ \text{mm}$) of 6:1 PDMS and baked at $80\ ^\circ\text{C}$ for 5 min. A thin layer of 15:1 PDMS was spin coated on the fluidic layer mold at 1300 RPM for 1 min. The device was designed such that the valve regions on the device were placed in areas surrounded by shallow fluidic channels, ensuring uniform coverage of these regions with a thin layer of PDMS. The PDMS on the fluidic layer mold was then baked at $80\ ^\circ\text{C}$ for 4 minutes. The PDMS was removed from the control layer mold, cut to match the size of the fluidic layer, and aligned with baked PDMS layer on the fluidic layer mold under a stereoscope. The fluidic layer mold with the aligned control layer was baked at $80\ ^\circ\text{C}$ for 5 min to promote adhesion between the control layer and the fluidic layer. Following this, 49.5 g of 10:1 PDMS was poured on the fluidic layer mold, covering all features on the fluidic layer mold with a 3-4 mm thick layer of PDMS. The fluidic layer mold was then baked for at least 20 minutes at $80\ ^\circ\text{C}$. Following this, the PDMS was removed from the fluidic layer mold and individual devices were cut. Fluidic access holes were punched into individual chips with sharpened needles (20 gauge; McMaster-Carr, Elmhurst, IL), bonded to thickness #1 cover glasses ($24\ \text{mm} \times 60\ \text{mm}$, thickness = ~ 0.13 to $0.16\ \text{mm}$; Ted Pella, Inc., Redding, CA) following O_2 plasma treatment (30 W, 500 mTorr, 45 s), and immediately baked at $80\ ^\circ\text{C}$

for at least 5 min to finalize device fabrication. All devices were subsequently treated with Aquapel (Pittsburgh Glass Works LLC, Pittsburgh, PA) to render their surface hydrophobic and fluorophilic [38]. Aquapel-treated devices were then dried at 80 °C for at least 1 hour prior to use.

4.2.4 Experimentation

A set of solenoid valves was used to control the on/off status of the individual microvalves in the microfluidic device. Connections between solenoid valves and microvalves were established via water-filled Tygon® microbore tubing (0.02-inch ID and 0.06-inch OD; Cole-Parmer, Vernon Hills, IL) with 23-gauge blunt needles (McMaster-Carr) inserted at designated valve holes. Microvalves were typically pressurized at ~40 psi. Valve operation sequences were programmed and controlled by custom software written in MATLAB (MathWorks, Natick, MA). This software allowed us to execute a predetermined sequence of valve actuation with independent time control for each actuation. The opening of a valve corresponding to an input on the device led to the injection of a sample fluid from that inlet into a central channel on the device. The volume of this droplet could be precisely controlled through variation of the opening time of the valve as well as the back pressure [62].

The carrier oil used to maintain the separation between sample plugs consisted of a perfluorocarbon FC-40 (3M, Two Harbors, MN) and a nonionic fluorosoluble surfactant 1H, 1H, 2H, 2H-Perfluoro-1-octanol (Sigma-Aldrich) (4:1 v/v). The carrier oil was loaded into Tygon microbore tubing and connected to the device via the designated oil inlet. Prior to generation of sample and reagent droplets, the carrier oil was injected to fill and prime the entire central fluidic channel. The testing of our platform was performed using a PCR buffer (1× Gold PCR buffer; Thermo Fisher Scientific, Waltham, MA) and food dyes (Ateco, Glen Cove, NY) as surrogates for different samples and reagents in order to enhance visualization. All samples and reagents were loaded into PTFE tubing (30 AWG; Cole-Parmer) and connected with the device through their designated inlets. All reagent input channels on the device were primed with the respective reagent. Any residual reagents in the central carrier fluid channel following this process were flushed out using the carrier oil. All the inputs on the device were kept

under constant pressure, with separate input pressures for the carrier oil (10 psi), sample inlets (5 psi), and all four reagent inputs (3 psi).

4.2.5 Data Acquisition and Analysis

Droplet generation, bifurcation, and fusion were observed with an inverted microscope (IX71; Olympus Corp., Japan) with either a 1.25 \times magnification objective lens (Olympus PlanAPO N 1.25 \times /0.04NA) or a 4 \times magnification objective lens (Olympus UPlanFl 4 \times /0.13NA). A digital single-lens reflex (DSLR) camera (EOS 60D; Canon, Inc., Japan) that was mounted on the microscope and interfaced via EOS Utility software was used to take images and videos of device operation. Screenshots were taken from videos via VLC media player (VideoLAN). Images were imported in ImageJ [140] and processed using its built-in functions. The area of the droplet was measured via the “Threshold” and “Analyze Particles” functions in ImageJ. Dusts and shadows on the images, which did not affect the generation, bifurcation, and fusion of droplets were digitally removed via Adobe Photoshop. Furthermore, the tone and the contrast of the images were also enhanced via Adobe Photoshop.

4.3 3. Results

4.3.1 Device Design and Workflow

We have designed a microfluidic device to support parallelized combinatorial droplet workflow (Figure 2). The microfluidic device employs a two-layer architecture where the flow of oil, sample droplets, and reagent droplets in the fluidic layer (Figure 2, blue) is regulated by designated microvalves in the valve layer (Figure 2, red). The fluidic channel – where the droplet generation, bifurcation, fusion, and detection occur – undergoes several splits, connects with reagent inlet channels, and eventually divides into 16 channels with the same length and hence the same fluidic resistance. The most upstream inlet is reserved for the carrier oil, which drives all flow on the device. Downstream to the oil inlet are two sample inlets with corresponding rinsing channels (Figure 2, insert micrograph 1) connected to the central carrier oil channel. Two pressure relief channels near the sample inlets ensure the uniformity of sample droplets by

decoupling droplet generation from fluidic resistance of the incubation channel. The central carrier oil channel splits into two identical halves at a bifurcating Y-junction (Figure 2, insert micrograph 2). For all four stages of bifurcation Y-junctions, the angle is 45° and the two outgoing channels shrink in width by a factor of $\sqrt{2}$ (e.g., for the first stage of bifurcating Y-junction, the single incoming channel has a width of $200\ \mu\text{m}$ and each of the two outgoing channels has a width of $140\ \mu\text{m}$) [133, 134]. After the first two stages of bifurcation, each of the four resulting fluidic channels is connected with a reagent channel that is individually controlled by a microvalve for programmable reagent injection (Figure 2, R1 – R4; insert micrograph 3). Importantly, in the general reagent injection area, the cross-section of fluid channels are designed such that the sample daughter droplets can be elongated to be several-fold longer than the width of the reagent inlet channel. As such, reagents can be directly injected into the sample droplets and fused, removing the need for droplet synchronization. Each fluidic channel subsequently goes through two additional bifurcating Y-junctions, resulting in 16 serpentine incubation channels to accommodate four replicates of the four different reaction conditions. Leveraging droplet splitting to produce replicates, which is important in all biochemical experiments, obviates serially generating replicates and thus enhances device throughput. All incubation channels are designed to have the same length to ensure equal fluidic resistance, which is critical for droplet uniformity. Finally, at the detection zone, the pitch between adjacent channels decreases to $50\ \mu\text{m}$ such that all 16 $50\text{-}\mu\text{m}$ -wide incubation channels can be viewed within a microscope viewing area (using a $4\times$ objective lens), thus facilitating parallel detection via microscopy (Figure 2, insert micrograph 4).

In our device, droplet bifurcation and subsequent parallelized reagent injection, droplet fusion, and droplet detection are performed in a streamlined workflow to maximize the throughput. Here, all microvalves are kept under positive pressure so that they are normally closed; they are opened on-demand to achieve injection. The carrier oil, samples, and reagents are pre-loaded into their designated inlets and are kept under constant pressure, so that when microvalves are opened, these fluids can be injected to form and subsequently maneuver droplets. Sample droplets are first generated by briefly opening the sample microvalve, and upon closing the sample microvalve and opening the oil microvalve, are pushed through the first two stages of bifurcating Y-junctions,

producing a total of four identical daughter droplets. As the sample droplets flow through the reagent injection region, the four reagent microvalves are opened momentarily to inject reagents directly into elongated sample daughter droplets and achieve droplet fusion. Fused sample-reagent droplets go through two additional bifurcating Y-junctions such that each injection of sample and reagents results in a total of 16 droplets (four replicates of four different conditions). Each daughter droplet then flows through its serpentine incubation channel and arrives simultaneously with all other daughter droplets in the same group at the detection zone, thus facilitating parallel detection via microscopy (see Supplementary Video S1). Notably, the volume of fused droplets is controlled to span the cross-section of all fluid channels, as this is critical to maintain the spatial indices of all droplets.

4.3.2 Uniform Droplet Splitting

We have achieved uniform droplet splitting in our device, which is a critical prerequisite to the parallelized operation of our device. To demonstrate this, we generated a series of droplets (volume = ~ 10 nL; frequency = 0.5 Hz) with black food dye as the sample because this dye produces sharp color contrast and is empirically found to travel through the device with minimal sticking, and thus facilitates downstream operation and analysis. We then allowed them to travel downstream and continuously bifurcate through four stages of bifurcation Y-junctions. By recording videos of droplet splitting at all Y-junctions and extracting screenshot images from the videos, we clearly observed droplets splitting into two even halves as they flow through a bifurcation Y-junction (Figure 3A). To quantitatively analyze the bifurcation performance across the four bifurcation stages, we used image analysis software to measure the areas of the pair of split droplets after splitting at each of the 15 Y-junctions and calculated the ratio of the area of each droplet over the combined area. As such, an area ratio of 50% for both daughter droplets indicates even droplet splitting. The area ratio of daughter droplets at the four different stages and the 15 Y-junctions consistently remained at $\sim 50\%$ (Figure 3B; $n = 10$ for each Y-junction), indicating uniform droplet splitting. Furthermore, uniform droplet bifurcation across the different stages of Y-junctions validates that Y-junctions enable

uniform droplet splitting even with different Y-junction channel dimensions and droplet volumes.

Of note, in order to achieve uniform droplet splitting, it is critical to maintain the same fluidic resistance across all fluidic channels that flow in parallel. Here, we have carefully examined our devices to ensure the fluid channels are free of obstructions due to defects in the master mold. We have also found a potential source for severely increasing the fluidic resistance of a particular fluid channel is an overlaying valve control channel, as that may cause the fluid channel to sag down and increase the fluidic resistance. In our design, we have avoided overlaying valve control channels on top of fluid channels. For the only occurrence, we designed the valve control channel to overlay the four fluid channels equally, and we narrowed the valve control channel to prevent it from sagging into the fluid channels. Finally, we have designed filter structures at all sample and reagent inlets to prevent channel clogging, which can also severely increase the fluidic resistance of a particular fluid channel and disrupt droplet splitting.

4.3.3 Parallelized Injection of Reagents with Individualized Calibration

We have designed our device to simultaneously inject multiple reagents in parallel. To demonstrate this capability, we pre-loaded each reagent inlet with a different color of food dye (orange, green, blue, and black in this case) and simultaneously actuated the microvalves that control the reagent inlets to form four reagent droplets in parallel. Indeed, a simultaneous actuation of all four reagent microvalves resulted in four independent reagent droplets in their respective channels (Figure 4A).

Importantly, the individually controlled reagent inlets in our device allow us to calibrate each inlet independently and to ensure consistent and accurate volume injection across parallel reagent channels. This design feature is important because the microvalves in our device, which are based on PDMS membranes, can vary in thickness as a result of the soft lithography fabrication process. Moreover, variations in reagent viscosity can lead to variability in droplet sizes as well [141, 142]. To show that we can use our individually addressable reagent inlets to correct reagent droplets that may have different sizes due to the aforementioned differences, we deliberately used four different colors of food dye (orange, green, blue, and black) as the reagents. When the four reagent

microvalves were opened with an identical opening time (e.g., 30 ms), the four resulting droplets could differ by as much as 44% in normalized droplet area (Figure 4B). Based on visually observing the initial size of the reagent droplets, we subsequently shortened or lengthened the opening time for each reagent microvalve. With such simple adjustments, we were able to generate reagent droplets with significantly improved uniformity; the variation in normalized droplet area reduced to < 12% (Figure 4C). Further improvements in the uniformity could be achieved by performing a few iterations of measuring the droplet areas via image analysis before fine-tuning the microvalve opening time.

4.3.4 **Reliable Droplet Fusion in Parallel**

Having demonstrated uniform droplet splitting and uniform reagent injection in parallel, we subsequently combined these two functions and demonstrated robust, parallelized fusion of sample and reagent droplets. We first confirmed reliable droplet fusion visually and qualitatively by using a polymerase chain reaction (PCR) buffer as the sample (due to its clear color and negligible sticking to the device) and four different colors of food dye as the four reagents. Here, we generated a series of sample droplets at ~0.25 Hz and moved them through the first two bifurcation stages. Importantly, our design enforced an elongated shape for each of the four bifurcated daughter droplets as they traveled past the four reagent inlets, thus allowing us to directly inject reagents into them for robust droplet fusion (Figure 5; also see Supplementary Video S2). Of note, we tuned the back pressure applied to the reagent inlets to prevent fission of sample droplets during reagent injection. In addition, our design gradually widened the channels immediately downstream to the reagent channels, which caused droplets to slow down following reagent injection and facilitated fusion of sample and reagent droplets that may not have fused at the time of reagent injection.

Parallelized fusion of sample droplets and reagent droplets was observed to maintain an efficiency of nearly 100% in our device. We quantitatively evaluated the fusion performance in all four channels of our device by performing the same droplet fusion experiment but using only the black food dye as the reagent in all four reagent channels in order to minimize potential experimental variations due to the viscosities of different

food dyes. Using video and image analysis to evaluate the droplet fusion in all four channels, we defined droplet fusion efficiency as the ratio between fused droplets and all droplets after the fusion step. The fusion efficiencies were between 98.1% (n = 52), 99.1% (n = 107), 99.1% (n = 107), and 94.5% (n = 55) for the four channels, indicating reliable droplet fusion. These results show that droplets could be reliably fused without having to pause momentarily at the reagent inlets. Such capacity for continuous yet reliable droplet fusion thus presents key feature for enhancing the throughput in our device.

4.3.5 Parallelized Droplet Imaging

We used microscopy to simultaneously image and hence analyze fused droplets in all 16 incubation channels. This imaging approach for parallelized detection is facilitated by designing the detection zone of the device to fit within the field of view of microscopes (under 4× microscope objective lens). To show parallelized droplet detection, we generated multiple groups of 16 droplets (four replicates of the four sample-reagent combination) and imaged them at the detection zone. Here, due to uniform droplet splitting, uniform reagent injection, and robust droplet fusion, the 16 droplets in each group had uniform sizes. For example, the droplet sizes in group 1 had only an 8.0% standard deviation and remained uniformly sized in group 20, with a standard variation of 6.6% (Figure 6). Importantly, the droplets traveled at relatively the same speed through their own incubation channels and thus allowed their spatial indices to be maintained. Indeed, for the droplets in group 1, we measured that the 16 droplets varied by only as much as 3.67 mm in position after traveling through the 100-mm-long incubation channels, equivalent to a 3.67% variation. For the droplets in group 20, the 16 droplets mostly maintained their positional orders relative to each other while the maximum difference in position was only 3.46 mm. We note that, because the detection area is only 2.5 mm in length, we combined and aligned two screenshots in order to measure the position of all 16 droplets in each group. Nevertheless, these results showed that the droplets in the parallel detection area could indeed be tracked via spatial indexing.

4.4 Discussion

The highly parallelized reagent assembly approach described in this work presents an alternative approach to device architecture for droplet microfluidics. Devices employing shear-flow droplet generation has capacity for extremely high throughput, but their limited capacity for in-line combinatorial assembly of reagents has confined their utility to simple, throughput-based applications such as digital PCR. Our parallelized design presents an alternative architecture with greater flexibility for reagent assembly, while demonstrating the potential for parallel processing to bridge the gap in throughput. For example, even operating under a conservative 0.25 Hz generation rate for sample droplets, which equates to a 4 Hz generation rate for fused sample-reagent droplets, a single parallelized combinatorial droplet device is capable of detecting nearly 0.35 million fused droplets per day. As such, this device has the potential to meet the need for high-throughput screening applications.

Maintaining balanced fluidic resistance across all fluidic channels in parallel is critical to robust long-term operation of our parallelized combinatorial droplet device. Increases in fluidic resistance in a single incubation channel may cause sample droplets to split unevenly at the first two stages of bifurcating Y-junctions and travel through these junctions at different speeds, which may subsequently disrupt droplet fusion and ultimately lead to operation failure. In this work, we have carefully removed potential sources for increasing the fluidic resistance in our devices, such as obstructions in fluidic channels and overlaying valve control channels. In addition, we observed that the reagent viscosity may also be important to device operation. For example, sample droplets that fused with a more viscous food dye tend to travel slower through the incubation channels when compared to those that fused with a less viscous food dye. Such differences can also lead to unbalanced fluidic resistance in the device. As such, implementing reactions involving reagents that vary in viscosities in the droplet format in our parallelized combinatorial droplet device may require additional characterization steps to ensure reliable operation.

We envision several routes towards improving our device. For example, for proof of concept, we have only implemented two stages of bifurcation prior to parallelized injection of four reagents. In our future iterations of the device, we envision increasing the number of bifurcation stages to three or four and the number of reagent channels to 8

or 16. For each reagent channel, we can further implement multiple reagent inlets. Thus, with the two post-fusion bifurcation stages for droplet replication, we can effectively improve the overall throughput of combinatorial droplet devices by 64-fold and beyond. We also plan to integrate sample inlets of the device to our previously reported serial sample loading system [143] so that the device can accept an unlimited number of samples from multi-well plates. Temperature-controlled heaters can be readily appended to the incubation region of the device to enable a host of biochemical assays that require elevated temperatures. Finally, we can implement wide-view imaging [33] to increase the area of detection and hence the capacity for parallel detection of droplets in our device.

4.5 *Conclusions*

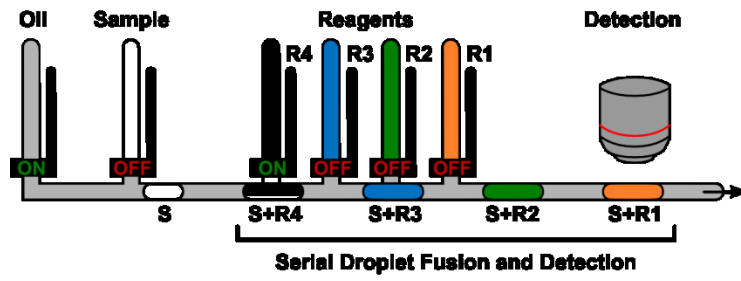
In summary, we present a parallelized combinatorial droplet device that enhances device throughput via droplet bifurcation, parallelized reagent injection, and parallelized droplet detection. We demonstrate that microfluidic droplets can split evenly at all Y-junctions across all four bifurcation stages in our device. We also show that we can simultaneously inject four independent reagents into their respective channels with equal volume, which can only be done by adjusting the valve opening time of each individually-addressable microvalve. Furthermore, we validate that sample and reagent droplets can be reliably fused in a continuous manner, which further enhances the device throughput. Finally, the fused sample and reagent droplets maintain their spatial indices and can be imaged in parallel via microscopy. Taken together, we have successfully parallelized the once-serial operation in combinatorial droplet devices and have improved the device throughput by 16-fold. Given its current performance and prospect for future improvements, we believe the parallelized combinatorial droplet device has the potential to meet the demand as a flexible and cost-effective tool that can perform high throughput screening applications.

4.6 *Acknowledgments*

We thank Dong Jin Shin for his valuable comments and feedback on this manuscript. We also thank the funding support from DARPA (Micro/Nano Fluidics Fundamentals

Focus (MF3) Center), National Institutes of Health (R01CA155305, U54CA151838, R21CA173390), National Science Foundation (0967375, 1159771), and DuPont Pioneer.

(A) Traditional Design (Serial Operation)



(B) Improved Design (Parallel Operation)

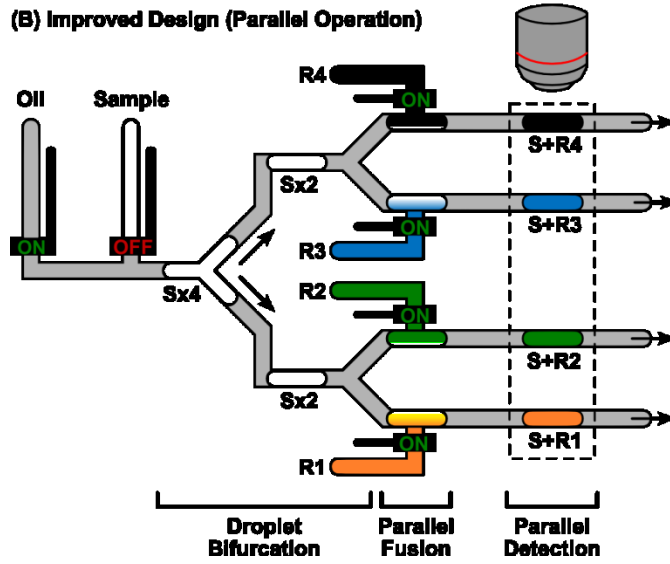


Figure 4.1. Improving Throughput of Combinatorial Droplet Devices via Parallelization.

(A) In the traditional design, sample droplets (S) are fused with designated reagents (R1 – R4) one at a time to generate the train of combinatorial droplets (S + R1, etc.), which maintain their spatial index within the single channel before they are sequentially optically detected. (B) The current design leverages parallelized operation via droplet bifurcation, parallel reagent injection, and parallel detection to improve the throughput. Specifically, each sample droplet first travels through bifurcating Y-junctions (two stages as shown here) and split into identical daughter droplets (four as shown here) before each daughter droplet is fused with its designated reagent via direct injection. Importantly, the reagents can be simultaneously injected into the daughter droplets, thereby facilitating improved throughput. Finally, detection of fused droplets can be performed one group at a time, further ensuring high-throughput operation within the device.

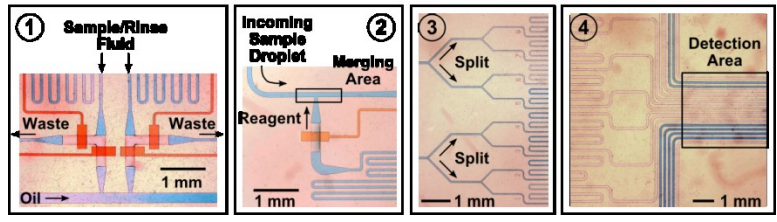
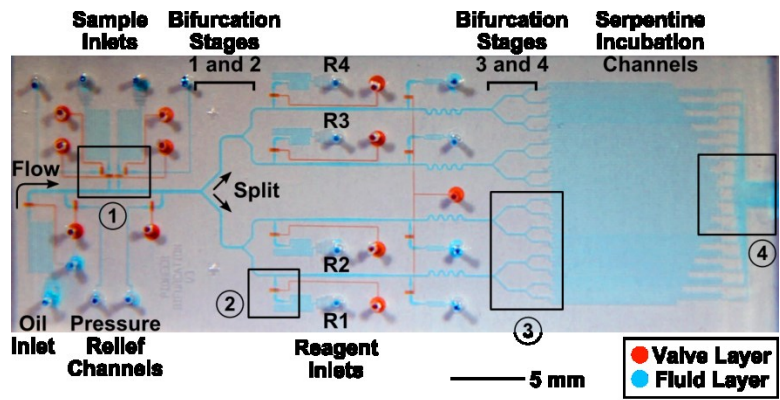
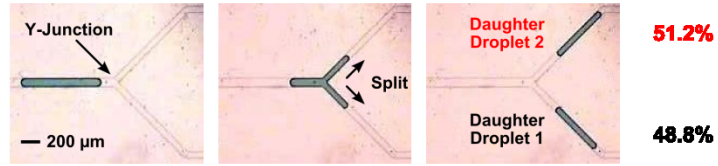


Figure 4.2. Parallelized Combinatorial Droplet Device.

The microfluidic device employs a two-layer architecture where the flow of oil, sample droplets, and reagent droplets in the fluid layer (blue) is regulated by designated valves in the valve layer (red). The most upstream inlet is reserved for the carrier oil, which drives droplet formation and flow. Downstream to the oil inlet are two sample inlets with corresponding rinsing channels (insert micrograph 1) connected to the fluid channel. The fluid channel splits into two identical halves at a bifurcating Y-junction and each of the four resulting fluid channels is connected with a reagent channel that is individually controlled by a microvalve for programmable reagent injection (R1 – R4; insert micrograph 2). In our device, reagents can be directly injected into the sample droplets and fused, removing the need for droplet synchronization. Each fluid channel subsequently goes through two additional bifurcating Y-junctions (insert micrograph 3), resulting in a total of 16 serpentine incubation channels to accommodate four replicates of the four different reaction conditions. Finally, at the detection zone, the pitch between adjacent channels decreases such that all 16 channels can be viewed within a microscope viewing area, thus facilitating parallel detection via microscopy (insert micrograph 4).

(A) Before Bifurcation During Bifurcation After Bifurcation Area Ratio



(B)

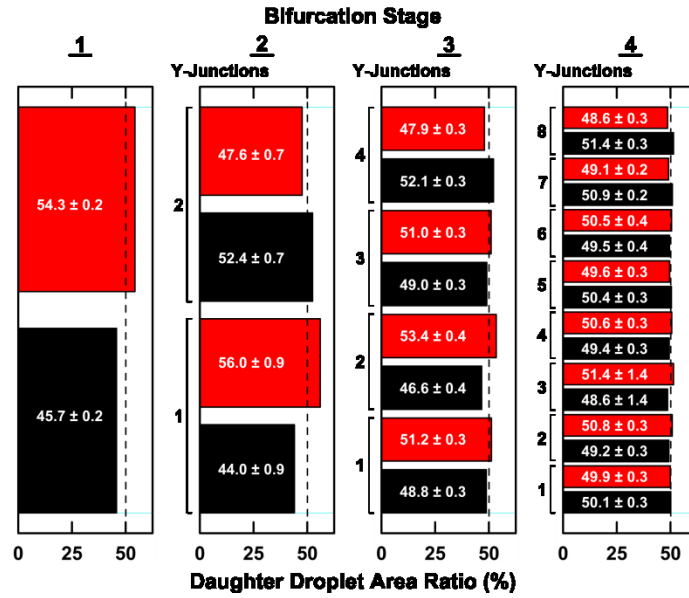


Figure 4.3. Uniformity of Droplet Bifurcation.

(A) In our device, microfluidic droplets split into two equal halves as they flow through a bifurcating Y-junction. To quantitatively analyze the bifurcation performance at the Y-junction, we measure the areas of the pair of daughter droplets after splitting and calculate the ratio of the area of each daughter droplet over the combined area of the two droplets. (B) We measured ~50% area ratio for all daughter droplets across the four bifurcation stages and the 15 Y-junctions (n = 10 for each Y-junction), suggesting that uniform droplet bifurcation is independent of channel dimensions and droplet volumes.

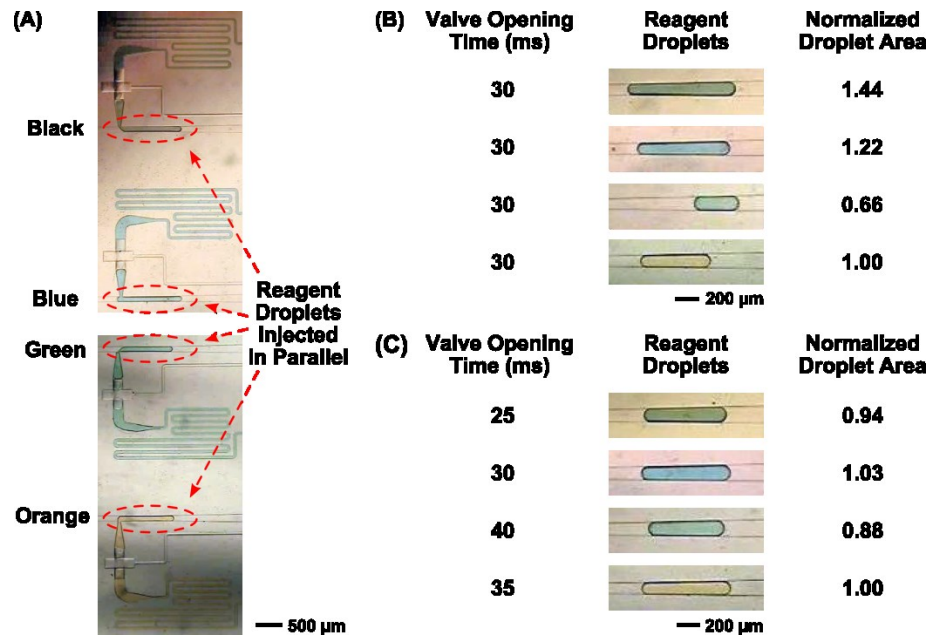


Figure 4.4 Parallelized Quadplex Injection of Reagent Droplets with Capacity for Individualized Calibration.

(A) Parallelized injection of multiple reagents can be readily achieved in our device, as a simultaneous actuation of all four reagent microvalves results in four independent reagent droplets in their respective channels. (B) Variations in reagent inlet microvalves and differences in the viscosity of food dyes can lead to reagents droplets with different sizes. For example, when we injected four different colors of food dyes with an identical microvalve opening time (*e.g.*, 30 ms) the four resulting reagent droplets can differ by as much as 44% in normalized droplet area. (C) By adjusting the microvalve opening time of each individually-addressable reagent microvalve, reagent droplets with significantly improved size uniformity can be generated.

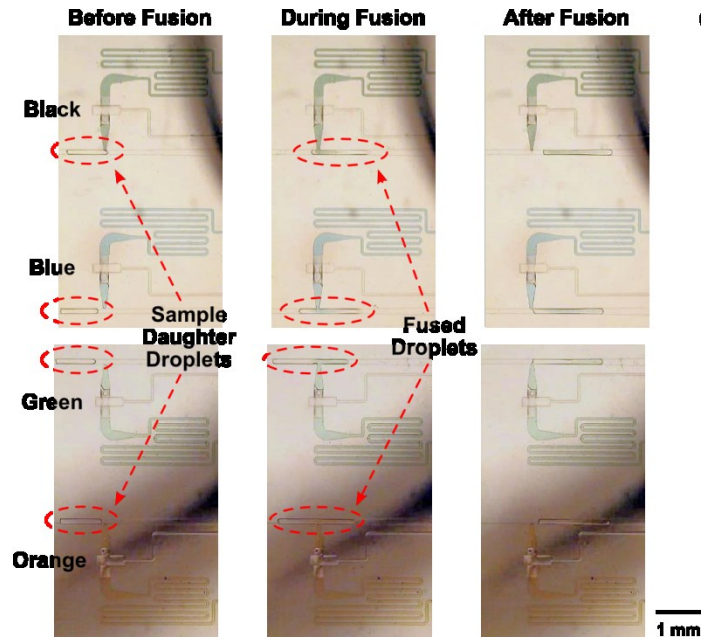
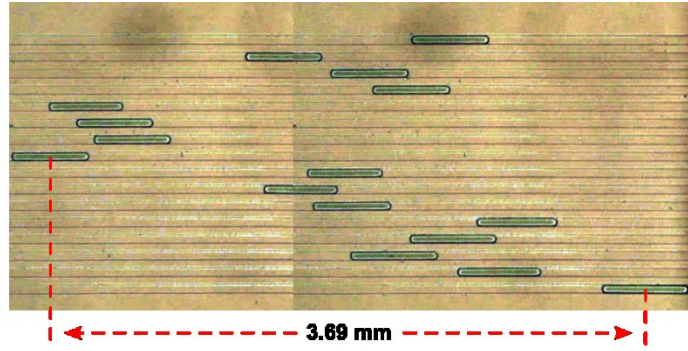


Figure 4.5. Parallel Fusion of Sample Droplets with Reagent Droplets.

In our device, the four split sample droplets (after two bifurcations) maintain an elongated shape as they travel past the four reagent inlets, allowing direct injection of reagents into them for robust droplet fusion simultaneously in all four channels.

Group 1



Group 20

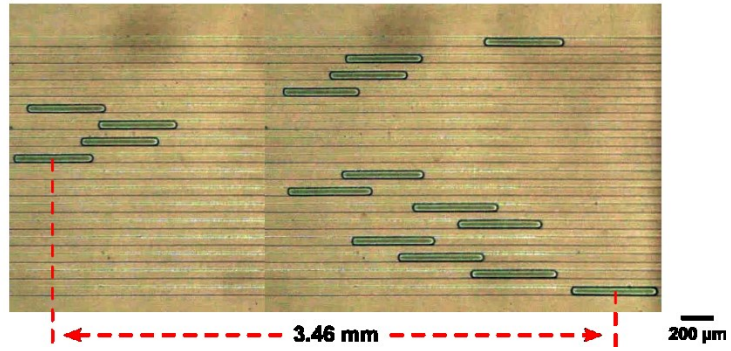


Figure 4.6. Imaging-Based Parallel Detection of Fused Droplets.

We generate multiple groups of 16 droplets (four replicates of the four sample-reagent combination) and image them at the detection zone via microscopy. Even droplet bifurcation, uniform reagent injection, and robust droplet fusion enable size uniformity for the 16 droplets. For example, the droplet sizes in group 1 and group 20 have only a standard deviation of 8.0% and 6.6%, respectively. Furthermore, the droplets travel at relatively the same speed through their own incubation channels and thus allow their spatial indices to be maintained. Indeed, for the droplets in group 1, the 16 droplets vary by only as much as 3.69 mm in position after traveling through the 100-mm-long incubation channels, equivalent to a 3.69% variation. For the droplets in group 20, the 16 droplets mostly maintain their positional orders while the maximum difference in position is only 3.46 mm.

5

A Nano Sample Processor for Genotyping

of Plant Samples for Marker-Assisted Selection

Maintaining global crop production is critical to human survival. As threats to the global food supply continue to mount, multinational seed companies are turning to genomics to accelerate the rate of crop improvement. DNA marker technology offers great promise in plant breeding. The key to wide-spread adoption of molecular breeding is the availability of flexible and cost-effective tools that can perform high-throughput genotyping to guide the crop development process. Towards that end, we have developed and demonstrated a programmable droplet-based microfluidic device for genotyping of Maize genomic DNA. A unique component of the microfluidic platform is the Nano Sample Processor (NSP), which overcomes traditional limitations associated with microfluidic devices. The NSP is a novel architecture which is capable of introducing an unlimited number of plant samples onto a microfluidic device for genotyping analysis.

5.1 Introduction

In the imminent future, the agriculture industry will have to maintain the stability of the global food supply despite exponential population growth [144]. The complexity of this task will be exacerbated by the decrease of arable land, emergence of new pests, and abiotic stress due to changing climate patterns [145]. In anticipation of this task, there has recently been a global concerted effort to collect, store, and characterize crop species [146]. In addition, sales of genetically modified (GM) crops have increased. In GM crops, genes are artificially inserted using genetic engineering techniques. A panel of genes may be inserted or a single gene may be overexpressed. Another modern-day approach to developing new crops is genomic selection (GS), in which genetic information informs the breeding process. In GS, a large plant population is screened and

genetic material intrinsic to a prospective plant is used. The plant varieties developed by this selective breeding are referred to as cultivars. Multinational seed companies are increasingly turning to genomic selection (GS) to fast-track the plant breeding process [147] instead of spending years physically identifying plants with desired traits. By allowing companies to sidestep the process of growing plants in the nascent stages of cultivar development, GS reduces costs and accelerates the crop discovery process. Furthermore, GS is profoundly different from genetic engineering technologies, in that GS allows scientists to harness natural biodiversity as opposed to artificially introducing traits. The burgeoning interest in molecular plant breeding has created a significant need for affordable, rapid, high-throughput genotyping technologies [146]. In GS, Single Nucleotide Polymorphisms (SNPs) are often chosen as molecular markers because of their abundance throughout the genome and stability over generations [148, 149]. Furthermore, the bi-allelic nature of SNPs facilitates allele calling and data storage [146].

The agriculture industry has already taken steps [150, 151] towards miniaturizing high-throughput genotyping. Microarrays are often used in SNP genotyping and rely on fixed sets of markers [152-154]. Array-based systems boast high multiplexing capacity. Often “universal” designs for a range of germplasms are used. To ensure applicability of designs across multiple species requires a large collection of SNPs, thereby increasing costs and the likelihood of ascertainment bias [146]. Other genotyping systems have been introduced to the market [138, 155-157]. Array TapeTM Technology (Douglas Scientific) is considered state-of-the-art and is used by large multinational seed companies [146]. This technology processes spools of Array TapeTM for assay setup, PCR, and fluorescent detection – genotyping up to 150,000 data points per day. Each individual reaction is 1.6 μL , which represents a 68% volume reduction compared to standard plate-based systems, which use at least 5 μL reaction volumes. However, the requirement for separate modules for liquid handling, thermocycling and detection impedes complete automation and increases costs. Because these aforementioned methods do not offer flexibility and use a large volume, they do not meet the requirements as an affordable, flexible, genotyping platform for agricultural applications.

Droplet microfluidics has the potential to satisfy the unmet needs for increased miniaturization, scalability and automation in genotyping. Each droplet is analogous to a

microcentrifuge tube and is separated by an immiscible carrier fluid, typically oil. The volume of droplets is typically 10^3 - 10^6 fold lower than those used in conventional bench-top techniques, drastically reducing cost. Droplets can be generated at kilohertz rates [158]. The utility of droplets has been demonstrated in applications ranging from single-cell [116, 159-161] and single-molecule analysis [114, 162] to particle synthesis [163-165]. Yet, limitations remain which prevent wide-spread adoption of droplet platforms, particularly for genotyping in agricultural applications. Firstly, a microfluidic device can at most accommodate 10-30 inlet channels due to small device footprint, thus limiting the number of samples that can be genotyped. The second obstacle is the ability (or lack thereof) of droplet devices to perform combinatorial operations. For example, genotyping applications require 10's or 100's of markers to be screened against millions of DNA samples. Currently, microfluidic devices excel at generating large populations of droplets of identical composition, but are less adept at performing the types of combinatorial operations that genotyping reactions require. Inherent to this concern is the lack of reliable fusion methods of sample droplets and reagent droplets. Several techniques to merge droplets have recently been proposed, including the picoinjector [105, 166] and electrocoalescence [167]. Electrocoalescence does not meet the requirements for robustness, because it requires precise synchronization of droplet streams. Flexibility is limited because electrocoalescence can only merge pre-formed droplets, and thus the ratio of the sample droplet to reagent droplets is fixed. In addition, both the picoinjector and electrocoalescence require optical barcodes to identify individual library compounds. Such barcodes place restrictions on the combinatorial screening power of platforms which utilize picoinjectors or electrocoalescence in droplet fusion modules.

Herein, a droplet-based platform for programmable SNP genotyping in agriculture is presented (Figure 1A). A microfluidic chip (Supplementary Figure 1) featuring the Nano Sample Processor was designed to accommodate a screening assay (Invader[®]) used commonly in large multinational seed companies. Using this platform, we demonstrate multiplexed genotyping of a library of Maize samples. To the best of our knowledge, this is the first time that the Invader[®] assay has been performed in a microdroplet format. The Nano Sample Processor (NSP) (Figure 2B) allows for a single sample inlet to process an

unlimited numbers of samples. We employ a fusion method which exploits local channel geometry for synchronization-free injection of reagents into each sample daughter droplet [62]. Furthermore, droplets are indexed by their order in a 1D array, enabling the identification of the each droplet. Spatial indexing obviates the need for an optical barcoding scheme [62]. Our device operates in a continuous flow fashion: as droplets are being generated, droplets further downstream are simultaneously being incubated, and near the outlet of the device, in-line fluorescent read-out of droplets is occurring. Because of continuous flow operation (assembly-line), its potential throughput is higher than array-based systems (batch processing) because idle time is eliminated. By incorporating novel design aspects such as the Nano Sample Processor, traditional limitations – which often relegate droplet devices to the analysis of large droplet populations with identical composition – are overcome.

5.2 *Materials and Methods*

5.2.1 **SNP Genotyping Workflow:**

The entire workflow is presented in Figure 1A. A short summary is presented here and each of the steps are discussed in more detail below. DNA was extracted from Maize leaf tissue or seed. DNA extraction was followed by 10-plex PCR amplification for 30 cycles. Following PCR-based amplification, samples were denatured to deactivate the Taq DNA Polymerase and snap-cooled for at least 5 minutes. Amplified Maize DNA was loaded onto the microfluidic device via the Nano Sample Processor (Figure 2B). DNA droplets (~ 5 nL) were generated and fused with SNP interrogating probes and Invader[®] reaction mix (~45 nL). DNA-probe droplets were incubated for ~20 minutes at 63 °C as they moved throughout the incubation channel. In-line biallelic readout was performed using a two-color fluorescence spectroscopy detection system. Each fluorophore corresponded to a different allele for each SNP site interrogated. This reaction enabled coincident detection of two alternative alleles present at a single SNP site for a particular cultivar. Raw fluorescence data in both channels was APD corrected. Average droplet intensities of droplets were subsequently normalized. The ratio of FAM/RED signal was then used to determine the final allelic call out for that specific DNA sample.

5.2.2 Multiplexed PCR:

DNA targets were extracted from 8 Maize samples. The crude DNA extracts were amplified using multiplexed PCR prior to the Invader[®] assay. Reagents for the multiplexed PCR included FastStart Taq DNA polymerase (Roche), 10x PCR gold buffer with 20 mM MgCl₂ (Roche), 10 mM dNTPs (Roche), and corresponding primers (IDT). The multiplexed PCR reaction contained 10 primer pairs. The reaction amplified 10 multiplex loci simultaneously (Supplementary Figure 4). Reagents were heated at 95 °C for 600 seconds and then thermocycled for 30 cycles: 95 °C for 30 seconds, 55 °C for 90 seconds, 72 °C for 150 seconds. After thermocycling, a final extension step was executed at 72 °C for 300 seconds. Prior to the SNP Invader[®] assay, genomic DNA targets were denatured at 100 °C for 20 minutes, snap-cooled, and then kept on ice until use.

5.2.3 Invader[®] Assay Chemistry:

The Invader[®] Assay (Figure 1B) utilizes two simultaneous isothermal amplification assays in a biplex format [168]. In the primary reaction, both the Invader[®] oligonucleotide and primary probe hybridize to the target of interest. An invasive structure is formed from the single-base overlap. This forms a 3-dimensional structure that is recognized by an enzyme which cleaves the 5' Arm of the primary probe. In the secondary reaction, the 5' arm of the probe binds to the FRET cassette. In this secondary FRET reaction, this structure is recognized by an enzyme which cleaves the fluorophore and a fluorescent signal is generated. The combination of both reactions can provide a ~10 million fold signal amplification. One cost advantage of the Invader[®] reaction is that it utilizes generic FRET cassettes, obviating the need for expensive TaqMan[®] chemistry that is customized for each sequence.

5.2.4 Off-chip SNP Genotyping Invader[®] Assay (Synthetic and Genomic Targets):

In the assay design stage, 10 polymorphic markers of interest were identified and selected. For markers 4, 5, 6, 7, and 9, synthetic target sets complementary to the probes

were manufactured by Integrated DNA Technologies (Coralville, Iowa) for initial testing. Each synthetic target set consisted of two oligos, “A” and “B”, one for each SNP allele. For all 10 markers, the Invader® probes were designed by Third Wave Technologies. The genomic targets consisted of DNA extracted from Maize seed. All genomic targets evaluated were known to be homozygous. For the genomic targets, the amplified PCR product (SNP) was used in the Invader® Assay SNP genotyping reaction. For off-chip experimental results, concentrations identical to those being compared in the droplet format were generated in 10 µL reactions in a 96-well plate. The fluorescence from the 96-well plate was then monitored on a CFX96 Real-Time PCR detection system (Bio-Rad Laboratories, Inc.). Fluorescence was monitored in FAM (excitation: 450-490 nm and emission: 510-530 nm) and Texas Red (excitation: 560-590 nm and emission: 610-650 nm). The Invader® assay was carried out using corresponding Invader® probes specific to the amplified targets, Cleavase XI FRET mix solution (Third Wave Technologies), Cleavase XI Enzyme solution (Third Wave Technologies) and MgCl₂ solution (Third Wave Technologies).

5.2.5 Hydrophobic Surface Treatment of Microfluidic Device:

To ensure the success of performing Invader® genotyping, droplets needed to flow smoothly throughout the device. In addition, droplet contents had to be retained from droplet generation to detection. This required optimization of the carrier fluid and modification of the surface treatment strategy. PDMS-based droplet microfluidic devices are conventionally treated with a hydrophobic surface treatment. Aquapel (PPG Industries, Pittsburgh, PA) is often used in conjunction with fluorinated carrier fluids [97, 159, 169]. However, Aquapel treatment was observed to be incompatible with the Invader® assay. Namely, Aquapel was found to cause the adsorption of small hydrophobic molecules, including FAM and Redmond Red fluorophores, out of the droplets and onto the PDMS side walls. These effects were more pronounced at elevated temperatures (~63°C), such that the DNA-Probe droplets could no longer be distinguished from the carrier phase (Supplementary Figure 3). Thus, the device fabrication was modified such that the control layer was below the fluidic channels.

Because PDMS is innately hydrophobic, no additional hydrophobic surface treatment was necessary.

5.2.6 Optimization of Carrier Fluid, Additives, and Surfactants:

Optimization of carrier fluid was performed for the droplet-based Invader[®] assay. Different mixtures of fluorinated oils, including: FC-40, FC-3283, HFE-7500 and Perfluorooctanol were evaluated. The addition of bovine serum albumin was found to improve small hydrophobic molecule (and thus fluorophore) retention within droplets. These results were consistent with those found in the literature [170]. However, BSA caused droplet sticking in the channels. A mixture of FC-40 and Perfluorooctanol (4:1 v/v) offered the optimal balance between droplet stability and small molecule retention among the carrier oils and surfactants that were evaluated.

5.2.7 On-chip SNP Genotyping Invader[®] Assay (Synthetic and Genomic Targets):

A set of solenoid valves was used to control the on/off status of the individual valves of the control layer on the microfluidic device. The control box was controlled by a MATLAB (Mathworks) program. To interface with the microfluidic device, all reagents were loaded into Tygon[®] microbore tubing (Cole-Parmer) and connected with the device through inlet and valve ports. Valves were pressurized at ~ 15 psi.

Once the control layer was primed, carrier fluid was loaded onto the fluidic layer through the inlet. The carrier phase for our experiments consisted of FC-40 (3M) and 1H, 1H, 2H, 2H-Perfluoro-1-octanol (Sigma Aldrich) (4:1 v/v) and was pressurized at 5 psi. The carrier fluid was allowed to wet the entire length of the central carrier fluid channel prior to droplet generation. All reagent inputs on the device were primed with the respective reagent. Any residual reagents in the central carrier fluid channel following this process were flushed out using the carrier fluid phase through the pressure relief channels.

Next, the valve actuation sequence programmed in MATLAB corresponding to the reagent combinations to be generated on the device was executed. Pressure-relief channels on either side of the droplet preparation region opened during generation to decouple downstream fluidic resistance and droplet volume. The DNA droplet (~5 nL) then entered the droplet preparation region and the carrier fluid flow was halted by

activating an upstream valve. A mixture containing SNP-interrogating probe, enzymes, and FRET cassettes (~45 nL) was injected directly into the DNA-containing droplet. The carrier fluid valve was released, and the droplet exited the preparation region. Subsequent DNA-probe droplets were processed in an assembly-line process. Each DNA sample was screened against a library of 10 SNP-interrogating probes, resulting in a sequence containing 10 droplets of different probe composition per DNA sample processed. Each DNA-probe droplet passed through a serpentine channel to promote mixing of reagents prior to entering the incubation region. The incubation region was maintained at a constant temperature of 63°C. After incubation, in-line fluorescence readout was performed on droplets using dual laser spectroscopy, where fluorescence intensity data was collected and analyzed.

5.2.8 Fluorescence Detection Setup and Data Analysis:

Spectroscopy data was acquired using a custom-built, dual laser excitation (488 nm, 552 nm) and dual emission channel (506-534 nm and 608-648 nm) fluorescence spectroscopy platform [123]. Data analysis was performed using custom scripts written in MATLAB [130]. The leading and falling edge of each droplet were identified as the location in a fluorescence data trace where the signal from the FAM dye reached three standard deviations about the background fluorescence of the continuous phase. Fluorescence data from the Red APD (Redmond Red) was analysed at each droplet location, as identified by the FAM signal. Integration time for photon binning was set at 10 *ms* for all peak counting experiments. For each sample, four data traces were analysed with each trace containing at least 10 visible droplets. MATLAB was used to identify droplets in a data trace and generate the average intensity and standard deviations for each reaction condition across its repeats. The average droplet intensity each droplet was then used to determine the final allelic call out for that specific DNA with probe. The average fluorescence intensity of a DNA-probe combination droplet was divided by the average fluorescence intensity of a probe-only control droplet. Data was analysed according to the following calculation (21):

$$\frac{FAM}{RED} ratio = \frac{\frac{RFU_{FAM_sample}}{RFU_{FAM_average_no_target_control}}}{\frac{RFU_{RED_sample}}{RFU_{RED_average_no_target_control}}}$$

If the FAM/RED ratio was <0.5, the call was determined to be RED. If the ratio was >0.5, the call was FAM. The value of 0.5 was determined as the threshold value by calculating the ratio of FAM/RED NTC droplets after on-chip incubation. The ratio of the raw fluorescence intensities of all individual 10 probes were calculated separately and used in normalization calculations. To easily visualize the data, the log of the FAM/RED ratio is used in the Figures 4 and 5.

$$\log\left(\frac{FAM}{RED} ratio_{RED}\right) < \log\left(\frac{FAM}{RED} ratio_{Threshold}\right) < \log\left(\frac{FAM}{RED} ratio_{FAM}\right)$$

$$\log\left(\frac{FAM}{RED} ratio_{Threshold}\right) = \log(0.5) = -0.301$$

5.3 Results

5.3.1 Droplet-Based Assay Overview:

The purpose of this work is to adapt Maize genotyping assays, which have traditionally been performed in multi-well plates or ArrayTape™, in a highly miniaturized, droplet-based format. For proof-of-concept demonstration, the isothermal Invader® assay was chosen. The workflow of the droplet-based assay is presented in Figure 1. Briefly, genomic DNA extracted from Maize leaf tissue or seed, which was provided to us by our industrial collaborator, was amplified by PCR. PCR-amplified DNA samples were heated to separate double-stranded PCR products and deactivate the Taq DNA polymerase and then snap-cooled before they were sequentially loaded into the microfluidic device via the Nano Sample Processor. In parallel, up to ten distinct Invader® reaction mix – each containing the reaction buffer, MgCl₂, Cleavase, FRET cassettes, and a specific set of Invader® probes that target a specific SNP site of the

samples – were loaded into the microfluidic device via designated reagent inlets. DNA droplets (~ 5 nL) were generated and fused with SNP interrogating probes and Invader[®] reaction mix (~45 nL). Fused DNA-probe droplets were incubated to perform the Invader reaction as they moved through the incubation channel, which was heated to 63 °C by a custom temperature apparatus. This reaction enabled the detection of two alternative alleles present at a single SNP site for a particular cultivar, with each allele corresponding to either a FAM-fluorophore-labelled probe or a Redmond Red (RED)-fluorophore-labelled probe.. Immediately after Invader reaction, droplets flowed through the detection region, where both FAM and RED fluorescence intensities were simultaneously measured using a two-color fluorescence spectroscopy detection system to achieve in-line, bi-allelic detection. After fluorescence signal processing, the ratio of FAM/RED signals was then used to determine the final allelic call out for that specific DNA.

5.3.2 Benchtop verification of Invader assays

The robustness of the Invader[®] assay was first verified by detecting the alleles for all synthetic and genomic DNA samples in bench-top experiments. Here, reaction mixtures containing the reaction buffer, MgCl₂, Invader[®] probes, Cleavase, FRET cassettes, and either synthetic targets or genomic targets were incubated at 63 °C for 30 minutes in a real-time PCR machine while FAM and Redmond Red (RED) fluorescence signals from these reactions were measured every 30 seconds. The results of these bench-top reactions served as an internal control for subsequent on-chip reactions. In addition, the bench-top results were cross-checked with internal data from our industrial collaborator to ensure accuracy.

Synthetic targets were first detected and the method for determining the specific allele was established. In this work, synthetic targets are single-stranded sequences, where targets “A” and “B” differ by only a single nucleotide and correspond to the RED allele and the FAM allele, respectively. In Figure 3A, two real-time Invader[®] amplification curves acquired from the pair of targets and the corresponding Invader probe set in Synthetic Target 4 are shown. Here, though both curves exhibited a phase of exponential increase immediately after the reactions commenced, but target “A” resulted in only an

increase in RED fluorescence (Figure 3A, bottom) and target “B” resulted in only an increase in FAM fluorescence (Figure 3A, top). Both curves plateaued after approximately 6 minutes. The plateau indicated that the cleavage of the fluorophores from all FRET cassettes had been exhausted. All real-time Invader[®] curves for synthetic targets exhibited the same phase of exponential amplification followed by a plateau phase. The time necessary to reach steady-state fluorescence levels was incorporated into the microfluidic chip design, and helped determine incubation channel length. Allele call-outs were performed by taking the ratio of the end-point intensities of the FAM to RED fluorescence. The value of 0.5 was determined as the threshold value by calculating the ratio of FAM/RED NTC. Specifically, if the FAM/RED ratio was < 0.5 , the call was determined to be RED. If the ratio was > 0.5 , the call was FAM. For Synthetic Target 4, target “B” indeed yielded a ratio of > 0.5 , corresponding to a FAM call; target “A” indeed yielded a ratio of < 0.5 , corresponding to a RED call.

Figure 3B summarizes the results of the Invader[®] assay performed off-chip for synthetic targets. In these reactions, Markers 4, 5, 6, 7 and 9 each had bi-allelic synthetic targets which differed at a single nucleotide. Each set of markers were screened against their respective probe. As expected, Synthetic “A” targets yielded a Redmond Red signal and “B” targets yielded a FAM signal. Having verified the Invader[®] assay in the simpler synthetic target case, bench-top validation of the assay using Maize genomic DNA was performed.

In Figure 3C, the results of 80 separate screening reactions for the genomic Maize screening are shown. DNA 1-8 were each amplified using 10-plex PCR (Supplementary Figure 4) and then screened against each of the 10 different probes for regions of interest. Each Maize sample (DNA 1-8) was found to have a unique fingerprint for all 10 markers. To ensure that the Invader[®] assay functioned optimally, heat denaturation of the PCR product and Taq polymerase was necessary prior to running the Invader[®] assay. If heat denaturation was omitted, several Invader reactions did not yield conclusive allele calls.

5.3.3 Sample loading into microfluidic device via Nano Sample Processor

A novel feature of the microfluidic device is the Nano Sample Processor, which is designed to deliver a library of samples to the microfluidic chip. Each NSP is comprised of an inlet channel and a rinsing channel and their designated valves. The sample loading, rinsing, and switching process is depicted in Figure 2B in a step-by-step manner. Briefly, sample 1 was loaded onto the device and was driven with compressed air. The rinsing valve was in the open (ON) position, allowing sample to pass through the inlet. Once Sample 1 was loaded into the device, both valves were closed (OFF). Droplets were then generated by opening the valve between the sample inlet channel and oil channel. Once enough sample droplets were generated, the sample inlet was closed and the rinsing valve was opened. Rinsing fluid was flown throughout the sample channel and followed by compressed air. Sample 2 was then loaded and sample droplet generation was initiated. Sample loading via the NSP is attractive because a large number of samples can be delivered to the microfluidic device without the need for additional sample inlets.

5.3.4 Robust droplet operation and optical detection in microfluidic device

To perform Invader[®] assays within droplets, the droplets needed to flow smoothly throughout the device. In addition, droplet contents must be retained from droplet generation to detection. These requirements necessitate optimization of the carrier fluid and modification of the surface treatment strategy. PDMS-based droplet microfluidic devices are conventionally treated with a hydrophobic surface treatment. Aquapel is often used in conjunction with fluorinated carrier fluids [97, 159, 169]. However, Aquapel treatment was observed to be incompatible with the Invader[®] assay. For example, when we generated droplets with a bench-top reacted Invader reaction in Aquapel-treated devices, we observed that FAM and Redmond Red fluorophores would leak out of the droplets and adsorb onto PDMS side walls. These effects were even more pronounced at elevated temperatures (~63 °C), such that the fluorescence in droplets could no longer be distinguished from the background fluorescence in the carrier phase (Supplementary Figure 3). Thus, the device fabrication was modified such that the control layer was below the fluidic channels. Because PDMS is innately hydrophobic, no additional hydrophobic surface treatment was necessary. A mixture of FC-40 and Perfluorooctanol

(4:1 v/v) offered the optimal balance between droplet stability and small molecule retention among the carrier oils and surfactants that were evaluated. After such optimization, we could reliably detect bench-top reacted Invader reaction in the form of droplets in our device (Figure 5.3).

5.3.5 On-Chip SNP Genotyping Invader[®] with Synthetic Targets

As the first step to demonstrating the droplet-based Invader[®] assay, we first genotyped the five pairs of synthetic targets. Invader[®] Probes, MgCl₂, Cleavase and FRET mix were mixed and then loaded on to the chip via a probe inlet. Target sets (“A” and “B”) were loaded through the two NSP inlets (Figure 2). After screening a target pair, another pair of synthetic targets was then loaded via the same sample inlet. Sample inlets were rinsed with water by opening the valve controlling the rinsing channel, thereby allowing water to rinse the sample inlet without proceeding further downstream into the chip. Synthetic target samples and reaction mix were mixed on-chip. Mixing was abetted by a serpentine channel region downstream from the droplet preparation region. After passing through the mixing region, samples were incubated at 63 °C. Droplet passage time through the incubation region was ~20 minutes.

A representative recorded fluorescence trace after incubation on chip is shown in Figure 4A. Sequences of each pair of synthetic targets were generated in an asymmetrical fashion – *B, B, A* – where *A* and *B* denote the Redmond Red and FAM alleles, respectively, for each synthetic target pair. This ensured the resulting droplets’ identities could be readily determined from the fluorescence data based on which synthetic target was generated as a duplicate. Multiple trains of droplets containing synthetic DNA were collected and its data corrected for APD. Figure 4A demonstrates that the sequence of droplets is maintained as they move from the droplet generation region towards the detection region. The spacing between the droplets is the carrier fluid. The height of the droplets is directly correlated with the droplet fluorescence intensity. For each sample-probe combination, the droplet intensity was found to be consistent with very little variation. Droplet intensities of the same content were grouped using a MATLAB script.

The resultant log of ratios of FAM signal to Redmond Red signal calculated for each droplet were used as an indication of the SNP allele present in the synthetic target pairs.

An average of all the ratios for the same set of droplets was then calculated and a final allele call out was determined based on this ratio. A ratio of greater than $\log(0.5)$ would result in a FAM call, while a ratio smaller than $\log(0.5)$ would result in a RED call. A comparison with the bench top data show that the on-chip Invader[®] assay with synthetic target achieved a 100% correct call out for each synthetic allele.

5.3.6 On-Chip SNP Genotyping Invader[®] with Genomic Targets

8 genomic Maize DNA samples were screened with 10 Invader[®] probes on-chip. The performance of the NSP was evaluated by processing all 8 DNA samples through the same inlet. Specifically, the potential for cross-contamination was evaluated. Multiplexing was performed as described above and trains of 10 droplets (one DNA sample at a time with each of the 10 probes) were generated continuously.

Because of the observed variation in fluorescence intensity based on probe, a ratiometric analysis was applied. The results from the on-chip multiplexed SNP Genotyping Invader[®] assay with a final SNP read out for each genomic sample with each probe is shown in Figure 5. A ratio $> \log(0.5)$ indicated a FAM call and similarly, a ratio $< \log(0.5)$ indicated a RED call. Of the 80 combinations, only one resulted in a mismatched call when compared to the bench top results (1.3%). However, this mismatched call out exhibits a $\log(\text{FAM}/\text{RED})$ ratio very close to $\log(0.5)$, suggesting that additional data points for these particular cases may be necessary. Furthermore, the standard deviations calculated for $n=3$ per DNA/probe combination had low variation, suggesting that the signals observed and consequent allelic call outs were robust. On-chip collected genotypic fingerprints for all 8 Maize samples matched the bench-top reactions.

5.4 Discussion

This platform represents the first embodiment of a droplet-based, continuous flow platform for agricultural applications. The presented Nano Sample Processor has the ability to introduce an unlimited number of DNA samples on to a microfluidic device, overcoming limitations to the number of samples that can be introduced on to the microfluidic device because of small footprint. All 8 Maize genomic samples analysed were introduced through the same inlet, and no measurable cross-contamination was

observed. It is important to note that the Invader[®] assay can perform up to a million fold amplification, thus had there been any cross-contamination between successive samples, this would have likely been observed during detection. Therefore, the rinsing channel that was incorporated into the NSP was found to be highly effective in curtailing cross-contamination between successive genomic DNA samples, and would likely to be able to be employed in platforms that utilize other amplification-based assays, i.e. the Polymerase Chain Reaction.

By employing a valve-based reagent fusion scheme, the microfluidic device was able to perform combinatorial screening, which plant genotyping requires, in a flexible way which most microfluidic platforms cannot offer. Droplets are reliably merged without the need for synchronization. This device is based on valve-based droplet generation technology, which combines the control offered by microfluidic valves with the high-throughput capacity of droplets. Furthermore, the device has the ability to generate as many DNA-probe replicates as desired. Performing more replicates may be especially valuable for specific markers that are close to the threshold for allele calling. Simultaneous operation of droplet generation, incubation, and read-out eliminates idle time compared to batch-processing methods such as with the Douglas Scientific Array Tape[™]. Finally, because the droplets maintain their order from droplet generation to read-out, the need for fluorescent barcoding is eliminated. Barcode-free continuous flow operation of this strategy implies unlimited potential screening capacity on a single device with precise composition control over the reaction content of each individual droplet.

One limitation of the current platform is that there is no option to keep samples cooled prior to processing on-chip. Specifically, we observed that it was important for DNA to be denatured prior to the Invader[®] genotyping step to ensure accurate allele calling. Some of the Maize-probe combinations are near the threshold for allele calling (i.e., DNA 2, Marker 5). It is likely this is due to partial re-hybridization of DNA prior to on-chip genotyping. Thus, future iterations should include a cooling element beneath the Nano Sample Processors to keep DNA samples in a denatured state (as a continuation of the snap-cooling process) prior to hybridization. In addition, the width of the cooling element

can be extended to be placed beneath probe inlets to preserve the integrity of Invader® enzymes for long operating periods.

In future iterations of the device, the NSP design can be integrated with probe inlets in addition to the sample inlets, allowing probes and samples to be switched on-demand and enhancing flexibility in setting up screening reactions. To enhance throughput, the device can be coupled to a robotic sampling system [143]. Additionally, to accommodate crude DNA samples, a filter inlet design could be incorporated on the microfluidic device itself or as an adapter to the tubing that is interfaced with the device.

This platform can potentially be adapted for many different assays. For example, the device can be modified such that the incubation channel loops over multiple heating zones for assays which require multiple temperature zones, such as the Polymerase Chain Reaction. In applications where droplet evaporation is a concern, our lab has developed an evaporation-resistant method for fabricating PDMS-based devices (unpublished work). We believe that the optimized surface chemistry and carrier fluid presented herein are applicable to a large number of assays. It is important to note that leakage of small hydrophobic molecules is dependent on assay chemistry and in particular, molecular structure and size and thus may require some fine-tuning. Herein we obtained optimal results by eliminating the use of Aquapel and fine tuning the carrier fluid. Another option is to tether small hydrophobic molecules such as fluorophores to larger molecules, such as antibodies, to prevent leakage out of droplets.

Because the integrated NSP is able to introduce a virtually unlimited number of samples, it has the potential to replace conventionally used robotic pipetting systems or Array Tape™ in agricultural GS applications. Additional benefits of the microfluidic droplet approach are the sequestration of reagents and DNA inside droplets, thereby minimizing cross-contamination between individual reactions. Furthermore, the cost per screening assay is dramatically lessened by reducing the reaction volume from 5 μ L down to 50 nL. We believe the device presented herein has the potential to fulfil the unmet need for increased miniaturization, flexibility and automation in GS for cultivar development.

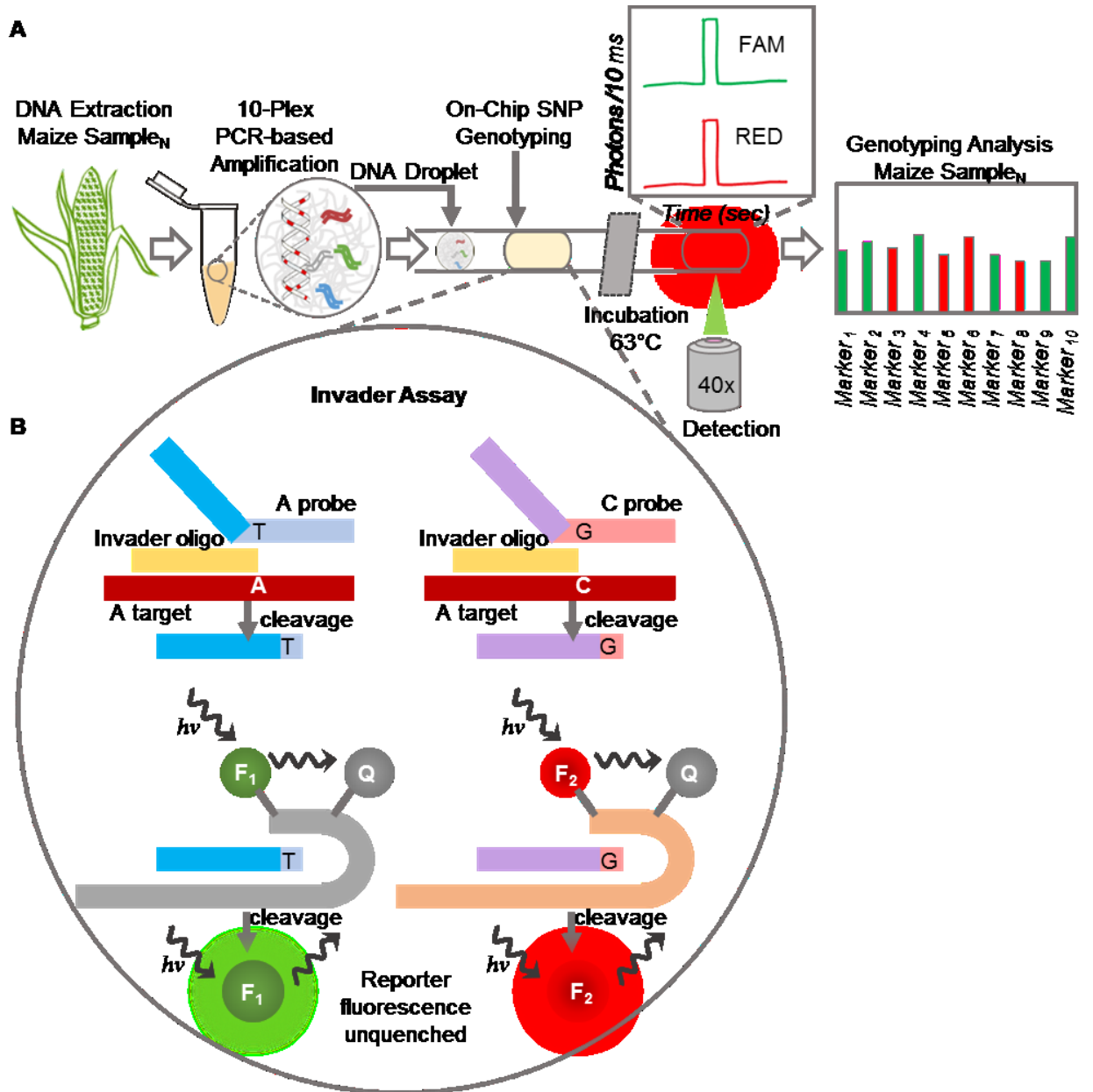


Figure 5.1. SNP Genotyping Workflow.

A) SNP Genotyping Workflow. DNA was extracted from leaf tissue or seed. DNA extraction was followed by 10-plex PCR amplification for 30 cycles. Following PCR-based amplification, samples were snap-cooled. Amplified DNA was loaded onto the microfluidic device via the sample inlet. DNA droplets (~ 5 nL) were generated and fused with SNP interrogating probes and Invader[®] reaction mix (~45 nL). DNA-probe droplets were incubated for ~ 20 minutes at 63°C as they moved throughout the incubation channel. In-line readout was performed using a two-color fluorescence spectroscopy detection system. Raw data was APD corrected. Average droplet intensities of droplets were normalized. The ratio of FAM/RED signal was then used to determine the final allelic call out for that specific DNA with probe. B) Invader[®] Assay Chemistry: In the primary reaction, both the Invader[®] oligonucleotide and primary probe hybridize to the target of interest. An invasive structure is formed from the single-base overlap. This forms a 3-dimensional structure that is recognized by an enzyme which cleaves the 5' Arm of the primary probe. In the secondary reaction, the 5' arm of the probe binds to the FRET cassette. In this secondary FRET reaction, this structure is recognized by an enzyme which cleaves the fluorophore and a fluorescent signal is generated.

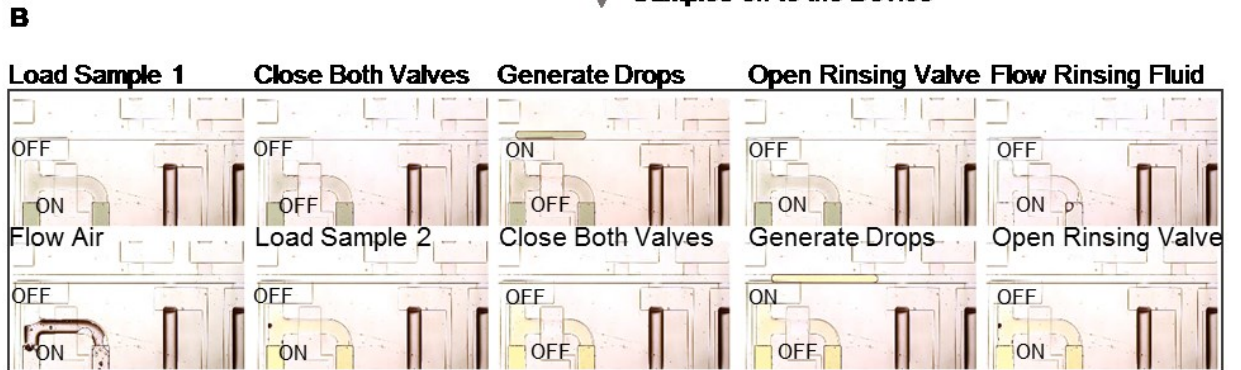
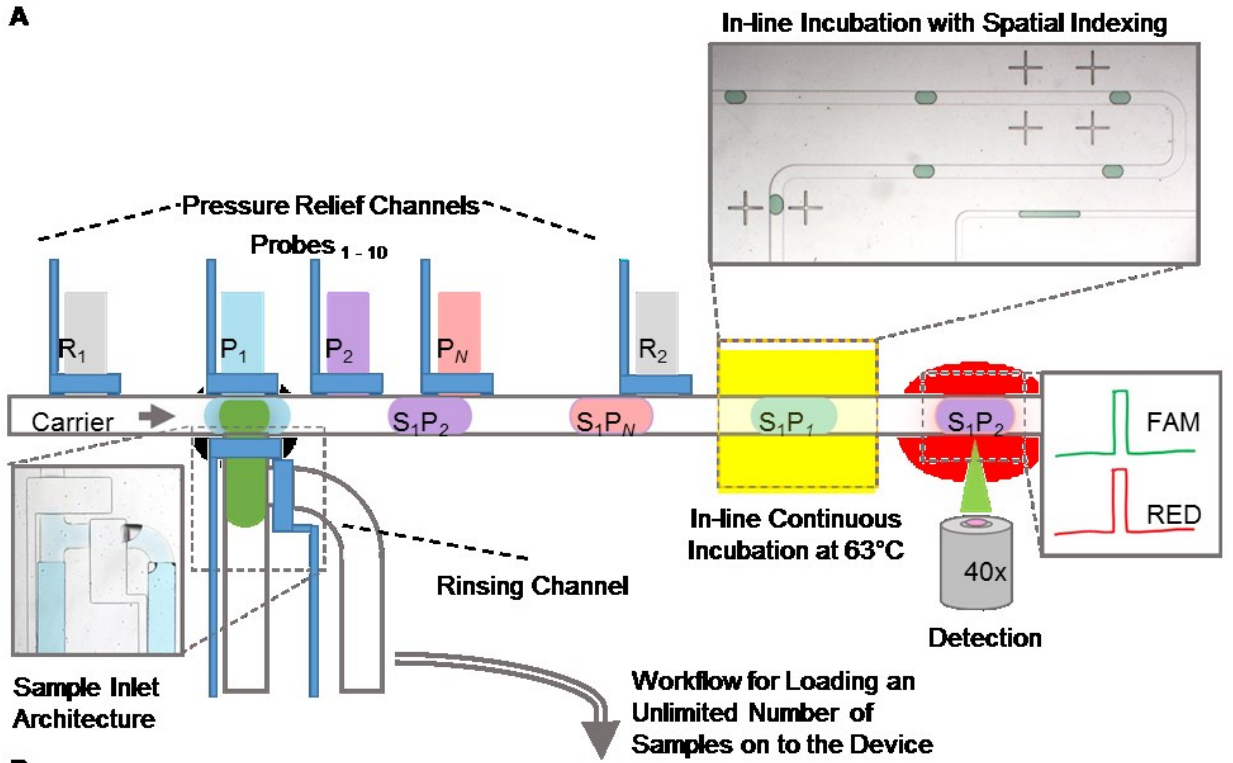
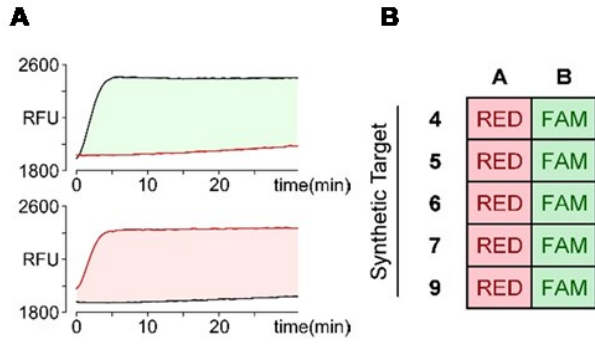


Figure 5.2. Microfluidic Chip Workflow.

A) Microfluidic Chip Workflow. Amplified DNA was loaded onto the device. Prior to the experiment, the desired sequence of reactions on the device was programmed. Each of the 8 DNA samples processed was screened against a library of 10 SNP-interrogating probes. A small amount of DNA (5 μ L) was introduced into the sample inlet and pressurized. In the design, a novel inlet architecture was designed to accommodate a rinsing channel, thus allowing for an unlimited number of samples to be processed through the same inlet without measurable cross-contamination. The valve chopped the sample and generated a small DNA droplet (~ 5 nL). Pressure-relief channels on either side of the droplet preparation region opened during generation to decouple fluidic resistance and droplet volume. The DNA droplet then entered the droplet preparation region and the carrier fluid flow was halted by activating an upstream valve. A mixture containing SNP-interrogating probe, enzymes and FRET cassettes (~45 nL) was injected directly into the DNA-containing droplet. The carrier fluid valve was released, and the droplet exited the preparation region. Subsequent DNA-probe droplets were processed in an assembly-line process. Each DNA-probe droplet passed through a serpentine channel to promote mixing of reagents prior to entering the incubation region. The incubation region was maintained at a constant temperature of 63°C. After incubation, in-line fluorescence readout was performed on droplets using dual laser spectroscopy, where fluorescence intensity data was collected and analysed. A unique feature of the platform was that the programmed sequence of droplets was spatially maintained on the device – from droplet preparation to droplet detection – consequently, there was no need for barcoding. B) Nano Sample Processor: Sample 1 was loaded onto the device and was driven with compressed air. The rinsing valve was in the open (ON) position, allowing sample to pass through the inlet. Once Sample 1 was loaded on to the device, both valves were closed (OFF). Droplets were then generated by opening the valve between the sample inlet channel and oil channel. Once enough sample droplets were generated, the sample inlet was closed and the rinsing valve was opened. Rinsing fluid was flown throughout the sample channel and followed by compressed air. Sample 2 was then loaded and sample droplet generation was initiated.



C

		Probe									
		1	2	3	4	5	6	7	8	9	10
DNA	1	FAM	FAM	RED	FAM	RED	RED	FAM	RED	FAM	FAM
	2	FAM	FAM	RED	FAM	RED	RED	FAM	RED	RED	RED
	3	RED	RED	RED	RED	RED	FAM	FAM	RED	RED	FAM
	4	FAM	FAM	FAM	RED	RED	RED	FAM	RED	RED	RED
	5	FAM	FAM	RED	RED	FAM	RED	RED	RED	RED	RED
	6	FAM	FAM	FAM	RED	FAM	FAM	FAM	FAM	RED	RED
	7	RED	RED	FAM	RED	RED	FAM	FAM	RED	RED	RED
	8	FAM	FAM	RED	RED	RED	FAM	FAM	RED	FAM	RED

Figure 5.3 Bench-top SNP Genotyping Invader® Assay Results.

A) Representative curves observed from the CFX96 real-time machine. The Invader® reaction was incubated at 63°C and a fluorescence reading was taken every 30 seconds. Within less than 10 minutes the Invader® reaction reached a plateau. Allele call-outs were performed by taking the ratio of the end-point intensities of the FAM to RED fluorescence. If the FAM/RED ratio was <0.5, the call was determined to be RED. If the ratio was >0.5, the call was FAM. The value of 0.5 was determined as the threshold value by calculating the ratio of FAM/RED NTC after incubation. In this example, the top graph would yield a FAM call and the bottom would yield a RED call. B) Bench top Invader® read out of synthetic target pairs with their corresponding probes. FAM represents the allele corresponding to the probe containing the FAM fluorophore (“B” target), and vice versa for RED as Redmond Red (“A” target). Allele call outs were correct for 100% of the cases. C) Bench top Invader® read out of multiplexed genomic targets with all 10 probes. This data was used as an internal control for on-chip experiments.

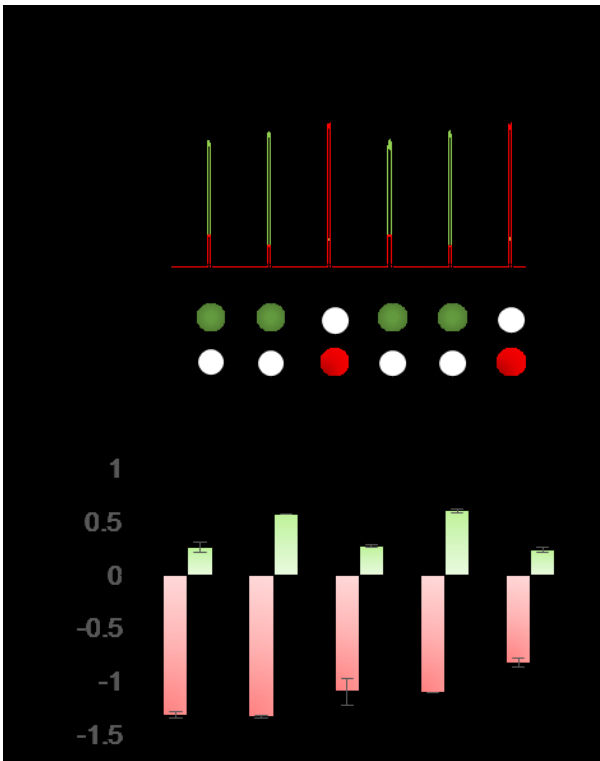


Figure 5.4. Synthetic Target Results.

A) Representative APD trace of the FAM fluorescence intensity as observed from real-time read out of the Invader[®] assay on chip using synthetic target 6. This trace contained two repeats of the same asymmetrical sequence, *B, B, A* such that the first two peaks observed correspond to droplets containing the same content (synthetic target type B). The third droplet in the sequence contains synthetic target type A. Allele calling was performed by taking the ratio of the FAM intensity to the RED intensity. If the ratio was >0.5 , the call was FAM. The value of 0.5 was determined as the threshold value by calculating the ratio of FAM/RED NTC after incubation. In this example, the first two droplets in the sequence would yield a FAM call and the third would yield a RED call. This matched the droplet generation sequence which was programmed in the MATLAB software controlling the pneumatic valves. B) Summary of synthetic target sets 4, 5, 6, 7, and 9.

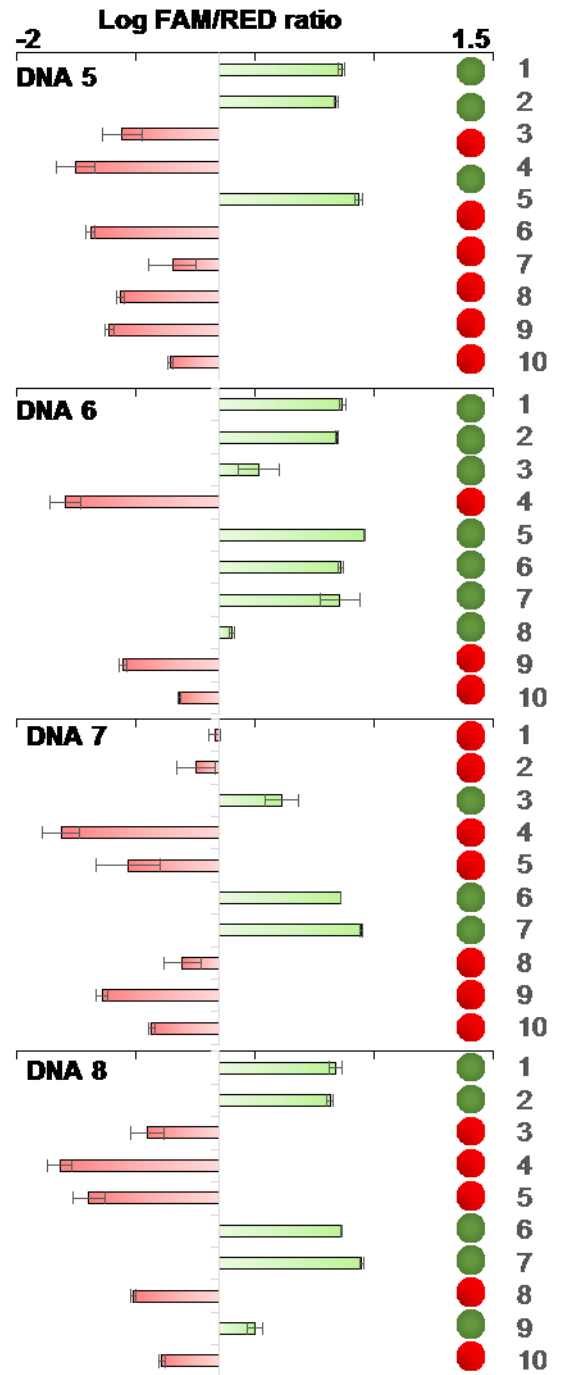
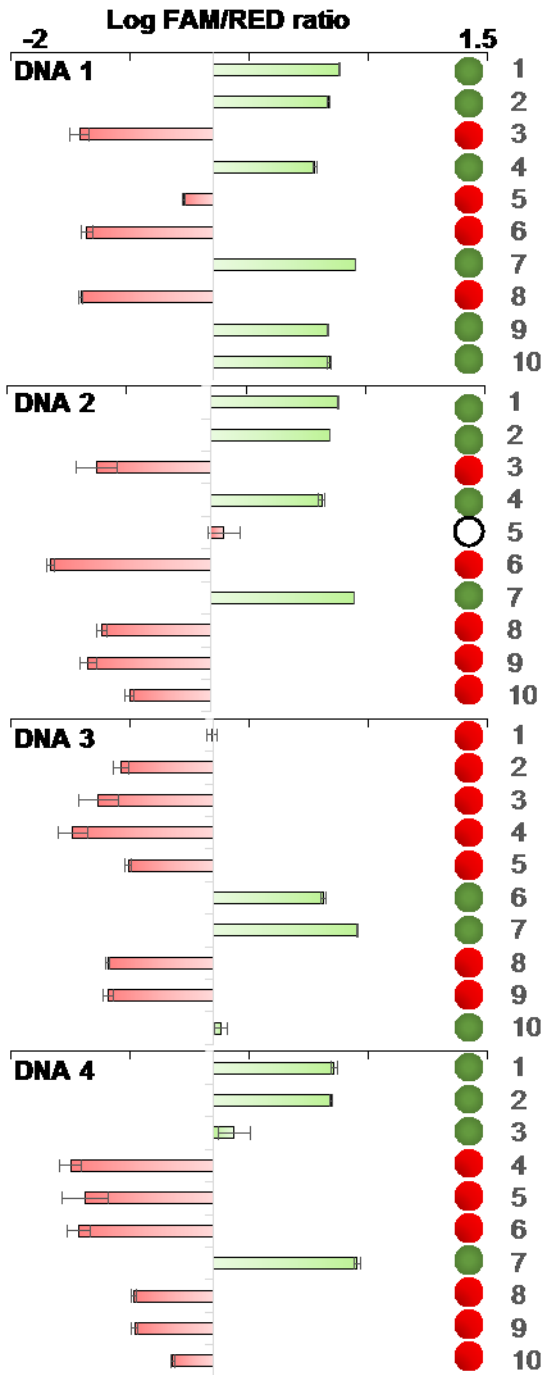


Figure 5.5. On-chip SNP Genotyping Invader[®] Assay of Genomic Targets.

Call out chart for all 80 multiplexed reactions with 8 genomic DNA samples against 10 Invader[®] probes. All Maize Targets 1 – 8 were screened against 10 SNP Markers. For all droplets, the FAM/RED ratio was calculated. For visualization, the log of the FAM/Red ratio is plotted here. Droplet sequences of 10 probes in sequential order were used for all genomic targets. Allele type is displayed in the chart as either green (FAM allele) or red (Redmond Red allele). Call out was determined by taking the average ratio of fluorescence intensities for FAM:Redmond Red, and are shown in the chart. Of 80 averaged reactions, only 1 resulted in a mismatched call (DNA2 with probe 5), resulting in a 98.8% call accuracy.

6

Ultra-thin, evaporation-resistant PDMS

devices for absolute quantification of DNA using digital PCR.

We present an array-based nanoliter digital PCR (dPCR) platform. The ultra-thin microfluidic device can accommodate high temperatures for extended periods, while minimizing evaporation. The device utilizes a very simple fabrication scheme, and can achieve a limit of detection of 100 attomolar of synthetic target. dPCR presents a feasible way to quantify rare targets, especially in high background. We demonstrate proof-of-concept use of this device to identify methylation of synthetic DNA in high background, a potential biomarker for many diseases. We believe that this simple and cost-effective device will encourage wider adoption of dPCR.

6.1 *Introduction*

Heterogeneous diseases such as cancer are characterized by a range of genetic and epigenetic alterations. Traditional bulk procedures measure ensemble signals (Figure 1), which have very low sensitivity for infrequent sequences within biological samples. Sensitive detection techniques such as dPCR are required to detect rare mutations within a milieu of wild-type DNA molecules. However, dPCR requires extensive miniaturization, as thousands of parallel reactions are required per sample.

Droplets indexed in high-density arrays enable high-throughput imaging. Different groups have developed dPCR systems. The “SlipChip” is one example [82], but has limited dynamic range due to large reaction volumes. Heyries [51] et al developed a megapixel digital PCR device that partitions based on surface tension. However, this approach requires expensive processes such as CVD. Another design includes a self-

compartmentalization chip [85]. However, a low-permeability fluorosilane polymer was required to prevent evaporation, thereby raising the cost and increasing the complexity of fabrication.

In this work, we have applied a unique fabrication method to build ultra-thin PDMS-based microfluidic devices for dPCR. The method can be adopted in any laboratory and obviates the need for complicated processes such as CVD or spin-coating of polymers, thereby limiting the time and cost of fabrication, as well as making dPCR technology more accessible

6.2 *Methods*

The goals of our study were twofold: (1) to examine whether the new fabrication method sufficiently inhibited evaporation and permitted repeated thermal cycling and (2) whether dPCR could be executed on the device. Our contribution to the field of dPCR is the development of a fabrication method that can cheaply and rapidly produce dPCR devices that are resistant to evaporation. This fabrication method is described in Figure 2.

6.2.1 **Device fabrication**

The device consists of five layers, a break-out of which is shown in Figure 3. One blank wafer is spun with 15:1 PDMS at 2100 rpm and another blank is spun with 6:1 PDMS at 100 rpm, which serves as a temporary layer. After baking for six minutes, the 6:1 blank layer is peeled from the wafer and placed over the 15:1 PDMS. This combination bakes for six more minutes to loosely bond the two PDMS layers. The two bonded PDMS layers are then removed from the wafer and attached to a thin glass slide via O₂ plasma bonding (15:1 side facing the glass). After bonding and a five minute bake, the temporary PDMS layer can be peeled from the chip, leaving just the thin layer. A similar process is used to fabricate the thin pattern layer, using 15:1 PDMS for the silanized pattern wafer (900 rpm) and 6:1 PDMS for a temporary blank layer (100 rpm). Finally, a thin glass coverslide is plasma bonded to the top PDMS layer to reduce evaporation, and an adaptor placed over the inlets to interface with tubing.

inlets and outlets of the device. The chip was placed in a vacuum chamber to evacuate air from the PDMS matrix and the channels within the device. The PCR reaction mixture

consisted of Magic Buffer (μl) , ROX (0.8 uL), dNTPs (10 mM, 0.8 uL), Forward and reverse primers (10 uM, 1.2 uL each), Platinum Taq Polymerase (0.2 uL), TAQ Probe (10 μM , .40 μl), DNA target (3.2 μl), 0.1% Tween-20 (2 μl), BSA (20 mg/ml, 2 μl), and water (24.2 μl). 1.1 g of uncured PDMS mixed at a ratio of 10:1 (base:crosslinker), and 5 g of silicone oil (100 cst) composed the oil phase.

6.2.2 Device Loading and Thermocycling

In the first step of the workflow, sample is loaded onto the microfluidic device by puncturing the tape, which pulls the reagents into the wells because of the negative pressure inside the channels. The wells are then partitioned using the PDMS/silicone oil mixture, which is loaded via pressurization at 10 psi until complete. The device is thermocycled on a flatbed peltier for up to 60 cycles (5 minutes of 95°C, then 60 cycles of 15 seconds at 95°C and 60 seconds at 60°C).

6.2.3 Imaging and Image Processing

Chips are imaged on a Typhoon 9410 Variable Mode Imager at 10 μm resolution. Fluorescent images are obtained for both the TaqMan probe (FAM) and the reference dye (ROX). Following detection, the images are imported into Matlab for processing and analysis. A mask is overlaid with the image file. The resulting image contains fluorescent data from only the areas of interest. The central pixels of each well are used to measure average intensity. Matlab's built-in bimodal population separation function, multithresh, is used to set a threshold for positive wells. Finally, the number of positive and negative wells are counted, and occupancy is calculated assuming a Poisson distribution of reaction mixture throughout the device.

6.2.4 Evaporation

The simple, thin-chip microfabrication technique employed reduced the evaporation by an order of magnitude compared to traditional microfluidic devices, which overcomes a critical problem for high temperature assays. Given the same reaction conditions, an average of 8% evaporation can be seen per well on the thin chip. In contrast, 80% of the reaction evaporates after 60 cycles on a device with standard thickness. This reduction

allows for assays that require many cycles to be completed on the microfluidic chip. The results of the comparison are shown in Figure 4.

6.2.5 Digital PCR

The microfluidic device can be used to perform digital PCR across a range of concentrations. The segmentation of the reaction mixture into many wells reduces the background such that single events become quantifiable. We demonstrated digital PCR for concentrations ranging from 100 – 0.1 fM. The calculated results and expected results match with 14% error, as shown in Figure 5. The automatic thresholding performed by Matlab defines an average signal to background ratio of 10:1 across chips. A sample raw image can be seen in Figure 6A. After processing, plotting the average fluorescent intensity of each well produces a bimodal histogram (Figure 6B). The two populations are separated by Matlab's multithresh, and the resulting number of positive and negative wells are counted. The occupancy can be calculated using the equation

$$\text{Occupancy} = N_{\text{total}} * \ln (N_{\text{total}}/N_{\text{negative}}) ,$$

which assumes a Poisson distribution of positive target throughout the wells of the chip.

6.3 Discussion

The development of a robust digital PCR device meets a clinical need for detection and quantification of rare genetic events. Rare mutations or allelic variations can be biomarkers of disease. A device that can quantify these rare events at a digital level can allow for early detection of these biomarkers. We have shown that this microfluidic device can quantify rare events, and performs at a robust and reproducible level.

The implementation of such a device is limited by fabrication and usability. The device presented here requires only simple fabrication techniques and is facile to use. Minimization of evaporation is essential for running PCR on a PDMS device. This challenge has led most other dPCR devices to employ a complex fabrication method [2, 3]. However, we demonstrate a technique that minimizes evaporation without any additional use of equipment or materials. In addition, the device presented here does not

require valves, which necessitate external operating equipment, but rather utilizes a single layer and a single inlet, minimizing the external equipment required to operate. This method allows wide adoption of dPCR throughout the microfluidic community.

Further improvements to this system include increasing the limit of detection and multiplexing the reaction. Increasing the limit of detection can be achieved by expanding the grid of wells, therefore increasing the partitioning of the sample. One challenge in incorporating an increased number of reaction wells is the resolution of the imaging system. A new, ultra-high resolution imaging mechanism is required in order to increase well density without expanding the size of the chip beyond feasible dimensions. Multiplexing the reactions on the device becomes less challenging with a high-resolution imaging system. Without separation of targets, however, care must be taken to avoid nonspecific amplification. Nevertheless, this method of fabrication will drive adaptation and progress in the field of digital PCR.

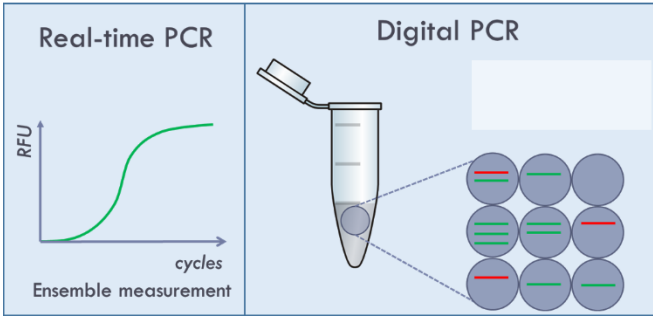


Figure 6.1. Ensemble versus Digital PCR.

In bulk experiments, rare targets will get lost in averaged signal. In digital PCR, each original DNA molecule is isolated in a unique reaction so that rare molecules can be observed and quantified.

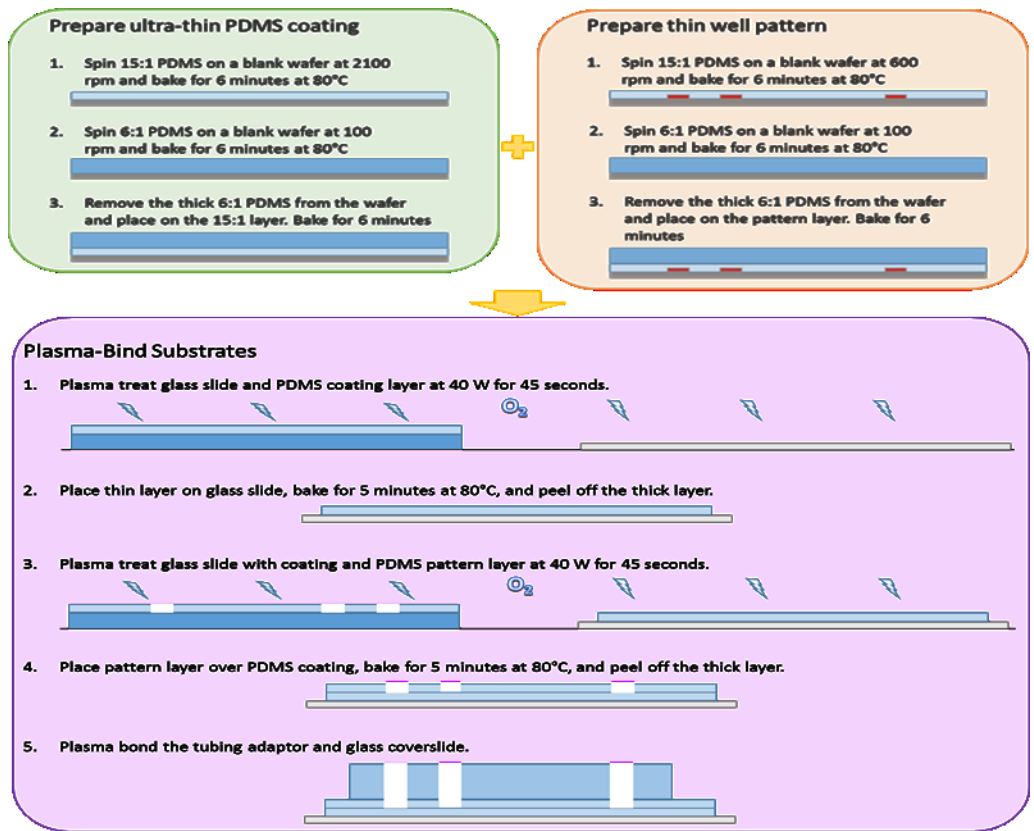


Figure 6.2. Fabrication steps for creation of ultra-thin microfluidic dPCR chip.

Fabrication steps for creation of an ultra-thin microfluidic dPCR chip. First, the thin layers are prepared by loose bonding with a sacrificial thick layer. Then, the layers are bonded via plasma treatment. After baking, the thick layer can be peeled off, leaving just the thin PDMS. Finally, a tubing adaptor and glass coverslide are plasma bonded to the chip.

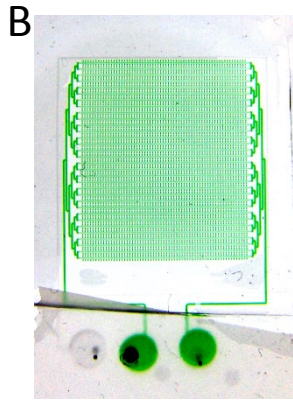
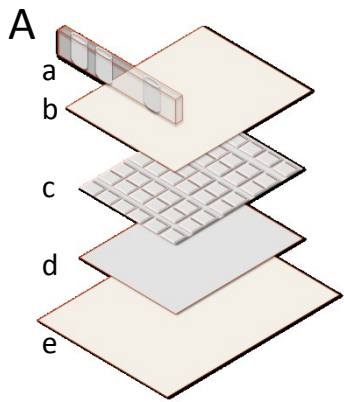


Figure 6.3. Device structure.

A. Exploded view of microfluidic chip. The device has five layers: a. Tubing adaptor, b. Glass coverslip, c. Thin reaction wells, d. Thin PDMS coating, e. Thin glass slide. B. Camera image of microfluidic chip filled with green indicator dye.

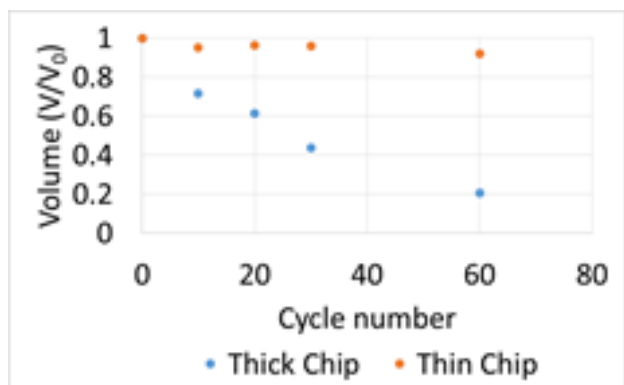


Figure 6.4. Evaporation during PCR.

Evaporation during PCR. Thick chips fabricated using conventional techniques experienced 80% evaporation. In contrast, the thin chips only experienced 8% volume loss after 60 cycles of thermal cycling (5 minutes of 95°C, then 60 cycles of 15 seconds at 95°C and 60 seconds at 60°C).

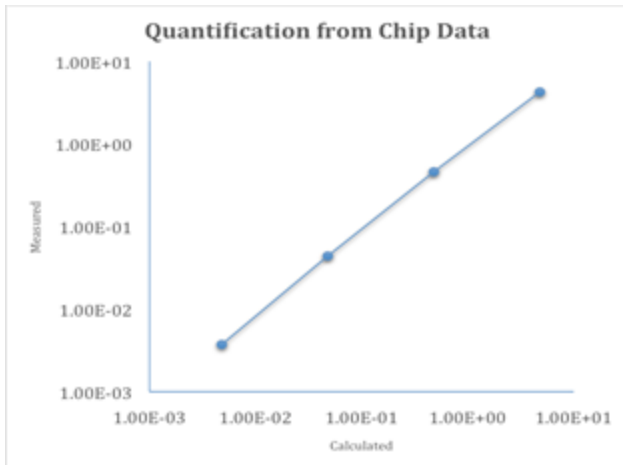


Figure 6.5. A comparison of expected and measured copies per well.

The expected value was calculated based on the stock concentration and reaction protocol. The measured value is obtained from digital counting and Poisson's occupancy equation.

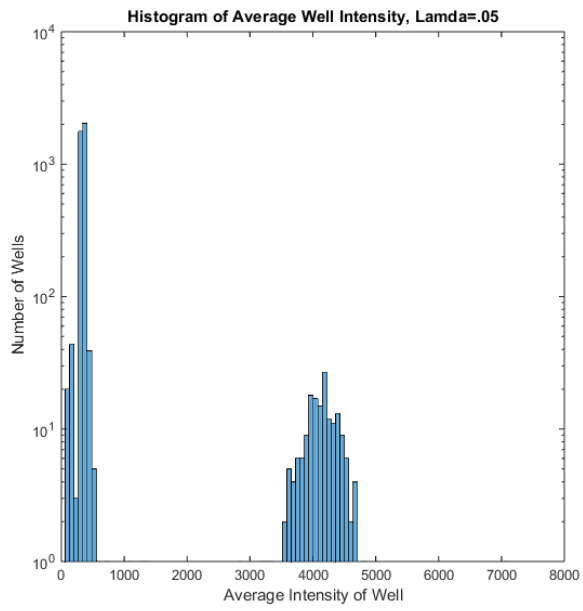
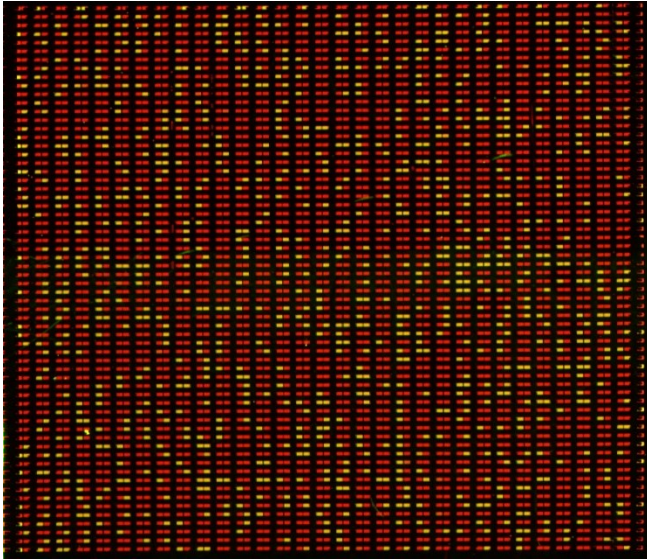


Figure 6.6. Experimental Results.

(A). Image of microfluidic chip from the Typhoon Scanner. The signal image (green) was obtained with 526 nm emission and 488 nm filter, and is overlaid with the reference image (red). After Matlab processing, average intensities of each well are obtained (B). The sample result shown had an expected copy number of 0.48 and a measured copy number of 0.44.

7

Conclusions and future work

Droplet microfluidics holds great promise as a tool in biology and medicine. The scope of this thesis work centered on extending the use of droplet microfluidic platforms.

In Chapter 3, we developed a solution for performing high-throughput screening operations using droplet microfluidics. We expect the platform described here to be a promising candidate for combinatorial screening applications using droplet microfluidics. In Chapter 4, we further developed this technology for increased throughput. Taken together, we have successfully parallelized the once-serial operation in combinatorial droplet devices and have improved the device throughput by 16-fold. Given its current performance and prospect for future improvements, we believe the parallelized combinatorial droplet device has the potential to meet the demand as a flexible and cost-effective tool that can perform high throughput screening applications. In Chapter 5, we applied this platform to an agricultural application. We believe the device presented herein has the potential to fulfil the unmet need for increased miniaturization, flexibility and automation in GS for cultivar development. In Chapter 6 we developed a static droplet array for nucleic acid sensing at a single molecule level. This thesis help lay the groundwork for use of droplet microfluidics in applications which require combinatorial analysis of samples.

Bibliography

1. Naylor, S., *Biomarkers: current perspectives and future prospects*. Expert review of molecular diagnostics, 2003. **3**(5): p. 525-9.
2. Bainbridge, M.N., et al., *De novo truncating mutations in ASXL3 are associated with a novel clinical phenotype with similarities to Bohring-Opitz syndrome*. Genome Med, 2013. **5**(2): p. 11.
3. Wallstrom, G., K.S. Anderson, and J. LaBaer, *Biomarker discovery for heterogeneous diseases*. Cancer Epidemiol Biomarkers Prev, 2013. **22**(5): p. 747-55.
4. Chin, L., et al., *Making sense of cancer genomic data*. Genes Dev, 2011. **25**(6): p. 534-55.
5. Thomas, R.K., et al., *Sensitive mutation detection in heterogeneous cancer specimens by massively parallel picoliter reactor sequencing*. Nat Med, 2006. **12**(7): p. 852-5.
6. Banoo, S., et al., *Evaluation of diagnostic tests for infectious diseases: general principles*. Nat Rev Microbiol, 2006. **4**(12 Suppl): p. S20-32.
7. Yang, S. and R.E. Rothman, *PCR-based diagnostics for infectious diseases: uses, limitations, and future applications in acute-care settings*. Lancet Infect Dis, 2004. **4**(6): p. 337-48.
8. Rost, S., et al., *Mutations in VKORC1 cause warfarin resistance and multiple coagulation factor deficiency type 2*. Nature, 2004. **427**(6974): p. 537-41.
9. Nahavandi, S., et al., *Microfluidic platforms for biomarker analysis*. Lab Chip, 2014. **14**(9): p. 1496-514.
10. Hung, L.-Y., et al., *Microfluidic platforms for discovery and detection of molecular biomarkers*. Microfluidics and Nanofluidics, 2014. **16**(5): p. 941-963.
11. Teh, S.Y., et al., *Droplet microfluidics*. Lab Chip, 2008. **8**(2): p. 198-220.
12. Taly, V., et al., *Detecting biomarkers with microdroplet technology*. Trends Mol Med, 2012. **18**(7): p. 405-16.
13. Devonshire, A.S., et al., *Application of next generation qPCR and sequencing platforms to mRNA biomarker analysis*. Methods, 2013. **59**(1): p. 89-100.
14. Theberge, A.B., et al., *Microdroplets in microfluidics: an evolving platform for discoveries in chemistry and biology*. Angew Chem Int Ed Engl, 2010. **49**(34): p. 5846-68.
15. Song, H., D.L. Chen, and R.F. Ismagilov, *Reactions in droplets in microfluidic channels*. Angew Chem Int Ed Engl, 2006. **45**(44): p. 7336-56.
16. Schneider, T., J. Kreutz, and D.T. Chiu, *The potential impact of droplet microfluidics in biology*. Anal Chem, 2013. **85**(7): p. 3476-82.
17. Pompano, R.R., et al., *Microfluidics using spatially defined arrays of droplets in one, two, and three dimensions*. Annu Rev Anal Chem (Palo Alto Calif), 2011. **4**: p. 59-81.
18. Dressler, O.J., et al., *Droplet-based microfluidics: enabling impact on drug discovery*. J Biomol Screen, 2014. **19**(4): p. 483-96.

19. Casadevall i Solvas, X. and A. deMello, *Droplet microfluidics: recent developments and future applications*. Chem Commun (Camb), 2011. **47**(7): p. 1936-42.
20. Velev, O.D., B.G. Prevo, and K.H. Bhatt, *On-chip manipulation of free droplets*. Nature, 2003. **426**(6966): p. 515-6.
21. Hunt, T.P., D. Issadore, and R.M. Westervelt, *Integrated circuit/microfluidic chip to programmably trap and move cells and droplets with dielectrophoresis*. Lab Chip, 2008. **8**(1): p. 81-7.
22. Chugh, D. and K.V. Kaler, *Leveraging liquid dielectrophoresis for microfluidic applications*. Biomed Mater, 2008. **3**(3): p. 034009.
23. Pollack, M.G., et al., *Applications of electrowetting-based digital microfluidics in clinical diagnostics*. Expert Rev Mol Diagn, 2011. **11**(4): p. 393-407.
24. Lu, H.W., et al., *A study of EWOD-driven droplets by PIV investigation*. Lab Chip, 2008. **8**(3): p. 456-61.
25. Sista, R., et al., *Development of a digital microfluidic platform for point of care testing*. Lab Chip, 2008. **8**(12): p. 2091-104.
26. Boles, D.J., et al., *Droplet-based pyrosequencing using digital microfluidics*. Anal Chem, 2011. **83**(22): p. 8439-47.
27. Long, Z., et al., *Fundamentals of magnet-actuated droplet manipulation on an open hydrophobic surface*. Lab Chip, 2009. **9**(11): p. 1567-75.
28. Im do, J., et al., *Electrophoresis of a charged droplet in a dielectric liquid for droplet actuation*. Anal Chem, 2011. **83**(13): p. 5168-74.
29. Hua, Z., et al., *Multiplexed real-time polymerase chain reaction on a digital microfluidic platform*. Anal Chem, 2010. **82**(6): p. 2310-6.
30. Shikida, M., et al., *Using wettability and interfacial tension to handle droplets of magnetic beads in a micro-chemical-analysis system*. Sensors and Actuators B: Chemical, 2006. **113**(1): p. 563-569.
31. Zhang, Y., et al., *A surface topography assisted droplet manipulation platform for biomarker detection and pathogen identification*. Lab Chip, 2011. **11**(3): p. 398-406.
32. Shin, D., Y. Zhang, and T.-H. Wang, *A droplet microfluidic approach to single-stream nucleic acid isolation and mutation detection*. Microfluidics and Nanofluidics, 2014: p. 1-6.
33. Zhang, Y. and T.H. Wang, *Full-Range Magnetic Manipulation of Droplets via Surface Energy Traps Enables Complex Bioassays*. Adv Mater, 2013.
34. Pipper, J., et al., *Catching bird flu in a droplet*. Nat Med, 2007. **13**(10): p. 1259-63.
35. Tsuchiya, H., et al., *On-chip polymerase chain reaction microdevice employing a magnetic droplet-manipulation system*. Sensors and Actuators B: Chemical, 2008. **130**(2): p. 583-588.
36. Ohashi, T., et al., *A simple device using magnetic transportation for droplet-based PCR*. Biomedical Microdevices, 2007. **9**(5): p. 695-702.
37. Shikida, M., et al., *A palmtop-sized rotary-drive-type biochemical analysis system by magnetic bead handling*. Journal of Micromechanics and Microengineering, 2008. **18**(3): p. 035034.

38. Neuzil, P., J. Pipper, and T.M. Hsieh, *Disposable real-time microPCR device: lab-on-a-chip at a low cost*. *Molecular BioSystems*, 2006. **2**(6-7): p. 292-298.
39. Rida, A., V. Fernandez, and M. Gijs, *Long-range transport of magnetic microbeads using simple planar coils placed in a uniform magnetostatic field*. *Applied Physics Letters*, 2003. **83**(12): p. 2396-2398.
40. Chiou, C.-H., et al., *Topography-assisted electromagnetic platform for blood-to-PCR in a droplet*. *Biosensors and Bioelectronics*, 2013. **50**: p. 91-99.
41. Pipper, J., et al., *Clockwork PCR including sample preparation*. *Angew Chem Int Ed Engl*, 2008. **47**(21): p. 3900-4.
42. Wixforth, A., *Acoustically driven planar microfluidics*. *Superlattices and Microstructures*, 2003. **33**(5): p. 389-396.
43. Yeo, L.Y. and J.R. Friend, *Ultrafast microfluidics using surface acoustic waves*. *Biomicrofluidics*, 2009. **3**(1): p. 012002.
44. Baudoin, M., et al., *Low power sessile droplets actuation via modulated surface acoustic waves*. *Applied Physics Letters*, 2012. **100**(15): p. 154102.
45. Fu, Y., et al., *Recent developments on ZnO films for acoustic wave based bio-sensing and microfluidic applications: a review*. *Sensors and Actuators B: Chemical*, 2010. **143**(2): p. 606-619.
46. Park, S.-Y., et al., *A light-induced dielectrophoretic droplet manipulation platform*. *Lab Chip*, 2009. **9**(22): p. 3228-3235.
47. Huang, C.-J., et al., *A biocompatible open-surface droplet manipulation platform for detection of multi-nucleotide polymorphism*. *Lab Chip*, 2014.
48. Lehmann, U., et al., *Droplet-Based DNA Purification in a Magnetic Lab-on-a-Chip*. *Angewandte Chemie International Edition*, 2006. **45**(19): p. 3062-3067.
49. Van Der Pol, B., et al., *Clinical evaluation of the BD ProbeTec Neisseria gonorrhoeae Qx amplified DNA assay on the BD Viper system with XTR technology*. (1537-4521 (Electronic)).
50. Men, Y., et al., *Digital polymerase chain reaction in an array of femtoliter polydimethylsiloxane microreactors*. *Anal Chem*, 2012. **84**(10): p. 4262-4266.
51. Heyries, K.A., et al., *Megapixel digital PCR*. *Nat Methods*, 2011. **8**(8): p. 649-651.
52. Sykes, P.J., et al., *Quantitation of targets for PCR by use of limiting dilution*. *Biotechniques*, 1992. **13**(3): p. 444-9.
53. Vogelstein, B. and K.W. Kinzler, *Digital PCR*. *Proc Natl Acad Sci U S A*, 1999. **96**(16): p. 9236-41.
54. Day, E., P.H. Dear, and F. McCaughan, *Digital PCR strategies in the development and analysis of molecular biomarkers for personalized medicine*. *Methods*, 2013. **59**(1): p. 101-7.
55. Dressman, D., et al., *Transforming single DNA molecules into fluorescent magnetic particles for detection and enumeration of genetic variations*. *Proc Natl Acad Sci U S A*, 2003. **100**(15): p. 8817-22.
56. Diehl, F., et al., *BEAMing: single-molecule PCR on microparticles in water-in-oil emulsions*. *Nat Methods*, 2006. **3**(7): p. 551-9.
57. Diehl, F., et al., *Circulating mutant DNA to assess tumor dynamics*. *Nat Med*, 2008. **14**(9): p. 985-90.

58. Pekin, D., et al., *Quantitative and sensitive detection of rare mutations using droplet-based microfluidics*. Lab on a chip, 2011. **11**(13): p. 2156-66.
59. Zhong, Q., et al., *Multiplex digital PCR: breaking the one target per color barrier of quantitative PCR*. Lab on a Chip, 2011. **11**(13): p. 2167-2174.
60. Taly, V., et al., *Multiplex picodroplet digital PCR to detect KRAS mutations in circulating DNA from the plasma of colorectal cancer patients*. Clinical chemistry, 2013. **59**(12): p. 1722-1731.
61. Pinheiro, L.B., et al., *Evaluation of a droplet digital polymerase chain reaction format for DNA copy number quantification*. Anal Chem, 2011. **84**(2): p. 1003-1011.
62. Zec, H., T.D. Rane, and T.H. Wang, *Microfluidic platform for on-demand generation of spatially indexed combinatorial droplets*. Lab on a chip, 2012. **12**(17): p. 3055-62.
63. Tewhey, R., et al., *Microdroplet-based PCR enrichment for large-scale targeted sequencing*. Nature biotechnology, 2009. **27**(11): p. 1025-1031.
64. Harismendy, O., et al., *Detection of low prevalence somatic mutations in solid tumors with ultra-deep targeted sequencing*. Genome Biol, 2011. **12**(12): p. R124.
65. Bonnefond, A., et al., *Highly Sensitive Diagnosis of 43 Monogenic Forms of Diabetes or Obesity Through One-Step PCR-Based Enrichment in Combination With Next-Generation Sequencing*. Diabetes care, 2014. **37**(2): p. 460-467.
66. Huebner, A., et al., *Quantitative detection of protein expression in single cells using droplet microfluidics*. Chemical communications, 2007(12): p. 1218-1220.
67. Joensson, H.N., et al., *Detection and Analysis of Low-Abundance Cell-Surface Biomarkers Using Enzymatic Amplification in Microfluidic Droplets*. Angewandte Chemie-International Edition, 2009. **48**(14): p. 2518-2521.
68. Boedicker, J.Q., M.E. Vincent, and R.F. Ismagilov, *Microfluidic Confinement of Single Cells of Bacteria in Small Volumes Initiates High-Density Behavior of Quorum Sensing and Growth and Reveals Its Variability*. Angewandte Chemie International Edition, 2009. **48**(32): p. 5908-5911.
69. Brouzes, E., et al., *Droplet microfluidic technology for single-cell high-throughput screening*. Proceedings of the National Academy of Sciences of the United States of America, 2009. **106**(34): p. 14195-200.
70. Zeng, Y., et al., *High-Performance Single Cell Genetic Analysis Using Microfluidic Emulsion Generator Arrays*. Analytical Chemistry, 2010. **82**(8): p. 3183-3190.
71. Rane, T.D., et al., *Droplet microfluidics for amplification-free genetic detection of single cells*. Lab Chip, 2012. **12**(18): p. 3341-3347.
72. Vogelstein, B. and D. Gillespie, *Preparative and analytical purification of DNA from agarose*. Proceedings of the National Academy of Sciences, 1979. **76**(2): p. 615-619.
73. Tang, Y.-W., G.W. Procop, and D.H. Persing, *Molecular diagnostics of infectious diseases*. Clinical chemistry, 1997. **43**(11): p. 2021-2038.
74. Caliendo, A.M., *Multiplex PCR and emerging technologies for the detection of respiratory pathogens*. Clinical infectious diseases, 2011. **52**(suppl 4): p. S326-S330.

75. Tsiatis, A.C., et al., *Comparison of Sanger Sequencing, Pyrosequencing, and Melting Curve Analysis for the Detection of *KRAS* Mutations: Diagnostic and Clinical Implications*. The Journal of Molecular Diagnostics, 2010. **12**(4): p. 425-432.
76. Wittwer, C.T., et al., *High-resolution genotyping by amplicon melting analysis using LCGreen*. Clinical chemistry, 2003. **49**(6): p. 853-860.
77. Wu, D.Y., et al., *Allele-specific enzymatic amplification of beta-globin genomic DNA for diagnosis of sickle cell anemia*. Proceedings of the National Academy of Sciences, 1989. **86**(8): p. 2757-2760.
78. Saiki, R.K., et al., *Diagnosis of sickle cell anemia and β -thalassemia with enzymatically amplified DNA and nonradioactive allele-specific oligonucleotide probes*. New England Journal of Medicine, 1988. **319**(9): p. 537-541.
79. Baker, M., *Digital PCR hits its stride*. Nat Methods, 2012. **9**(6): p. 541.
80. Du, W., et al., *SlipChip*. Lab Chip, 2009. **9**(16): p. 2286-2292.
81. Shen, F., et al., *Nanoliter multiplex PCR arrays on a SlipChip*. Anal Chem, 2010. **82**(11): p. 4606-4612.
82. Shen, F., et al., *Digital PCR on a SlipChip*. Lab Chip, 2010. **10**(20): p. 2666-2672.
83. Shen, F., et al., *Digital isothermal quantification of nucleic acids via simultaneous chemical initiation of recombinase polymerase amplification reactions on SlipChip*. Analytical chemistry, 2011. **83**(9): p. 3533-40.
84. Shen, F., et al., *Multiplexed quantification of nucleic acids with large dynamic range using multivolume digital RT-PCR on a rotational SlipChip tested with HIV and hepatitis C viral load*. Journal of the American Chemical Society, 2011. **133**(44): p. 17705-17712.
85. Zhu, Q., et al., *Digital PCR on an integrated self-priming compartmentalization chip*. Lab Chip, 2014. **14**(6): p. 1176-85.
86. Sundberg, S.O., et al., *Spinning disk platform for microfluidic digital polymerase chain reaction*. Anal Chem, 2010. **82**(4): p. 1546-50.
87. Hu, M., et al., *Ultrasensitive, multiplexed detection of cancer biomarkers directly in serum by using a quantum dot-based microfluidic protein chip*. ACS Nano, 2010. **4**(1): p. 488-94.
88. Huebner, A., et al., *Microdroplets: a sea of applications?* Lab on a Chip, 2008. **8**(8): p. 1244-1254.
89. Teh, S.-Y., et al., *Droplet microfluidics*. Lab on a Chip, 2008. **8**(2): p. 198-220.
90. Pompano, R.R., et al., *Microfluidics using spatially defined arrays of droplets in one, two, and three dimensions*. Annual Review of Analytical Chemistry, 2011. **4**: p. 59-81.
91. Guo, M.T., et al., *Droplet microfluidics for high-throughput biological assays*. Lab on a Chip, 2012. **12**(12): p. 2146-2155.
92. Song, H., D.L. Chen, and R.F. Ismagilov, *Reactions in droplets in microfluidic channels*. Angewandte chemie international edition, 2006. **45**(44): p. 7336-7356.
93. Kumaresan, P., et al., *High-throughput single copy DNA amplification and cell analysis in engineered nanoliter droplets*. Analytical chemistry, 2008. **80**(10): p. 3522-3529.
94. Kiss, M.M., et al., *High-throughput quantitative polymerase chain reaction in picoliter droplets*. Analytical chemistry, 2008. **80**(23): p. 8975-8981.

95. Beer, N.R., et al., *On-chip, real-time, single-copy polymerase chain reaction in picoliter droplets*. Analytical Chemistry, 2007. **79**(22): p. 8471-8475.
96. Clausell-Tormos, J., et al., *Droplet-based microfluidic platforms for the encapsulation and screening of mammalian cells and multicellular organisms*. Chemistry & biology, 2008. **15**(5): p. 427-437.
97. Baret, J.C., et al., *Fluorescence-activated droplet sorting (FADS): efficient microfluidic cell sorting based on enzymatic activity*. Lab on a chip, 2009. **9**(13): p. 1850-8.
98. Shi, W., et al., *Droplet microfluidics for characterizing the neurotoxin-induced responses in individual *Caenorhabditis elegans**. Lab on a Chip, 2010. **10**(21): p. 2855-2863.
99. Shi, W., et al., *Droplet-based microfluidic system for individual *Caenorhabditis elegans* assay*. Lab on a Chip, 2008. **8**(9): p. 1432-1435.
100. Sobrino, B., M. Brión, and A. Carracedo, *SNPs in forensic genetics: a review on SNP typing methodologies*. Forensic science international, 2005. **154**(2): p. 181-194.
101. Gupta, P., S. Rustgi, and R. Mir, *Array-based high-throughput DNA markers for crop improvement*. Heredity, 2008. **101**(1): p. 5-18.
102. Ragoussis, J., *Genotyping technologies for genetic research*. Annual review of genomics and human genetics, 2009. **10**: p. 117-133.
103. Veldhuisen, B., C. Van Der Schoot, and M. De Haas, *Blood group genotyping: from patient to high-throughput donor screening*. Vox sanguinis, 2009. **97**(3): p. 198-206.
104. Theberge, A.B., et al., *Microfluidic platform for combinatorial synthesis in picolitre droplets*. Lab on a chip, 2012. **12**(7): p. 1320-1326.
105. Abate, A.R., et al., *High-throughput injection with microfluidics using picoinjectors*. Proceedings of the National Academy of Sciences, 2010. **107**(45): p. 19163-19166.
106. Li, L., et al., *Nanoliter microfluidic hybrid method for simultaneous screening and optimization validated with crystallization of membrane proteins*. Proceedings of the National Academy of Sciences, 2006. **103**(51): p. 19243-19248.
107. Boedicker, J.Q., et al., *Detecting bacteria and determining their susceptibility to antibiotics by stochastic confinement in nanoliter droplets using plug-based microfluidics*. Lab on a Chip, 2008. **8**(8): p. 1265-1272.
108. Zeng, S., et al., *Microvalve-actuated precise control of individual droplets in microfluidic devices*. Lab Chip, 2009. **9**(10): p. 1340-1343.
109. Guo, F., et al., *Valve-based microfluidic device for droplet on-demand operation and static assay*. Applied Physics Letters, 2010. **97**(23): p. 233701.
110. Wang, H., et al., *A rapid pathway toward a superb gene delivery system: programming structural and functional diversity into a supramolecular nanoparticle library*. ACS nano, 2010. **4**(10): p. 6235-6243.
111. Unger, M.A., et al., *Monolithic microfabricated valves and pumps by multilayer soft lithography*. Science, 2000. **288**(5463): p. 113-116.

112. Puleo, C.M. and T.-H. Wang, *Microfluidic means of achieving attomolar detection limits with molecular beacon probes*. *Lab on a Chip*, 2009. **9**(8): p. 1065-1072.
113. Puleo, C., et al., *Coupling confocal fluorescence detection and recirculating microfluidic control for single particle analysis in discrete nanoliter volumes*. *Lab on a Chip*, 2008. **8**(5): p. 822-825.
114. Rane, T.D., et al., *Counting single molecules in sub-nanolitre droplets*. *Lab on a chip*, 2010. **10**(2): p. 161-4.
115. Schneider, T., J. Kreutz, and D.T. Chiu, *The Potential Impact of Droplet Microfluidics in Biology*. *Analytical Chemistry*, 2013. **85**(7): p. 3476-3482.
116. Rane, T.D., et al., *Droplet microfluidics for amplification-free genetic detection of single cells*. *Lab on a chip*, 2012. **12**(18): p. 3341-7.
117. Cho, S., et al., *Droplet-Based Microfluidic Platform for High-Throughput, Multi-Parameter Screening of Photosensitizer Activity*. *Analytical Chemistry*, 2013. **85**(18): p. 8866-8872.
118. Song, H. and R.F. Ismagilov, *Millisecond kinetics on a microfluidic chip using nanoliters of reagents*. *Journal of the American Chemical Society*, 2003. **125**(47): p. 14613-14619.
119. Han, Z.Y., et al., *Measuring Rapid Enzymatic Kinetics by Electrochemical Method in Droplet-Based Microfluidic Devices with Pneumatic Valves*. *Analytical Chemistry*, 2009. **81**(14): p. 5840-5845.
120. Shestopalov, I., J.D. Tice, and R.F. Ismagilov, *Multi-step synthesis of nanoparticles performed on millisecond time scale in a microfluidic droplet-based system*. *Lab on a Chip*, 2004. **4**(4): p. 316-321.
121. Shum, H.C., J.W. Kim, and D.A. Weitz, *Microfluidic fabrication of monodisperse biocompatible and biodegradable polymersomes with controlled permeability*. *Journal of the American Chemical Society*, 2008. **130**(29): p. 9543-9549.
122. Hindson, B.J., et al., *High-Throughput Droplet Digital PCR System for Absolute Quantitation of DNA Copy Number*. *Analytical Chemistry*, 2011. **83**(22): p. 8604-8610.
123. Rane, T.D., et al., *Microfluidic continuous flow digital loop-mediated isothermal amplification (LAMP)*. *Lab on a chip*, 2015. **15**(3): p. 776-82.
124. Ng, E.X., et al., *Low-volume multiplexed proteolytic activity assay and inhibitor analysis through a pico-injector array*. *Lab on a Chip*, 2015. **15**(4): p. 1153-1159.
125. Kaminski, T.S., et al., *Automated generation of libraries of nL droplets*. *Lab on a Chip*, 2012. **12**(20): p. 3995-4002.
126. Guo, F., et al., *Valve-based microfluidic device for droplet on-demand operation and static assay*. *Applied Physics Letters*, 2010. **97**(23).
127. Jambovane, S., et al., *Creation of Stepwise Concentration Gradient in Picoliter Droplets for Parallel Reactions of Matrix Metalloproteinase II and IX*. *Analytical Chemistry*, 2011. **83**(9): p. 3358-3364.
128. Xiang, X., et al., *Real-time luminescence-based colorimetric determination of double-strand DNA in droplet on demand*. *Biosensors & Bioelectronics*, 2012. **32**(1): p. 43-49.

129. Chen, J.Y., et al., *Assembly-line manipulation of droplets in microfluidic platform for fluorescence encoding and simultaneous multiplexed DNA detection*. *Talanta*, 2015. **134**: p. 271-277.
130. Rane, T.D., H.C. Zec, and T.H. Wang, *A barcode-free combinatorial screening platform for matrix metalloproteinase screening*. *Analytical chemistry*, 2015. **87**(3): p. 1950-6.
131. Link, D.R., et al., *Geometrically mediated breakup of drops in microfluidic devices*. *Physical Review Letters*, 2004. **92**(5).
132. Menetrier-Deremble, L. and P. Tabeling, *Droplet breakup in microfluidic junctions of arbitrary angles*. *Physical Review E*, 2006. **74**(3).
133. Hatch, A.C., et al., *Tunable 3D droplet self-assembly for ultra-high-density digital micro-reactor arrays*. *Lab on a Chip*, 2011. **11**(15): p. 2509-2517.
134. Hatch, A.C., et al., *1-Million droplet array with wide-field fluorescence imaging for digital PCR*. *Lab on a Chip*, 2011. **11**(22): p. 3838-3845.
135. Vertti-Quintero, N., et al., *Behavior of liquid plugs at bifurcations in a microfluidic tree network*. *Biomicrofluidics*, 2012. **6**(3).
136. Verbruggen, B., et al., *Separation of magnetic microparticles in segmented flow using asymmetric splitting regimes*. *Microfluidics and Nanofluidics*, 2015. **18**(1): p. 91-102.
137. Yoon, D.H., et al., *Active and Precise Control of Microdroplet Division Using Horizontal Pneumatic Valves in Bifurcating Microchannel*. *Micromachines*, 2013. **4**(2): p. 197-205.
138. Chan, M., et al., *Evaluation of nanofluidics technology for high-throughput SNP genotyping in a clinical setting*. *The Journal of molecular diagnostics : JMD*, 2011. **13**(3): p. 305-12.
139. Unger, M.A., et al., *Monolithic microfabricated valves and pumps by multilayer soft lithography*. *Science*, 2000. **288**(5463): p. 113-116.
140. Schneider, C.A., W.S. Rasband, and K.W. Eliceiri, *NIH Image to ImageJ: 25 years of image analysis*. *Nature Methods*, 2012. **9**(7): p. 671-675.
141. Tice, J.D., A.D. Lyon, and R.F. Ismagilov, *Effects of viscosity on droplet formation and mixing in microfluidic channels*. *Analytica Chimica Acta*, 2004. **507**(1): p. 73-77.
142. Wehking, J.D., et al., *Effects of viscosity, interfacial tension, and flow geometry on droplet formation in a microfluidic T-junction*. *Microfluidics and Nanofluidics*, 2014. **16**(3): p. 441-453.
143. Rane, T.D., H.C. Zec, and T.H. Wang, *A serial sample loading system: interfacing multiwell plates with microfluidic devices*. *Journal of laboratory automation*, 2012. **17**(5): p. 370-7.
144. Neethirajan, S., et al., *Microfluidics for food, agriculture and biosystems industries*. *Lab on a chip*, 2011. **11**(9): p. 1574-86.
145. Tester, M. and P. Langridge, *Breeding technologies to increase crop production in a changing world*. *Science*, 2010. **327**(5967): p. 818-22.
146. Thomson, M.J., *High-throughput SNP genotyping to accelerate crop improvement*. *Plant Breeding and Biotechnology*, 2014. **2**(3): p. 195-212.
147. Rivers, J., et al., *Genomic breeding for food, environment and livelihoods*. *Food Security*, 2015. **7**(2): p. 375-382.

148. Prashar, S., et al., *Stability of midge tolerant varietal blends over 3-4 successive generations: high-speed/high-throughput, SNP-DNA fingerprinting in grain seeds*. Journal of Plant Molecular Biology and Biotechnology, 2012. **3**(2): p. 1-10.
149. Mammadov, J.A., et al., *Development of highly polymorphic SNP markers from the complexity reduced portion of maize [*Zea mays L.*] genome for use in marker-assisted breeding*. TAG. Theoretical and applied genetics. Theoretische und angewandte Genetik, 2010. **121**(3): p. 577-88.
150. Fan, J.B., et al., *Highly parallel SNP genotyping*. Cold Spring Harbor symposia on quantitative biology, 2003. **68**: p. 69-78.
151. Hyten, D.L., et al., *High-throughput genotyping with the GoldenGate assay in the complex genome of soybean*. TAG. Theoretical and applied genetics. Theoretische und angewandte Genetik, 2008. **116**(7): p. 945-52.
152. Shen, R., et al., *High-throughput SNP genotyping on universal bead arrays*. Mutation research, 2005. **573**(1-2): p. 70-82.
153. Steemers, F.J., et al., *Whole-genome genotyping with the single-base extension assay*. Nature methods, 2006. **3**(1): p. 31-3.
154. Hoffmann, T.J., et al., *Next generation genome-wide association tool: design and coverage of a high-throughput European-optimized SNP array*. Genomics, 2011. **98**(2): p. 79-89.
155. Seeb, J.E., et al., *SNP genotyping by the 5'-nuclease reaction: advances in high-throughput genotyping with nonmodel organisms*. Methods in molecular biology, 2009. **578**: p. 277-92.
156. Berthier-Schaad, Y., et al., *Reliability of high-throughput genotyping of whole genome amplified DNA in SNP genotyping studies*. Electrophoresis, 2007. **28**(16): p. 2812-7.
157. Magee, D.A., et al., *Technical note: High fidelity of whole-genome amplified sheep (*Ovis aries*) deoxyribonucleic acid using a high-density single nucleotide polymorphism array-based genotyping platform*. Journal of animal science, 2010. **88**(10): p. 3183-6.
158. Bardin, D., et al., *Parallel generation of uniform fine droplets at hundreds of kilohertz in a flow-focusing module*. Biomicrofluidics, 2013. **7**(3): p. 34112.
159. Brouzes, E., et al., *Droplet microfluidic technology for single-cell high-throughput screening*. Proceedings of the National Academy of Sciences of the United States of America, 2009. **106**(34): p. 14195-14200.
160. Mazutis, L., et al., *Single-cell analysis and sorting using droplet-based microfluidics*. Nature protocols, 2013. **8**(5): p. 870-891.
161. Klein, A.M., et al., *Droplet Barcoding for Single-Cell Transcriptomics Applied to Embryonic Stem Cells*. Cell, 2015. **161**(5): p. 1187-1201.
162. Mazutis, L., et al., *Droplet-based microfluidic systems for high-throughput single DNA molecule isothermal amplification and analysis*. Analytical chemistry, 2009. **81**(12): p. 4813-21.
163. Valencia, P.M., et al., *Microfluidic technologies for accelerating the clinical translation of nanoparticles*. Nature nanotechnology, 2012. **7**(10): p. 623-9.
164. Zhang, J., et al., *One-step fabrication of supramolecular microcapsules from microfluidic droplets*. Science, 2012. **335**(6069): p. 690-4.

165. Lignos, I., et al., *Facile droplet-based microfluidic synthesis of monodisperse IV–VI semiconductor nanocrystals with coupled in-line NIR fluorescence detection*. Chemistry of Materials, 2014. **26**(9): p. 2975-2982.
166. Rhee, M., et al., *Pressure stabilizer for reproducible picoinjection in droplet microfluidic systems*. Lab on a chip, 2014. **14**(23): p. 4533-9.
167. Ahn, K., et al., *Electrocoalescence of drops synchronized by size-dependent flow in microfluidic channels*. Applied Physics Letters, 2006. **88**(26): p. 264105.
168. Olivier, M., *The Invader assay for SNP genotyping*. Mutation research, 2005. **573**(1-2): p. 103-10.
169. Koster, S., et al., *Drop-based microfluidic devices for encapsulation of single cells*. Lab on a chip, 2008. **8**(7): p. 1110-5.
170. Courtois, F., et al., *Controlling the retention of small molecules in emulsion microdroplets for use in cell-based assays*. Analytical chemistry, 2009. **81**(8): p. 3008-3016.

Curriculum Vitae

HELENA ZEC

hzec1@jhmi.edu

410.402.3303

4000 North Charles Street #1003, Baltimore MD 21218

Education

Johns Hopkins University, School of Medicine (JHU) Ph.D. Candidate in Biomedical Engineering	Baltimore, Maryland August 2008-present
Swiss Federal Institute of Technology (ETH) M.S. in Biomedical Engineering	Zürich, Switzerland August 2006-June 2008
Worcester Polytechnic Institute (WPI) B.S. in Biomedical Engineering	Worcester, Massachusetts August 2002-June 2006

Honors and Awards

- Names **2015-2016 Regional Candidate for the White House Fellowship.**
- **Transducer Research Foundation Travel Award (January 2014):** Awarded grant (\$250) to travel to San Francisco, USA to present research projects.
- **Graduate Student Award Travel Award (November 2013):** Awarded grant (\$300) to travel to Berlin, Germany to attend the Falling Walls Conference.
- **AT Kearney Scholarship for Falling Walls Conference,** The International Conference on Future Breakthroughs in Science and Society (Berlin, November 2013): One out of 100 young researchers and entrepreneurs selected world-wide to present research in Berlin to a panel of “luminaries from the worlds of academia, research and business”.
- **Johns Hopkins Business and Consulting Club 2013 Case Competition (May 2013):** Our team placed second in the JHBCC 2013 Competition out of 33 teams Hopkins-wide (\$500).
- **Philanthropic Education Organization Scholar Award (April 2013):** Merit-based award (\$15000) awarded to 85 women doctoral candidates selected from across the US and Canada.
- **Martin Luther King, Jr. Award for Community Service (January 2013):** Nominated by the Incentive Mentoring Program. This year the award was presented by Benjamin Jealous, (then) President of NAACP. The MLK Award recognizes and encourages significant voluntary community by 8 faculty, staff and students at Johns Hopkins University (\$200 donated to charity of choice).
- **Inaugural Global Young Scientists Summit in Singapore (January 20-25, 2013):** Nominated to attend Summit (280 students selected world-wide). The program addresses the key areas of science & research, technology innovation & society and solutions to global challenges.
- **Baden-Württemberg Post Conference Programme for Young Scientists to the 62nd Meeting of Nobel Laureates in Lindau (July 07 – 11, 2012):** One of 20 young researchers selected world-wide to attend post-conference program organized by Baden-Württemberg International. Program consisted of visiting various research institutions in Germany, meeting fellow researchers and learning about employment opportunities.

- **62nd Lindau Meeting of Nobel Laureates in Lindau. Germany dedicated to Physics (July 1-6, 2012):** Received “Young Researcher Award” to attend Nobel Laureates meeting. One of 550 young researchers world-wide (72 US students) selected to participate in this meeting with more than 25 Nobel Laureates in attendance to exchange ideas, discuss projects and build international networks (Sponsored by Mars, Inc).
- **MicroTas Student Travel Grant (2009):** Awarded grant (\$500) to travel to S. Korea to present research projects.
- **Medtronic Fellowship (2008):** Selected from the entire incoming BME class at Johns Hopkins (~35 students) for fellowship (\$28500) for first year of graduate school.
- **Whitaker International Fellow Scholarship (2007):** Awarded grant (\$28000) to complete Master thesis at ETH Zürich (11 fellows selected across the US).
- **Rotary International Ambassadorial Scholarship (2006):** Was awarded a grant (\$25000) to obtain a Master’s degree at ETH Zürich.
- **Rita Schaffer Undergraduate Award (2006):** Recognized as student leader developing initiatives that strengthen my community (\$400).

Professional Experience

- **Allied Minds Fellows Program, August 2015 – Present: *Research Assistant:*** I am involved with scouting, diligence, market discovery, and investment analysis for Allied Minds. Founded in 2006, Allied Minds is a publicly-traded venture capital company (LSE: ALM, market cap US\$1B+, 2014 FTSE 250).
- **Harvard Medical School, Center for Engineering in Medicine (PI: Mehmet Toner), April 2006 – September 2006: *Researcher:*** Worked with a novel microfluidic device capable of selective separation of rare circulating epithelial cells from whole blood samples of cancer patients.

Journal Publications (*denotes equal contribution)

1. H.C. Zec, T.H. Wang “Nanoliter array for digital methylation-specific PCR” *in preparation*
2. H.C. Zec, T.D. Rane, W.C. Chu, V.W. Wang, T.H. Wang. "A microfluidic droplet platform for multiplexed single nucleotide polymorphism analysis of an array plant genomic DNA samples." *in preparation*
3. T.D. Rane, H.C. Zec, T.H. Wang. “A barcode-free combinatorial screening platform for matrix metatalloproteinase screening”, *Analytical Chemistry* 2015, 87 (3), pp 1950–1956
4. T.D. Rane, L. Chen, H.C. Zec, T.H. Wang. "Microfluidic continuous flow digital loop-mediated isothermal amplification", *Lab on a Chip* 2015 Jan 22;15(3):776-82
5. H.C. Zec, D.J. Shin, T.H. Wang “Novel droplet platforms for biomarker detection: implications for molecular diagnostics”, *Expert Reviews for Molecular Diagnostics* Sep;14(7):787-80
6. T.D. Rane*, H.C. Zec*, T.H. Wang "A Serial Sample Loading System Interfacing Multiwell Plates with Microfluidic Devices." *Journal of laboratory automation* 17, no. 5 (2012): 370-377.
7. T.D. Rane, H.C. Zec, C. Puleo, A.P. Lee, T.H. Wang. "Droplet microfluidics for amplification-free genetic detection of single cells." *Lab on a Chip* 12, no. 18 (2012): 3341-3347.
8. H.C. Zec*, T.D. Rane*, T.H. Wang. "Microfluidic platform for on-demand generation of spatially indexed combinatorial droplets." *Lab on a Chip* 12, no. 17 (2012): 3055-3062.

Peer-reviewed Conference Papers (*denotes equal contribution)

1. Transducers, 2015, Alaska, USA, July '15: "Ultra-thin, evaporation-resistant PDMS devices for absolute quantification of DNA using digital PCR." H.C. Zec, and T.H. Wang
2. MicroTas, 2014, San Antonio, Texas, USA, Oct '14: "Continuous flow digital loop-mediated isothermal amplification (LAMP) in droplets." T.D. Rane, L. Chen, H.C. Zec, and T.H. Wang
3. MicroTas, 2014, San Antonio, Texas, USA, Oct '14: "Method for controlling water evaporation in PDMS-based microfluidic devices." H.C. Zec, C.O. Keefe, and T.H. Wang
4. H.C. Zec, T.D. Rane, P. Ma, T.H. Wang. "Parallelization of fission and fusion operations for high throughput generation of combinatorial droplets." In Micro Electro Mechanical Systems (MEMS), 2014 IEEE 27th International Conference on, pp. 334-337. IEEE, 2014.
5. MicroTas 2013, Freiburg, Germany, Oct '13: "A Multiplexed Microfluidic Droplet Platform for Matrix Metalloproteinase Screening" T. Rane, H. Zec, T.H. Wang
6. H.C. Zec, T.D. Rane, W.C. Chu, V.W. Wang, T.H. Wang. "A microfluidic droplet platform for multiplexed single nucleotide polymorphism analysis of an array plant genomic DNA samples." In Micro Electro Mechanical Systems (MEMS), 2013 IEEE 26th International Conference on, pp. 263-266. IEEE, 2013.
7. H.C. Zec, T.D. Rane, W.C. Chu, T.H. Wang. "Microfluidic Combinatorial Screening Platform." In ASME 2012 10th International Conference on Nanochannels, Microchannels, and Minichannels collocated with the ASME 2012 Heat Transfer Summer Conference and the ASME 2012 Fluids Engineering Division Summer Meeting, pp. 91-96. American Society of Mechanical Engineers, 2012.
8. IEEE 24th International Conference on Micro Electro Mechanical System, Cancun, Mexico, Jan '11: "High-throughput single-cell pathogen detection on a droplet microfluidic platform" T.D. Rane, H. Zec, C. Puleo, A.P. Lee, T.H. Wang
9. MicroTas 2009, Jeju, South Korea, Nov '09 "Micro-evaporator as Interconnects tom Low-Volume Microfluidic Components" H.C. Zec, C.M. Puleo, Y. Song, T.H. Wang
10. MicroTas 2009, Jeju, South Korea, Nov '09: "Analyte Detection in Droplets: One Molecule at a Time" T.D. Rane, C.M. Puleo, H. Zec, K.J. Liu, Y. Zhang, A.P. Lee, T.H. Wang

Conferences / Invited Talks

1. JHU CCNE Site Visit, April '14: "A Multiplexed Microfluidic Droplet Platform for Screening"
2. JHU INBT Spring Mini-Symposium, April '13: "A droplet platform for multiplexed single nucleotide polymorphism analysis."
3. MF3 IAB Meeting, Arlington, Virginia, Dec '10: "A programmable multiplexed microfluidic platform". H. Zec, T.Rane, T.H. Wang
4. BMES 2009 Annual Fall Scientific Meeting, Pittsburgh, PA, Oct'09: "Droplet-based micro-evaporator for biomolecular detection" H.Zec, C. Puleo, T.H. Wang
5. Swiss Society of Biomedical Engineering Meeting, Neuchatel, Switzerland, Sept'07: "Optimization of Undecalcified Bone Cryosectioning for Bone Cell Identification, Counting and Isolation" H.Zec, E. Wasserman, R. Müller

6. 32nd Annual Northeast Bioengineering Conference, Lafayette College, Easton, PA, Apr'05: "Fixation Techniques: A Cyclic Failure Analysis", H. Zec, D. Decoteau, D. Flannery, A. Hart, R. Dunn, M.D., K. Billiar, Ph.D.
7. 31st Annual Northeast Bioengineering Conference, Stevens Institute of Technology, Hoboken, New Jersey, Apr'05: "A Humidifier for Olfaction Studies During Functional Magnetic Resonance Imaging", M. Corcoran, H. Zec.

Patents

1. U.S. Patent App 'System and Method for Screening a Library of Samples' Inventors: Jeff T.H. Wang, H.C. Zec, T.D. Rane, W.C. Chu. JHU Reference Number: C11803
2. U.S. Patent App "Parallelization of Fission and Fusion Operations for High Throughput Generation of Combinatorial Droplets" Inventors: Jeff T.H. Wang, H.C. Zec, T.D. Rane

Teaching Experience

Delivered guest lecture for Manufacturing Engineering 530.354 (Spring 2014)
 Teaching Assistant for 'BioSensing and BioMEMS' class (Spring 2014, Spring 2011): Taught two lab sessions and graded lab reports.
 Teaching Assistant for 'Cell and Tissue Engineering Lab' (Spring 2013, Spring 2012, Spring 2011): Taught two lab sessions and graded lab reports.
 Teaching Assistant for 'Microfabrication Lab' (Fall 2011): Taught all lab sessions, graded all lab reports and homework sets.
 Teaching Assistant for 'Modeling and Design' (Fall 2010): Prepared lectures, graded lab reports and homework sets.

JHU research mentor for undergraduates:

Christopher Glover (Class of 2015, BME, University of Missouri)
 Lily Liu (Class of 2014, BME, JHU)
 Polly Ma (Class of 2016, BME, JHU) - Received Provost Undergraduate Research Award Fall 2014. Selected for summer internship in IMEC, Belgium (2014).
 Jeffrey Knox (Class of 2014, BME, JHU)
 Melissa Gosse (Class of 2013, BME, JHU) – Selected for 2012 NNIN REU Program at ASU NanoFab, Arizona State University. Current position: Associate Engineer at Canon Life Sciences.
 Elmer Rho (Class of 2015, BME, JHU)
 Mackenzie Crocker (Class of 2013, Chemical and Biomolecular Engineering, JHU)
 Kutay Muslu (Class of 2014, BME, JHU)

JHU research mentor for Senior Design Projects:

Frank Qin (Class of 2012, BME, JHU) – "Microfluidic Static Droplet Arrays". Current position: Technical services at EPIC.
 Joseph Choi (Class of 2012, BME, JHU) – "Microfluidic Static Droplet Arrays". Current position: Masters student at JSPH.
 Thanapoom Boonipat (Class of 2011, BME, JHU) "Novel Programmable Multiplexed Droplet Microfluidic Device". Current position: Medical Student, Dartmouth Medical School.
 Tae Hong Min (Class of 2010, BME, JHU).

Advisor to high school undergraduate students:

Yiyi Sun, Garrison Forest School, Women in Science in Engineering (Spring 2013)

Kori Davis, Dunbar High School, The Incentive Mentoring Program (Summer 2012)
Vivian Wang, High School Student (Summer 2012)